








EX LIBRIS  
UNIVERSITATIS  
ALBERTENSIS

The Bruce Peel  
Special Collections  
Library



Digitized by the Internet Archive  
in 2025 with funding from  
University of Alberta Library

<https://archive.org/details/0162014232472>













**University of Alberta**

**Library Release Form**

**Name of Author:** Yu Liu

**Title of Thesis:** Hybrid Composite/Metal Pipe — Theoretical Analysis and  
Experimental Study

**Degree:** Master of Science

**Year this Degree Granted:** 2001

Permission is hereby granted to the University of Alberta Library to reproduce single copies of this thesis and to lend or sell such copies for private, scholarly or scientific research purposes only.

The author reserves all other publication and other rights in association with the copyright in the thesis, and except as herein before provided, neither the thesis nor any substantial portion thereof may be printed or otherwise reproduced in any material form whatever without the author's prior written permission.







UNIVERSITY OF ALBERTA

**Hybrid Composite/Metal Pipe**  
**— Theoretical Analysis and Experimental Study**

By

Yu Liu



A thesis submitted to the Faculty of Graduate Studies in partial fulfillment of the  
requirements for the degree Masters of Science

Department of Mechanical Engineering

Edmonton, Alberta

Fall, 2001





University of Alberta

Faculty of Graduate Studies and Research

The undersigned certify that they have read, and recommend to the Faculty of Graduate Studies and Research for acceptance, a thesis entitled Hybrid Composite/Metal Pipe – Theoretical Analysis and Experimental Study submitted by Yu Liu in partial fulfillment of the requirements for the degree of Master of Science.





## **Abstract**

An analytical model is developed which is capable of predicting the stress-strain response of a hybrid polymeric composite/metal pipe under any combination of biaxial loading histories. Two programs are developed using MatLab code to carry out the parametric study. These two programs can determine the required internal pressure that will cause desired residual stresses in the metallic liner and the polymeric composite wrap. The programs can also simulate the loading, unloading and reloading process of the hybrid pipe.

Hybrid composite/steel pipe specimens were manufactured with a tubular rolling method. Uniaxial and biaxial loading tests were carried out. The predicted results by the current theoretical model were compared with the experiments and with the results from a finite element analysis. They were found to be in a very good agreement.





---

## ACKNOWLEDGEMENTS

The author wishes to express his thanks to Dr. Zihui Xia for his guidance and patience throughout this endeavor.

Gratitude is extended to Alan W. Wharmby, Mike Martens, Dr. John Wolodko and Mr. Bernie Faulkner, who helped me to use the experimental facility and the associate testing procedure.

I also wish to take this opportunity to express my thanks to the other members of the ACME Group, past and present, for offering support and excellent technical discussions during the weekly group meetings. Dr. F. Ellyin, Garret Meijer, Yu Chen, Dr. Xueli Han, Yafei Hu, Yunfa Zhang, Cecelia Lingheche and Pierre Mertiny were all helpful, and it was a pleasure to be among them.

I am especially grateful to my wife for being a supportive companion throughout this study, and earlier time.





---

## INDEX

|   |           |
|---|-----------|
| <b>CHAPTER 1 INTRODUCTION .....</b>   | <b>1</b>  |
| 1.1 Introduction .....  | 1         |
| 1.2 Review of traditional pipes .....   | 3         |
| 1.3 Review of composite pipes .....   | 4         |
| 1.4 Hybrid composite/metal pipes .....  | 6         |
| 1.5 Introduction of the present work.....   | 10        |
| <b>CHAPTER 2 THEORETICAL ANALYSIS .....</b>   | <b>12</b> |
| 2.1 Introduction .....  | 12        |
| 2.2 Constitutive model for the polymeric composite wrap.....                                | 12        |
| 2.2.1 Methodology of analysis of a composite structure .....                                | 12        |
| 2.2.2 Hooke's law for a two-dimensional unidirectional lamina .....                         | 15        |
| 2.2.3 Hooke's law for a two-dimensional angle lamina .....                                  | 16        |
| 2.2.4 Stress-strain relationships for a laminate .....                                      | 18        |
| 2.3 Advanced constitutive model for the metallic liner.....                                 | 23        |
| 2.3.1 Introduction of Ellyin and Xia's model .....  | 23        |
| 2.3.2 Stress-strain relation .....  | 25        |
| 2.3.3 Evolution of the yield surface .....  | 28        |
| 2.3.4 Determination of tangent modulus, $E_t$ .....   | 31        |
| 2.4 Integral analysis model for the hybrid composite/metal pipe.....                        | 32        |
| 2.4.1 Basic assumptions .....   | 32        |
| 2.4.2 Load analysis .....   | 32        |
| 2.4.3 Elastic stage.....  | 34        |
| 2.4.4 Monotonic plastic loading stage.....  | 38        |
| 2.4.5 Elastic unloading and plastic reloading .....   | 42        |
| 2.5 Numerical program development.....  | 46        |
| 2.5.1 Input parameters .....  | 46        |
| 2.5.2 Failure analysis of HPD1 .....  | 48        |
| 2.5.3 Output parameters.....  | 49        |
| 2.5.3 Examples .....  | 50        |
| 2.5.3.1 Example 1: Metallic liner alone.....  | 50        |
| 2.5.3.2 Example 2: Proof pressure prediction with the use of program HPD1 .....             | 52        |
| 2.5.3.3 Example 3: Uniaxial loading-reloading simulation with the use of program HPD2 ..... | 55        |
| 2.5.3.4 Example 4: Biaxial loading-reloading simulation with the use of program HPD2 .....  | 56        |
| 2.5.3.5 Example 5: Weight saving calculation.....   | 57        |



---

|  |            |
|--|------------|
| <b>CHAPTER 3 EXPERIMENTAL VERIFICATION .....</b>               | <b>59</b>  |
| 3.1 Introduction .....   | 59         |
| 3.2 Tubular specimen design .....                              | 59         |
| 3.3 Tubular specimen manufacturing .....                       | 63         |
| 3.3 Testing apparatus .....                                    | 74         |
| 3.3.1 MTS testing machine .....                                | 74         |
| 3.3.2 Gripping system .....                                    | 77         |
| 3.3.3 Data acquisition .....                                   | 82         |
| 3.4 Testing procedure & results .....                          | 84         |
| 3.4.1 Introduction .....                                       | 84         |
| 3.4.2 Steel liner test .....                                   | 85         |
| 3.4.3 Hybrid pipe specimen test .....                          | 87         |
| 3.4.3.1 Uniaxial test (1H:0A) .....                            | 87         |
| 3.4.3.2 Biaxial test I (2H:1A) .....                           | 89         |
| 3.4.3.3 Biaxial test II (2H:1A) .....                          | 92         |
| <b>CHAPTER 4 FINITE ELEMENT ANALYSIS AND COMPARISONS .....</b> | <b>96</b>  |
| 4.1 Introduction .....   | 96         |
| 4.2 Finite element model .....                                 | 96         |
| 4.3 Element type .....   | 97         |
| 4.4 Material properties .....                                  | 98         |
| 4.4.1 Material properties of the steel .....                   | 98         |
| 4.4.2 Material properties of composite wrap .....              | 99         |
| 4.5 Loading conditions .....                                   | 99         |
| 4.6 Loading history .....                                      | 100        |
| 4.7 Comparisons .....  | 100        |
| 4.7.1 Uniaxial tests ( $\kappa = 0$ ) .....                    | 100        |
| 4.7.2 Biaxial loading case I ( $\kappa = 1$ , 2H:1A) .....     | 102        |
| 4.7.3 Biaxial loading case II ( $\kappa = 1$ , 2H:1A) .....    | 106        |
| 4.7.4 Failure observation .....                                | 109        |
| <b>CHAPTER 5 SUMMARY &amp; CONCLUSIONS .....</b>               | <b>111</b> |
| <b>BIBLIOGRAPHY .....</b>                                      | <b>116</b> |





---

# LIST OF TABLES

TABLE 1.1 COMPARISON OF OPERATING COST OF TRANSPORTATION SYSTEMS [1] ..... 3

TABLE 3-1 MATERIAL PROPERTIES OF 3M TYPE 1003 E-GLASS FIBER/EPOXY RESIN  
COMPOSITE AS MANUFACTURED AT THE UNIVERSITY OF ALBERTA [41]..... 68

TABLE 3-2 SPECIMENS TESTED ..... 85

TABLE 3-3 STRESS-STRAIN CURVE POINTS FOR THE STEEL..... 86





---

## LIST OF FIGURES

|   |    |
|---|----|
| FIGURE 2-1 SCHEMATIC OF ANALYSIS OF LAMINATED COMPOSITE [17] .....                            | 14 |
| FIGURE 2-2 COORDINATE SYSTEM FOR A UNIDIRECTIONAL LAMINA .....                                | 15 |
| FIGURE 2-3 COORDINATE SYSTEMS FOR AN ANGLE LAMINA.....  | 16 |
| FIGURE 2-4 A LAMINATE CONSISTS OF 4 LAMINAE .....   | 19 |
| FIGURE 2-5 COORDINATE LOCATIONS OF PLYS IN A LAMINATE [17] .....                              | 20 |
| FIGURE 2-6 CONSTITUTIVE MODEL OF THE METAL [14].....  | 25 |
| FIGURE 2-7 LOADING STATUS OF THE HYBRID COMPOSITE PIPE.....                                   | 33 |
| FIGURE 2-8 FREE-BODY DIAGRAMS FOR THE METALLIC LINER AND COMPOSITE WRAP ...                   | 35 |
| FIGURE 2-9 MULTI-LINEAR STRESS-STRAIN CURVE OF THE METAL .....                                | 38 |
| FIGURE 2-10 SCHEMATIC ABOUT DETERMINE TANGENT MODULUS.....                                    | 45 |
| FIGURE 2-11 STRESS-STRAIN RELATIONSHIP FOR MULTI-LINEAR KINEMATIC HARDENING<br>MATERIAL ..... | 50 |
| FIGURE 2-12 RESPONSE OF THE METALLIC LINER.....   | 51 |
| FIGURE 2-13 PROOF PRESSURE PREDICTION AND FAILURE ANALYSIS BY HPD1 .....                      | 54 |
| FIGURE 2-14 PRESSURE-HOOP STRAIN CURVE UNDER UNIAXIAL-LOADING CONDITION ...                   | 56 |
| FIGURE 2-15 PRESSURE-HOOP STRAIN CURVE UNDER BIAXIAL-LOADING CONDITION .....                  | 57 |
| FIGURE 3-1 DRAWING OF THE HYBRID COMPOSITE/STEEL SPECIMEN (UNIT: MM).....                     | 62 |
| FIGURE 3-2 (A) PICTURE OF THE ROLLING TABLE, (B) LAYOUT OF THE ROLLING TABLE...               | 65 |
| FIGURE 3-3 RELATIONSHIP BETWEEN THE TEMPLATE AND THE STEEL MENDRAL .....                      | 67 |
| FIGURE 3-4 LAMINATE CUTTING .....   | 69 |
| FIGURE 3-5 PLACE THE PREPREG LAYER ON THE FLAT PLATE .....                                    | 70 |
| FIGURE 3-6 SPECIMEN IN THE CURING OVEN.....   | 73 |
| FIGURE 3-7 FINISHED TUBULAR SPECIMEN.....   | 74 |
| FIGURE 3-8 MTS MACHINE .....  | 76 |



|  |     |
|--|-----|
| FIGURE 3-9 SCHEMATIC DRAWING OF THE GRIPPING SYSTEM [42] .....   | 78  |
| FIGURE 3-10 INSTRON HYDRAULIC SCREW DRIVEN TESTING MACHINE.....  | 80  |
| FIGURE 3-11 FINISHED SPECIMEN MOUNTED IN THE GRIPPING SYSTEM .....   | 81  |
| FIGURE 3-12 (A) AXIAL EXTENSOMETER (B) HOOP EXTENSOMETER.....  | 82  |
| FIGURE 3-13 MARKING THE POSITION OF EXTENSOMETERS ON THE SPECIMEN.....   | 83  |
| FIGURE 3-14 DATA ACQUISITION SYSTEM.....   | 84  |
| FIGURE 3-15 EXPERIMENTAL STRESS-STRAIN CURVE OF STEEL WITH POINTS USED IN<br>MULTILINEAR KINEMATIC HARDENING MODEL ..... | 87  |
| FIGURE 3-16 UNIAXIAL $P - \varepsilon_h$ CURVES .....  | 88  |
| FIGURE 3-17 (A) $P - \varepsilon_h$ CURVE OF BIAXIAL LOADING TEST ONE .....  | 90  |
| FIGURE 3-17 (B) $P - \varepsilon_a$ CURVE OF BIAXIAL LOADING TEST ONE .....  | 91  |
| FIGURE 3-18 (A) $P - \varepsilon_h$ CURVE OF BIAXIAL LOADING TEST TWO .....  | 93  |
| FIGURE 3-18 (B) $P - \varepsilon_a$ CURVE OF BIAXIAL LOADING TEST TWO .....  | 94  |
| FIGURE 4-1 AXISYMMETRIC LOADING CONDITIONS OF THE HYBRID COMPOSITE PIPE.....   | 97  |
| FIGURE 4-2 PICTORIAL SUMMARY OF ELEMENT PLANE42 .....  | 97  |
| FIGURE 4-3 STRESS-STRAIN RELATIONSHIP FOR MULTILINEAR KINEMATIC HARDENING<br>MATERIAL .....                              | 98  |
| FIGURE 4-4 UNIAXIAL PRESSURE-HOOP STRAIN CURVES.....   | 101 |
| FIGURE 4-5 PRESSURE-HOOP STRAIN CURVES OF BIAXIAL TEST ONE.....  | 103 |
| FIGURE 4-6 PRESSURE-HOOP STRAIN CURVES OF BIAXIAL TEST ONE.....  | 105 |
| FIGURE 4-7 PRESSURE-HOOP STRAIN CURVES OF BIAXIAL TEST TWO .....   | 107 |
| FIGURE 4-8 PRESSURE-AXIAL STRAIN CURVES OF BIAXIAL TEST TWO.....   | 108 |





---

## Chapter 1 Introduction

### 1.1 Introduction

Pipelines play an important role in the daily lives of most people in the world, however, the influence is rather passive and the majorities are unaware of it. For example, the modern society lives on oil and gas that are major supplies of energy. Pipelines are the principal means of transporting oil and gas from their source to the ultimate destination. In 1991, according to the United Nations Gas Facts, there were about 3.2 million kilometers of transmission pipeline through out the world [1]. With the steady rise of world trade, it is safe to say that this number would have increased significantly since then.

In addition to direct use, such as to heat houses, to cook meals, etc., oil and gas can also be used to generate electric power, which is of significant importance to the modern society. Oil and gas are also the major raw materials for the petrochemical industry to produce many useful products, such as gasoline, diesel oil, jet fuel, propane, polyethylene and lubricants. All these demands for gas and oil require an effective way for transportation, and this leads to the development of the modern pipeline industry.

In 1859, Col. Edwin Drake struck oil in Titusville, Pennsylvania and there was the need for a more efficient means of transporting oil. This led to the first natural gas transportation pipeline in North America, which was 2-inch in diameter, and 5.5 miles long [2]. In Canada, gas pipelines were built along the south Saskatchewan River and in Turner valley to supply Calgary, Lethbridge and other towns in the 1950's. The discovery



of Leduc field in Alberta in 1947 lead to the major interprovincial pipeline in Canada built to supply eastern Canada and the United States. The pipeline was built in 1950 with a 20-inch diameter pipe between Edmonton and Regina, and an 18-inch diameter pipe on the eastern section. This pipeline ran 1,120 miles in length and it cost \$90 million. In 1953, this pipeline was extended to Sarnia, and in 1957 from Sarnia to Toronto. This time a 30-inch diameter pipe was used, and at the time, it was the biggest (diameter) line ever used to carrying crude oil [3]. Ever since then, the pipeline industry has grown enormously. By the end of 1997, there was approximately 266,000 km of energy-related pipelines in Alberta alone [4], and this number is steadily increasing with the increasing demand for oil and gas.

Compared with other transportation forms such as trucks, marine tankers and rail tankers, pipelines offer the following advantages [1]:

- They can move large quantities of hydrocarbons.
- They traverse long distances. For instance, in countries like Canada, U.S.A., Russia and Saudi Arabia where the major oil and gas fields are located, thousands of miles away from the major centers of the population and industry, they provide the best alternative.
- Most of the pipelines are buried underground, so they do not interfere with environmental activities.
- They have low operating costs as shown in the following table.





Table 1.1 Comparison of operating cost of transportation systems [1]

| Transportation systems | %Energy content used per 1000 km |
|------------------------|----------------------------------|
| Rail                   | 0.8-1.0                          |
| Truck                  | 3.2-5.4                          |
| Tankers (LNG)          | 0.8-1.1                          |
| Pipeline               | <0.5                             |

Based on the great demand for oil and gas, and the advantages that pipelines offer in transportation, it is predictable that the pipeline industry will be growing significantly. Large efforts are being made on the design and safe operation of pipelines. The materials used are also changing with the development of new technologies.

## ***1.2 Review of traditional pipes***

Traditionally, carbon steel has been almost exclusive choice for pipelines. Carbon steel pipelines are widely used to gather or collect the natural gas, crude oil or water. They are used to transport substances over distances from hundreds of meters to hundreds of kilometers. They are also used to distribute natural gas, water, water-refined liquids, and so on, to the end users. However, this type of pipe easily corrodes.

Cast iron is another material that can be used in pipeline systems. They are extensively used in water and natural gas distribution. They often withstand harsh conditions better, but cast iron has relatively low resistance to impact and as such is not an ideal material for the transportation of hazardous materials.



Alloy steels are also used as pipeline materials under certain service conditions.

These metallic materials have the disadvantages of high weight, low corrosion resistance, etc. Different methods are lately being developed to overcome the weakness in corrosion resistance. One way is to use an outside wrapping such as coal tar or glass fiber wrapping. These wrappings are not designed to take load. A weakness of this method is that corrosion will still occur at locations where the wrapping was improperly installed or was damaged. Another method is the cathodic protection. By applying a suitable voltage on pipes, or add additional metals such as zinc, magnesium or aluminum as the sacrifice anode, the pipe is turned into a cathode, and this prevents the iron in the pipe passing into the solution as an ion, thus suppresses the steel corrosion. The combination of these two techniques can minimize the corrosion rate [5].

### ***1.3 Review of composite pipes***

The composite pipe industry started from World War II, when people were seeking a viable alternative to protected steel, stainless steel and other exotic materials that were in short supply at that time. Its early applications included well casing and oil field gathering lines. Some of these have been in service for more than 30 years and are still fully functional. Today, because of its design flexibility and other advantages, low pressure composite pipelines are widely used and becoming the “system of choice” in the offshore oil and gas industry as well as the petrochemical industry all over the world.

Compared with traditional materials used for pipes, such as protected steel, stainless steel and other materials, these composite materials offer [6]:



- Exceptional corrosion resistance where temperatures are under  $250^{\circ}F$  ( $120^{\circ}C$ )
- Low installed cost (no hot work permits required), minimum maintenance (no repainting cost), low life cycle cost with over twenty years case histories in sea water service
- Excellent hydraulic characteristics, with resistance to erosion and fouling
- Lightweight (Six-inch composite pipe weights approximately four pounds per foot vs. twenty pounds per foot for Sch. 40 carbon steel pipe)
- High strength to weight ratio
- Flexibility of design to meet customer needs

However, composite pipes also have their own disadvantages, such as not fully developed material model, relatively complex material behavior, and there is also some difficulty with the joint technology. Among all these disadvantages, its limited capability in transporting high-pressure hydrocarbons is the key factor that limits its application. While transporting high-pressure fluids, due to the weak nature of matrix, the filament wind composite pipe is very likely to leak, and currently this limits the composite pipeline of being used for low-pressure transportation only. However, attracted by many advantages that a composite pipeline possesses, researchers and scientists are looking for different ways to overcome the abovementioned disadvantage, among which a hybrid composite/metal pipe is a very promising technology.





## **1.4 Hybrid composite/metal pipes**

A hybrid composite/metal (fiber glass/steel) pipe was developed for high-pressure pipeline use in 2000 [2]. It is made of a steel liner overwrapped with glass fiber/epoxy outside and can be used in transporting high-pressure natural gas. This hybrid composite pipe with a steel liner has many advantages over the steel pipe and the composite pipe.

Compared with traditional steel pipes, the hybrid composite/metal pipe has the following advantages:

- It can save considerable weight. For example, in aerospace applications, composite tanks overwrapped on a load sharing metallic liner could save 40% weight or more compared to the homogenous metal vessels.
- It can be optimized according to working conditions.
- The outside composite wrap protects the entire pipe from external corrosion, thus does not require the regular corrosion resistance protection used on steel pipes.

Compared with composite pipe, the internal metallic liner of the hybrid composite/metal pipe introduces many advantages over the composite pipes:

- The internal metallic liner can serve as a seal, which may effectively solve the problem of leakage under high-pressure transportation
- A beneficial compressive residual stress state can also be introduced, much as in autofrettage of an all metal thick-walled pipe. The pressure required to obtain this stress state is called proof pressure. The pipe is preloaded to the proof pressure, and after unloading, a compressive residual stress is created in the metallic liner, and a



tensile residual stress in the composite wrap. These residual stresses could increase the elastic range of the hybrid pipe as a whole. The bonding between the liner and the fiber wrap is also improved. The compressive residual stress could decrease the initiation and propagation of micro-cracks, thus increases the liner's ability to resist fatigue loading.

- The metallic liner can also function as a mandrel, which avoids the removal process of the internal mandrel that is required when fabricating purely composite pipes. Thus it reduces the cost of fabrication.

Based on these advantages, one could predict a bright future for the hybrid composite/metal pipe. Therefore, it is appropriate to study this type of pipe in greater detail.

As hybrid composite/metal pipe is a newly developed technique, there are relatively few reports in the open literatures. However, composite/metal pressure vessels have been utilized in transporting high-pressure fluids for a long time, and the cylindrical section of the pressure vessel is similar to the hybrid composite/metal pipe. Therefore some of the analytical methods used for pressure vessel design can provide useful insight to the current study.

The applications of composites in pressure vessels up to 1977 were reviewed in the Energy Technology Conference in Houston, Texas [7]. Different liners are used in these applications, and there are basically two approaches to the implementation of composite materials in high pressure vessels [8]: (a) to reinforce a thin metallic liner with composite wrap and (b) reinforce a thick load sharing metallic liner with composite wrap. Thin





liners could save more weight than the thick ones, and thus have higher load to weight ratio, but they also have their own problems. Thin liners tend to buckle during the decompression phase and are hard to manufacture. While using hybrid composite/metal pipelines to transport high-pressure natural gas, the weight factor is not so crucial, and thick liner is a better choice. For this reason, the literature review here will focus on the researches done concerning pressure vessels with thick metallic liner.

Shorkrieh and Rad [9] studied the effect of the sealing liner on displacement and stress fields of a composite cylinder, which was based on Aramid fibers and epoxy resin overwrap manufactured by filament winding method. This study showed that the liner has significant effect in reducing the displacement and stress fields. Ignoring its effect could lead to major error in the design. However, in their study the steel liner was considered to be linear elastic only and no experimental data was provided.

Lifshitz [10] presented a method to calculate stress and strain in non-symmetric filament-wound pressure vessels with thick metallic liners. In this study, the calculation was based on classical laminate theory and failure analysis was also carried out. The plastic yielding of the liner and transverse cracking of the composite were not considered to be final failure of the pressure vessel, and the liner and the composite were modeled by reduced properties after yielding or transverse cracking. In other words, the metallic liner was considered to be elastic-perfect plastic and no strain hardening effects were considered.

In 2000, Kabir [11] carried out a finite element analysis on composite pressure vessels with a load sharing metallic liner. He modeled the liner as an elastic, ideally



plastic material, and modeled the composite overwrap as a quasi-isotropic elastic material.

Liu and Hirano [12] presented the structural design and analysis of a FRP (fiber reinforced plastics) pressure vessel with a load-carrying metallic liner. The design was based on netting analysis and membrane theory, and the FEM analysis was carried out utilizing shell element.

In all the above analyses, the metallic liner is assumed to be elastic-perfect plastic only. However, for strain-hardening materials such as steel, this assumption could not fully exploit the capacity of the steel liner. There is need to model the metallic liner with more accurate material models. Swanson and Offolter [13] gave the basic equations for the analysis of a fiber composite cylinder wrapped over a ductile liner. In their model, within the linear range, the stiffness of the laminated cylinder is constructed by using classical laminate theory. In plastic part, an incremental tangential matrix is employed based on classical plastic theory. Their study considers the strain-hardening properties of the metallic liner. However, the classical plastic theory is adequate only for simple monotonic loading but does not properly describe the material behavior under cyclic or nonproportional loading. While considering the loading condition of the metallic liner, it is usually under nonproportional loading conditions due to the existence of the composite overwrap and introduction of the residual stresses. Thus, it is necessary to adopt a more accurate constitutive model to describe the behavior of the metallic liner, which is one of the objectives of the current study.



---

### **1.5 Introduction of the present work**

The current study focuses on a hybrid polymeric composite/metal pipe used in high-pressure natural gas transportation. There are three objectives for the current study:

1. To develop a more accurate theoretical analysis model for the hybrid composite/metal pipe;
2. To develop special computer program based on the theoretical model to facilitate the design of hybrid pipes;
3. To conduct experiments to validate the theoretical model.

The constitutive models of the metallic liner and the composite wrap are constructed separately. The metallic liner is assumed to be elastoplastic material, and an advanced constitutive model, Ellyin and Xia [14, 15 and 16] is used. The composite wrap is assumed to be an orthotropic elastic material, and its constitutive model is built with classical laminate theory. Based on the assumptions that there is perfect bonding between the metallic liner and the composite wrap, and that the strains are the same for the metallic liner and the fiber wrap (based on the thin-walled pipe assumption), the stress-strain response of the pipe can be derived.

To facilitate the calculation and design, two programs are developed using MatLab computer code. These two programs can predict the proof pressure, simulate the loading, unloading and reloading of the hybrid composite pipe, and carry out failure analysis. With these two programs, the design of the hybrid composite/metal pipe is greatly facilitated.





---

Experiments are also carried out to confirm the theoretical analysis. Tubular specimens are designed and manufactured using a tubular rolling method. The specimen is mounted on a MTS machine with a specially designed gripping system, which prevents the specimen from slippage while high axial tension is applied. Uniaxial and biaxial tests are carried out, and unloading and reloading procedure is introduced during the tests.

Finally, FEM model is also built using ANSYS as an additional method for comparison with the analytical solutions and experimental results. Both uniaxial and biaxial loading conditions are modeled, and the loading, unloading and reloading process are simulated. All the numerical results are compared with the theoretical predictions and the experimental results.



## **Chapter 2 Theoretical analysis**

### **2.1 Introduction**

To analyze the properties of the hybrid composite/metal pipe, it is first necessary to obtain the material properties of the metallic liner and the composite wrap, i.e. the constitutive models for both materials. This chapter will introduce an advanced constitutive model for the metallic liner that is complemented based on Ellyin and Xia's model. A complete description and derivation of the constitutive relationship can be found in references [14], [15] and [16]. The constitutive model for the composite wrap is constructed based on the classical laminate theory, of which a brief introduction is also given in this chapter. The integral analysis model of the hybrid composite pipe is given next, and two specific programs are developed using Matlab code, too. These two programs can predict the required proof pressure, and simulate loading, unloading and reloading properties of the hybrid composite pipe. Finally, examples are given to help understand and verify the functions of these two programs.

### **2.2 Constitutive model for the polymeric composite wrap**

#### **2.2.1 Methodology of analysis of a composite structure**

A composite material usually consists of two or more constituents and hence the mechanical analysis of it is different from that of the conventional materials such as metals and alloys. Before proceeding to the analysis, it is necessary to explain some terminologies for composite materials.



A composite structure is generally a laminated structure made of various laminae stacked together in a specific order. A lamina (also called a ply or a layer) is a single flat layer of unidirectional fibers or woven fibers encapsulated in a matrix. A laminate is a stack of laminae, and each lamina can have different fiber direction and can be made of different material systems.

The procedure to analysis a composite structure is illustrated in Figure 2-1[17]. First, the lamina is modeled on a micromechanical scale. It considers properties of the two constituents: fiber and matrix, and relates them with the volume fraction or mass fraction of fiber. Thus one can obtain the material properties for a single lamina. This is called *Micromechanics of a lamina*.

Secondly, the lamina is modeled on a macromechanical scale. The lamina is assumed to be a homogenous orthotropic layer. The stress-strain relationship is first formulated for a unidirectional lamina, and then for an angle lamina. The corresponding global engineering constants can also be obtained. This is called *Macromechanics of a lamina*.

Knowing the macromechanics of a single lamina, one develops the *Macromechanics of a laminate*. Based on the global properties of each lamina, lamina direction and stacking sequence of laminae, the stress-strain relation for the whole laminate can also be derived.





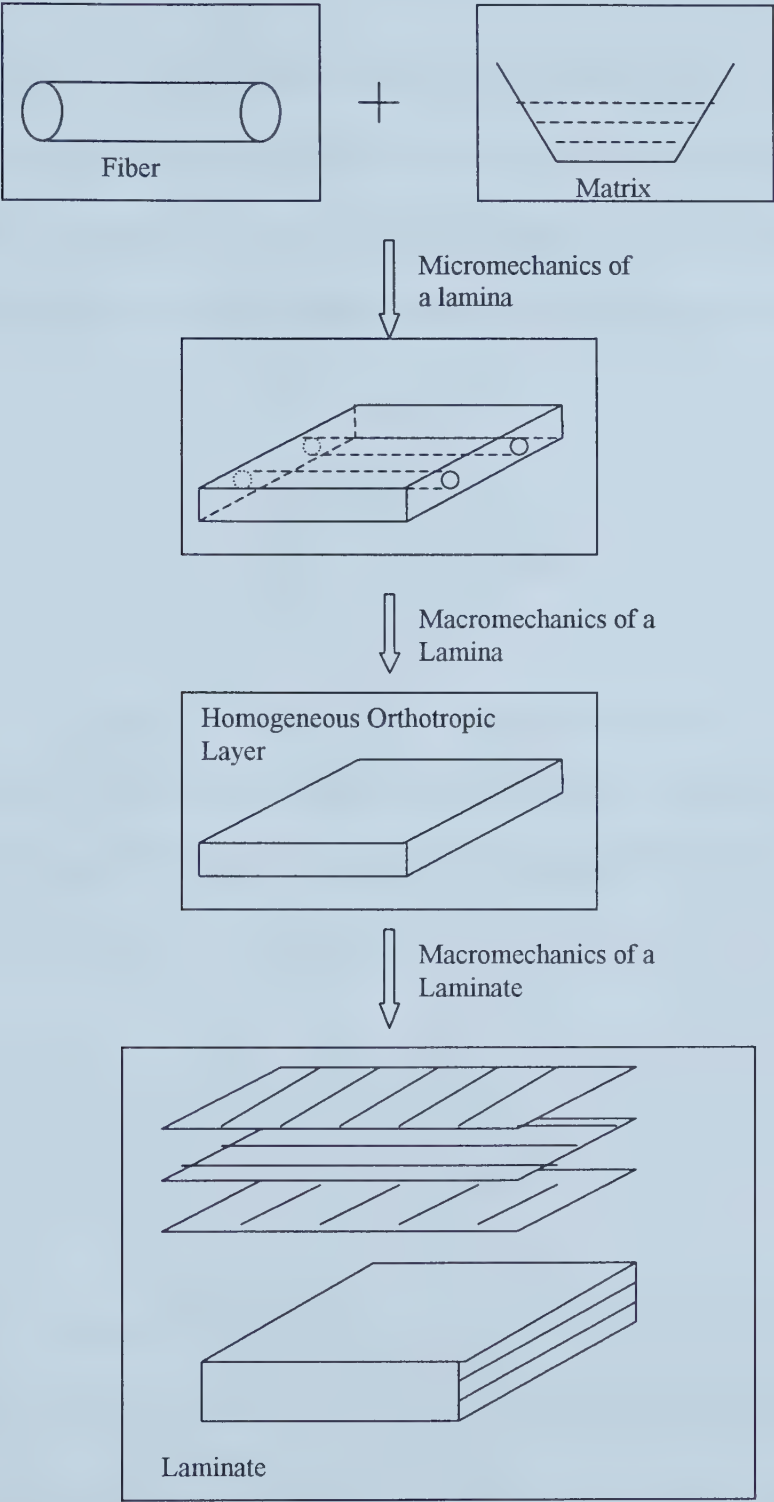


Figure 2-1 Schematic of analysis of laminated composite [17]



### 2.2.2 Hooke's law for a two-dimensional unidirectional lamina

A lamina is generally very thin and it is reasonable to assume that it is under a plane stress condition when there is no out-of-plane load applied. Thus the three-dimensional stress-strain relationship for a lamina can be reduced to a two dimensional one.

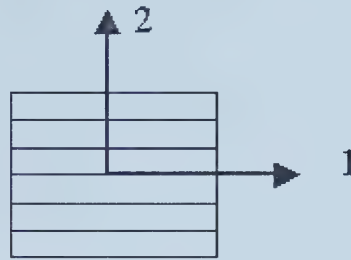


Figure 2-2 Coordinate system for a unidirectional lamina

The coordinate system for a unidirectional lamina is shown in Figure 2-2. The axes in the 1-2 coordinate system are called the local axes or the material axes where direction 1 is along the fiber direction. Based on Hooke's law, one can obtain

$$\begin{bmatrix} \varepsilon_1 \\ \varepsilon_2 \\ \gamma_{12} \end{bmatrix} = \begin{bmatrix} S_{11} & S_{12} & 0 \\ S_{12} & S_{22} & 0 \\ 0 & 0 & S_{66} \end{bmatrix} \begin{bmatrix} \sigma_1 \\ \sigma_2 \\ \tau_{12} \end{bmatrix} = \begin{bmatrix} \frac{1}{E_1} & -\frac{\nu_{12}}{E_1} & 0 \\ -\frac{\nu_{21}}{E_2} & \frac{1}{E_2} & 0 \\ 0 & 0 & \frac{1}{G_{12}} \end{bmatrix} \begin{bmatrix} \sigma_1 \\ \sigma_2 \\ \tau_{12} \end{bmatrix}, \quad (2.1)$$

where  $E_1$  is the longitudinal elastic modulus,  $E_2$  is the transverse elastic modulus, and  $G_{12}$  is the shear modulus, and  $\nu_{12}$  and  $\nu_{21}$  are the major and minor Poisson's ratio, respectively. Noting the relationship  $\frac{\nu_{12}}{E_1} = \frac{\nu_{21}}{E_2}$ , there are four independent engineering constants for a lamina.



Inverting the above equation gives

$$\begin{bmatrix} \sigma_1 \\ \sigma_2 \\ \tau_{12} \end{bmatrix} = \begin{bmatrix} Q_{11} & Q_{12} & 0 \\ Q_{12} & Q_{22} & 0 \\ 0 & 0 & Q_{66} \end{bmatrix} \begin{bmatrix} \varepsilon_1 \\ \varepsilon_2 \\ \gamma_{12} \end{bmatrix}, \quad (2.2)$$

where  $Q_{ij}$  are the reduced stiffness coefficients, and they are related to the engineering constants as

$$\begin{aligned} Q_{11} &= E_1 / (1 - \nu_{21}\nu_{12}), & Q_{12} &= \nu_{12}E_2 / (1 - \nu_{21}\nu_{12}), \\ Q_{22} &= E_2 / (1 - \nu_{21}\nu_{12}), & Q_{66} &= G_{12}. \end{aligned} \quad (2.3)$$

### 2.2.3 Hooke's law for a two-dimensional angle lamina

Generally, a laminate consists of lamina in different directions, which makes it necessary to develop the stress-strain relationship for an angle lamina.

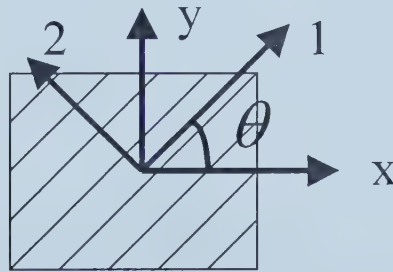


Figure 2-3 Coordinate systems for an angle lamina

The coordinate systems used for an angle lamina is shown in Figure 2-3. The axes in the 1-2 coordinate system are the local axes (material axes), where axis 1 is the longitudinal direction of the fibers, and axis 2 is the direction perpendicular to it, or axis 2





is called the transverse direction. The axes in the x-y coordinate system are the global axes, or the off-axes. The angle between axis 1 and x is  $\theta$ .

The stress-strain relationship in the local coordinate system is already achieved in the above section, equation (2.2). Based on tensor transformation rule, the global and local stresses and strains relate to each other by the transformation matrix  $[T]$ :

$$\begin{bmatrix} \sigma_x \\ \sigma_y \\ \tau_{xy} \end{bmatrix} = [T]^{-1} \begin{bmatrix} \sigma_1 \\ \sigma_2 \\ \tau_{12} \end{bmatrix} = \begin{bmatrix} c^2 & s^2 & -2sc \\ s^2 & c^2 & 2sc \\ sc & -sc & c^2 - s^2 \end{bmatrix} \begin{bmatrix} \sigma_1 \\ \sigma_2 \\ \tau_{12} \end{bmatrix}, \quad (2.4)$$

$$\begin{bmatrix} \varepsilon_1 \\ \varepsilon_2 \\ \gamma_{12}/2 \end{bmatrix} = [T] \begin{bmatrix} \varepsilon_x \\ \varepsilon_y \\ \gamma_{xy}/2 \end{bmatrix} = \begin{bmatrix} c^2 & s^2 & 2sc \\ s^2 & c^2 & -2sc \\ -sc & sc & c^2 - s^2 \end{bmatrix} \begin{bmatrix} \varepsilon_x \\ \varepsilon_y \\ \gamma_{xy}/2 \end{bmatrix}, \quad (2.5)$$

where  $c = \cos\theta$  and  $s = \sin\theta$ .

Equation (2.5) can be rewritten as

$$\begin{bmatrix} \varepsilon_1 \\ \varepsilon_2 \\ \gamma_{12} \end{bmatrix} = [R][T][R]^{-1} \begin{bmatrix} \varepsilon_x \\ \varepsilon_y \\ \gamma_{xy} \end{bmatrix}, \quad (2.6)$$

where  $[R]$  is the Reuter matrix and is defined as

$$[R] = \begin{bmatrix} 1 & 0 & 0 \\ 0 & 1 & 0 \\ 0 & 0 & 2 \end{bmatrix}. \quad (2.7)$$

Substituting (2.2) and (2.6) into equation (2.4), one can obtain

$$\begin{bmatrix} \sigma_x \\ \sigma_y \\ \tau_{xy} \end{bmatrix} = [T]^{-1} [Q][R][T][R]^{-1} \begin{bmatrix} \varepsilon_x \\ \varepsilon_y \\ \gamma_{xy} \end{bmatrix} = [\bar{Q}] \begin{bmatrix} \varepsilon_x \\ \varepsilon_y \\ \gamma_{xy} \end{bmatrix}, \quad (2.8)$$



where  $\bar{Q}_{ij}$  are given as

$$\begin{aligned}
 \bar{Q}_{11} &= Q_{11}c^4 + Q_{22}s^4 + 2(Q_{12} + 2Q_{66})s^2c^2, \\
 \bar{Q}_{12} &= (Q_{11} + Q_{22} - 4Q_{66})s^2c^2 + Q_{12}(c^4 + s^4), \\
 \bar{Q}_{22} &= Q_{11}s^4 + Q_{22}c^4 + 2(Q_{12} + 2Q_{66})s^2c^2, \\
 \bar{Q}_{16} &= (Q_{11} - Q_{12} - 2Q_{66})c^3s - (Q_{22} - Q_{12} - 2Q_{66})s^3c, \\
 \bar{Q}_{26} &= (Q_{11} - Q_{12} - 2Q_{66})cs^3 - (Q_{22} - Q_{12} - 2Q_{66})c^3s, \\
 \bar{Q}_{66} &= (Q_{11} + Q_{22} - 2Q_{12} - 2Q_{66})s^2c^2 + Q_{66}(c^4 + s^4).
 \end{aligned} \tag{2.9}$$

#### 2.2.4 Stress-strain relationships for a laminate

As shown in Figure 2-4, several laminae bonded together form a laminate. A real structure generally is a laminate structure, not a single lamina only. This is because a lamina is usually very thin (in the order of 0.125mm), which limits its capacity to withstand a realistic load. On the other hand, a unidirectional lamina is very weak in its transverse direction. Even if several unidirectional laminae stacked together in the same direction, it is still only suitable for unidirectional loading. Therefore, it is desirable to have laminae in different directions to meet different loading conditions. To optimize the cost and materials used, one need to understand the mechanical behavior of the laminate, which is related to the material properties of each single lamina, ply angle, and stacking sequence.



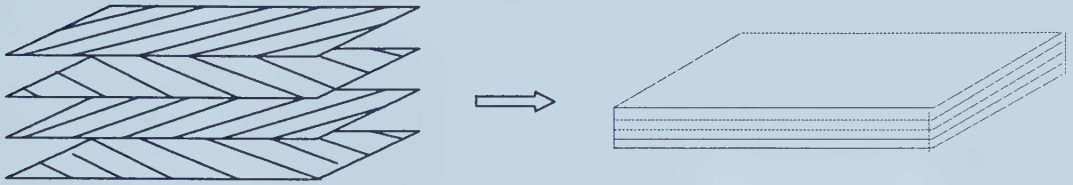


Figure 2-4 A laminate consists of 4 laminae

Classical laminate theory is the one that is most often used when analyzing the mechanical properties of a laminate. In the classical laminate theory, the following assumptions are made:

- The laminate is very thin and is under plane stress state.
- A straight line perpendicular to the middle-plane of laminate remains straight and perpendicular to the middle-plane during deformation.
- Displacements are small in comparison to the thickness of the laminate.
- Each lamina is orthotropic elastic and perfect bonding between neighboring laminae.

Based on the above assumptions the strains at any point along the thickness of a laminate can be related to the mid-plane deformation as

$$\begin{bmatrix} \varepsilon_x \\ \varepsilon_y \\ \gamma_{xy} \end{bmatrix} = \begin{bmatrix} \varepsilon_x^0 \\ \varepsilon_y^0 \\ \gamma_{xy}^0 \end{bmatrix} + z \begin{bmatrix} \kappa_x \\ \kappa_y \\ \kappa_{xy} \end{bmatrix}, \quad (2.10)$$

where  $\begin{bmatrix} \varepsilon_x^0 & \varepsilon_y^0 & \gamma_{xy}^0 \end{bmatrix}^T$  are the mid-plane strains, and  $\begin{bmatrix} \kappa_x & \kappa_y & \kappa_{xy} \end{bmatrix}^T$  are the mid-plane curvatures.





Substituting equation (2.10) into equation (2.8), the stresses for each lamina can be calculated as

$$\begin{bmatrix} \sigma_x \\ \sigma_y \\ \tau_{xy} \end{bmatrix} = [\bar{Q}] \begin{bmatrix} \varepsilon_x \\ \varepsilon_y \\ \gamma_{xy} \end{bmatrix} = [\bar{Q}] \begin{bmatrix} \varepsilon_x^0 \\ \varepsilon_y^0 \\ \gamma_{xy}^0 \end{bmatrix} + z [\bar{Q}] \begin{bmatrix} \kappa_x \\ \kappa_y \\ \kappa_{xy} \end{bmatrix}. \quad (2.11)$$

The next step is to find out the mid-plane strains and mid-plane curvatures when known loads are applied. To accomplish this, consider a laminate made of  $n$  plies, each ply have a thickness of  $t_k$ , and establish a coordinate system as shown in Figure 2-5.

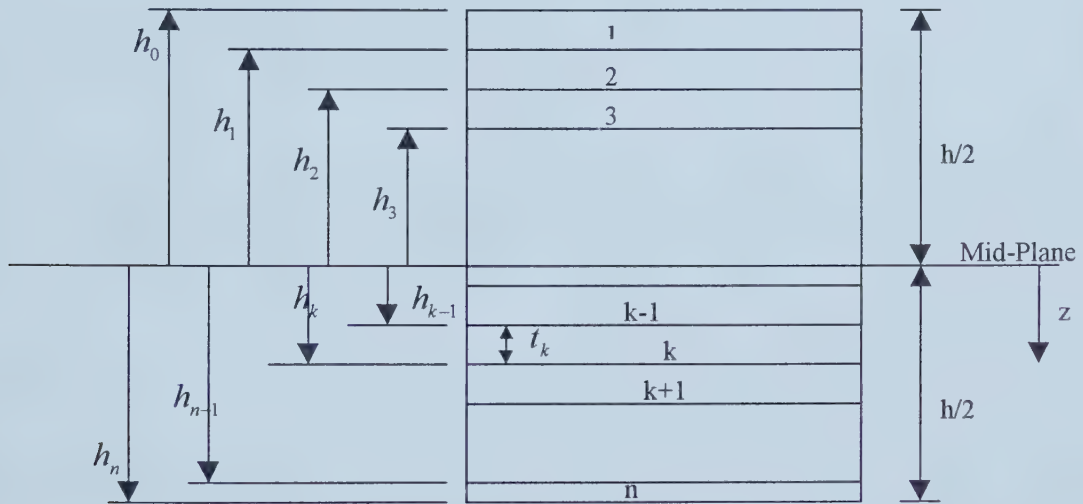


Figure 2-5 Coordinate locations of plies in a laminate [17]

The resultant forces and moments can be obtained by doing integration along the thickness based on the stresses in each lamina, which can be written as

$$\begin{bmatrix} N_x \\ N_y \\ N_{xy} \end{bmatrix} = \int_{-h/2}^{h/2} \begin{bmatrix} \sigma_x \\ \sigma_y \\ \tau_{xy} \end{bmatrix} dz = \sum_{k=1}^n \int_{h_{k-1}}^{h_k} \begin{bmatrix} \sigma_x \\ \sigma_y \\ \tau_{xy} \end{bmatrix} dz, \quad (2.12a)$$



$$\begin{bmatrix} M_x \\ M_y \\ M_{xy} \end{bmatrix} = \int_{-h/2}^{h/2} \begin{bmatrix} \sigma_x \\ \sigma_y \\ \tau_{xy} \end{bmatrix} z dz = \sum_{k=1}^n \int_{h_{k-1}}^{h_k} \begin{bmatrix} \sigma_x \\ \sigma_y \\ \tau_{xy} \end{bmatrix} z dz, \quad (2.12b)$$

where  $N_x$  and  $N_y$  are the normal force per unit length,  $N_{xy}$  is the shear force per unit length,  $M_x$  and  $M_y$  are the bending moments per unit length, and  $M_{xy}$  is the twisting moments per unit length.

Substituting equation (2.11) into equation (2.12), and the resultant forces and moments can be rewritten in terms of the mid-plane strains and curvatures:

$$\begin{bmatrix} N_x \\ N_y \\ N_{xy} \end{bmatrix} = \left[ \sum_{k=1}^n [\bar{Q}]_k \int_{h_{k-1}}^{h_k} dz \right] \begin{bmatrix} \varepsilon_x^0 \\ \varepsilon_y^0 \\ \gamma_{xy}^0 \end{bmatrix} + \left[ \sum_{k=1}^n [\bar{Q}]_k \int_{h_{k-1}}^{h_k} z dz \right] \begin{bmatrix} \kappa_x \\ \kappa_y \\ \kappa_{xy} \end{bmatrix} = [A] \begin{bmatrix} \varepsilon_x^0 \\ \varepsilon_y^0 \\ \gamma_{xy}^0 \end{bmatrix} + [B] \begin{bmatrix} \kappa_x \\ \kappa_y \\ \kappa_{xy} \end{bmatrix}, \quad (2.13a)$$

$$\begin{bmatrix} M_x \\ M_y \\ M_{xy} \end{bmatrix} = \left[ \sum_{k=1}^n [\bar{Q}]_k \int_{h_{k-1}}^{h_k} z dz \right] \begin{bmatrix} \varepsilon_x^0 \\ \varepsilon_y^0 \\ \gamma_{xy}^0 \end{bmatrix} + \left[ \sum_{k=1}^n [\bar{Q}]_k \int_{h_{k-1}}^{h_k} z^2 dz \right] \begin{bmatrix} \kappa_x \\ \kappa_y \\ \kappa_{xy} \end{bmatrix} = [B] \begin{bmatrix} \varepsilon_x^0 \\ \varepsilon_y^0 \\ \gamma_{xy}^0 \end{bmatrix} + [D] \begin{bmatrix} \kappa_x \\ \kappa_y \\ \kappa_{xy} \end{bmatrix}, \quad (2.13b)$$

where

$$[A] = \sum_{k=1}^n [\bar{Q}]_k (h_k - h_{k-1}), \quad (2.14a)$$

$$[B] = \sum_{k=1}^n [\bar{Q}]_k \frac{1}{2} (h_k^2 - h_{k-1}^2), \quad (2.14b)$$

$$[D] = \sum_{k=1}^n [\bar{Q}]_k \frac{1}{3} (h_k^3 - h_{k-1}^3). \quad (2.14c)$$

The matrices  $[A]$ ,  $[B]$  and  $[D]$  are called the extensional, coupling and bending stiffness matrices, respectively.



In the current study, the laminate is taken to be angle ply  $[\pm\theta]$ , and it is subjected to biaxial in-plane loading and the composite wrap is axisymmetric. Assuming that each ply has the same thickness, then from (2.14), the following results can be obtained,

$$[A] = h \begin{bmatrix} \bar{Q}_{11} & \bar{Q}_{12} & 0 \\ \bar{Q}_{12} & \bar{Q}_{22} & 0 \\ 0 & 0 & \bar{Q}_{66} \end{bmatrix}, [B] = \begin{bmatrix} B_{11} & B_{12} & B_{13} \\ B_{12} & B_{22} & B_{23} \\ B_{13} & B_{23} & B_{66} \end{bmatrix}, [D] = \begin{bmatrix} D_{11} & D_{12} & 0 \\ D_{12} & D_{22} & 0 \\ 0 & 0 & D_{66} \end{bmatrix}. \quad (2.15)$$

The composite wrap here is axisymmetric, and this prevents the cylindrical composite wrap from undergoing any change of curvature, which means that  $[\kappa] = 0$ .

Hence, for the angle ply laminate, and in the current study, (2.13) could be simplified as

$$\begin{bmatrix} N_x \\ N_y \\ N_{xy} \end{bmatrix} = h \begin{bmatrix} \bar{Q}_{11} & \bar{Q}_{12} & 0 \\ \bar{Q}_{12} & \bar{Q}_{22} & 0 \\ 0 & 0 & \bar{Q}_{66} \end{bmatrix} \begin{bmatrix} \varepsilon_x^0 \\ \varepsilon_y^0 \\ \gamma_{xy}^0 \end{bmatrix}, \quad (2.16a)$$

$$\begin{bmatrix} M_x \\ M_y \\ M_{xy} \end{bmatrix} = \begin{bmatrix} B_{11} & B_{12} & B_{13} \\ B_{12} & B_{22} & B_{23} \\ B_{13} & B_{23} & B_{66} \end{bmatrix} \begin{bmatrix} \varepsilon_x^0 \\ \varepsilon_y^0 \\ \gamma_{xy}^0 \end{bmatrix}. \quad (2.16b)$$

For a symmetric laminate, the coupling matrix  $[B] = 0$ . In the current study, the composite laminate is an angle ply, and  $[B] \neq 0$ . However, to make this a symmetric laminate requires only an additional layer of lamina, i.e. from  $[\pm\theta]_n$  to  $[(\pm\theta)_n, +\theta]$ . Thus, it can be further assumed that the coupling matrix  $[B] = 0$  and this leads to

$$\begin{bmatrix} M_x & M_y & M_{xy} \end{bmatrix}^T = \{0\}. \quad (2.17)$$





From equation (2.10) and the fact that  $[\kappa] = 0$ , the following relationship can be deduced:

$[\varepsilon_x \quad \varepsilon_y \quad \gamma_{xy}]^T = [\varepsilon_x^0 \quad \varepsilon_y^0 \quad \gamma_{xy}^0]^T$ . The relationship between the average stresses and the resultant forces can be written as

$$[\sigma_x \quad \sigma_y \quad \tau_{xy}]^T = [N_x \quad N_y \quad N_{xy}]^T / h. \quad (2.18)$$

Substituting equation (2.18) into equation (2.16), and equation (2.16) can be rewritten as

$$\begin{bmatrix} \sigma_x \\ \sigma_y \\ \tau_{xy} \end{bmatrix} = \begin{bmatrix} \bar{Q}_{11} & \bar{Q}_{12} & 0 \\ \bar{Q}_{12} & \bar{Q}_{22} & 0 \\ 0 & 0 & \bar{Q}_{66} \end{bmatrix} \begin{bmatrix} \varepsilon_x \\ \varepsilon_y \\ \gamma_{xy} \end{bmatrix}. \quad (2.19)$$

This is the stress-strain relationship for the composite wrap, which will be used in the later chapters to analyze the response of the integrated hybrid composite pipe.

## 2.3 Advanced constitutive model for the metallic liner

### 2.3.1 Introduction of Ellyin and Xia's model

Metals and alloys are very important engineering materials and they are widely used in industries. The demand for appropriate constitutive laws to simulate their behavior is critical to providing reliable solutions for existing engineering problems. Experimental observations indicate that metals have complex plastic behavior, and the classical plastic constitutive models are inadequate for simulating these behaviors. Ellyin and Xia [14, 15, and 16] have developed a rate independent elastic-plastic constitutive model (Figure 2-6), which is comprehensive and relatively simple to implement.



In this model, three hypersurfaces are defined: a yield surface, a stress memory surface and a strain memory surface.

The yield surface is the locus of the elastic region, and it can be expressed as

$$\varphi_y = f_y(\sigma_{ij} - \alpha_{ij}) - \sigma_y^2 = 0, \quad (2.20)$$

where  $\alpha_{ij}$  specifies the location of the center of the yield surface, and  $\sigma_y$  (yield stress) defines the radius of the yield surface. For von-Mises materials such as metal,

$$f_y = \frac{3}{2} \bar{s}_{ij} \bar{s}_{ij}, \quad (2.21)$$

where  $\bar{s}_{ij} = \bar{\sigma}_{ij} - \delta_{ij} \bar{\sigma}_{kk} / 3$  and  $\bar{\sigma}_{ij} = \sigma_{ij} - \alpha_{ij}$ .

The stress memory surface defines the maximum stress experienced during loading history. In the current study, the center of this surface locates at the origin, and the radius of this surface is determined by the maximum equivalent stress experienced during previous loading history,

$$\varphi_m = \frac{3}{2} s_{ij} s_{ij} - \sigma_{eff, \max}^2 = 0, \quad (2.22)$$

where  $s_{ij} = \sigma_{ij} - \frac{1}{3} \delta_{ij} \sigma_{kk}$ .

The strain memory surface specifies the maximum equivalent strain encountered during previous loading history:

$$\varphi_m = \frac{2}{3} e_{ij} e_{ij} - \varepsilon_{eff, \max}^2 = 0, \quad (2.23)$$

where  $e_{ij} = \varepsilon_{ij} - \frac{1}{3} \delta_{ij} \varepsilon_{kk}$ .



This model also introduced two types of plastic loading: one is termed monotonic loading (ML), and the other is termed reloading (RL). In the monotonic loading case, the stress memory surface expands with the movement of the yielding surface, and these two surfaces remain tangent to each other at the current stress point. For the reloading case, after elastic unloading, plastic deformation takes place again. During this stage, the yield surface is within the memory surface, and the memory surface remains unchanged. For different plastic loading cases, the evolution rule of the yield surface and the calculation of tangent modulus are also different.

In the current study, this constitutive model is adopted for the metallic liner, and the detailed analyses are given in the following sections.

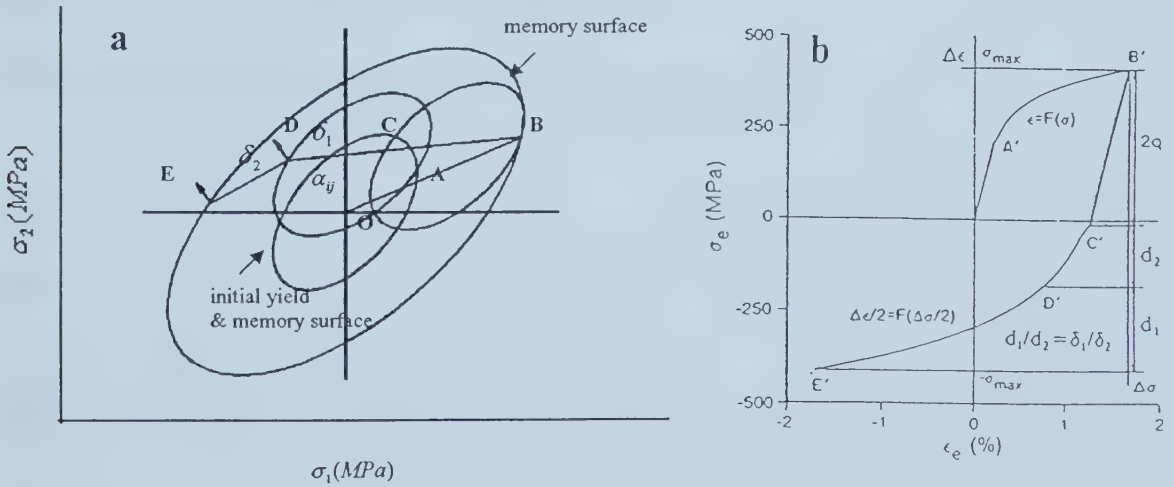


Figure 2-6 Constitutive model of the metal [14]

### 2.3.2 Stress-strain relation

It can be assumed that the total strain increment can be decomposed into elastic and plastic parts, i.e.





$$d\varepsilon_{ij} = d\varepsilon_{ij}^e + d\varepsilon_{ij}^p. \quad (2.24)$$

Generalized Hooke's law determines the relationship between the increment of elastic strain and the stress increment

$$d\varepsilon_{ij}^e = \frac{1}{E}[(1+\nu)\delta_{ik}\delta_{jl} - \nu\delta_{ij}\delta_{kl}]d\sigma_{kl}. \quad (2.25)$$

Since the metallic liner is under biaxial plane stress state, the elastic stress-strain relationship of it can be simplified as

$$\begin{bmatrix} \varepsilon_x^e \\ \varepsilon_y^e \end{bmatrix} = \begin{bmatrix} \frac{1}{E_{s1}} & -\frac{\nu}{E_{s1}} \\ -\frac{\nu}{E_{s1}} & \frac{1}{E_{s1}} \end{bmatrix} \begin{bmatrix} \sigma_x \\ \sigma_y \end{bmatrix}, \quad (2.26)$$

where  $E_{s1} = E$ , the Young's modulus of the metal.

The increment of plastic strain is determined by the flow rule

$$d\varepsilon_{ij}^p = cg \frac{\partial f_y}{\partial \sigma_{ij}} \frac{\partial f_y}{\partial \sigma_{kl}} d\sigma_{kl}, \quad (2.27)$$

where

$$c = 1 \quad \text{for} \quad \frac{\partial f_y}{\partial \sigma_{kl}} d\sigma_{kl} \geq 0 \quad \text{and} \quad f_y(\sigma_{ij} - \alpha_{ij}) - \sigma_y^2 = 0,$$

$$c = 0 \quad \text{for} \quad \frac{\partial f_y}{\partial \sigma_{kl}} d\sigma_{kl} < 0 \quad \text{or} \quad f_y(\sigma_{ij} - \alpha_{ij}) - \sigma_y^2 < 0.$$

For von-Mises material that is in a plane-stress state,

$$f_y = \bar{\sigma}_x^2 + \bar{\sigma}_y^2 - \bar{\sigma}_x \bar{\sigma}_y + 3\bar{\tau}_{xy}^2. \quad (2.28)$$



The metallic liner in the current study is assumed to be a multi-linear kinematic hardening material, and for multi-linear hardening materials,

$$g = \frac{1}{4\sigma_y^2} \left( \frac{1}{E_t} - \frac{1}{E_{s1}} \right), \quad (2.29)$$

where  $E_t$  is the tangent modulus of the metal.

Equation (2.27) is simplified as

$$\begin{bmatrix} d\epsilon_x^p \\ d\epsilon_y^p \\ d\epsilon_{xy}^p \end{bmatrix} = g \begin{bmatrix} (2\bar{\sigma}_x - \bar{\sigma}_y)^2 & (2\bar{\sigma}_x - \bar{\sigma}_y)(2\bar{\sigma}_y - \bar{\sigma}_x) & 6(2\bar{\sigma}_x - \bar{\sigma}_y)\bar{\tau}_{xy} \\ (2\bar{\sigma}_x - \bar{\sigma}_y)(2\bar{\sigma}_y - \bar{\sigma}_x) & (2\bar{\sigma}_y - \bar{\sigma}_x)^2 & 6(2\bar{\sigma}_x - \bar{\sigma}_y)\bar{\tau}_{xy} \\ 6(2\bar{\sigma}_x - \bar{\sigma}_y)\bar{\tau}_{xy} & 6(2\bar{\sigma}_y - \bar{\sigma}_x)\bar{\tau}_{xy} & 36\bar{\tau}_{xy}^2 \end{bmatrix} \begin{bmatrix} d\sigma_x \\ d\sigma_y \\ d\tau_{xy} \end{bmatrix}. \quad (2.30)$$

Further considering the metallic liner to be in biaxial loading condition without shear stress due to the axisymmetry of the pipe, then the above equation can be simplified as

$$\begin{bmatrix} d\epsilon_x^p \\ d\epsilon_y^p \end{bmatrix} = g \begin{bmatrix} (2\bar{\sigma}_x - \bar{\sigma}_y)^2 & (2\bar{\sigma}_x - \bar{\sigma}_y)(2\bar{\sigma}_y - \bar{\sigma}_x) \\ (2\bar{\sigma}_x - \bar{\sigma}_y)(2\bar{\sigma}_y - \bar{\sigma}_x) & (2\bar{\sigma}_y - \bar{\sigma}_x)^2 \end{bmatrix} \begin{bmatrix} d\sigma_x \\ d\sigma_y \end{bmatrix}. \quad (2.31)$$

The elastic part of the stress-strain increment relationship of the metallic liner can be written as

$$\begin{bmatrix} d\epsilon_x^e \\ d\epsilon_y^e \end{bmatrix} = \begin{bmatrix} 1/E_{s1} & -\nu/E_{s1} \\ -\nu/E_{s1} & 1/E_{s1} \end{bmatrix} \begin{bmatrix} d\sigma_x \\ d\sigma_y \end{bmatrix}. \quad (2.32)$$

Thus, the increment stress-strain relationship of the metallic liner can be written as

$$\begin{bmatrix} d\epsilon_x \\ d\epsilon_y \end{bmatrix} = \begin{bmatrix} g(2\bar{\sigma}_x - \bar{\sigma}_y)^2 + 1/E_{s1} & g(2\bar{\sigma}_x - \bar{\sigma}_y)(2\bar{\sigma}_y - \bar{\sigma}_x) - \nu/E_{s1} \\ g(2\bar{\sigma}_x - \bar{\sigma}_y)(2\bar{\sigma}_y - \bar{\sigma}_x) - \nu/E_{s1} & g(2\bar{\sigma}_y - \bar{\sigma}_x)^2 + 1/E_{s1} \end{bmatrix} \begin{bmatrix} d\sigma_x \\ d\sigma_y \end{bmatrix} \quad (2.33)$$



### 2.3.3 Evolution of the yield surface

For kinematic hardening materials, a translation tensor  $\alpha_{ij}$  is introduced to describe the rigid translation of the initial yield surface  $\phi(\sigma_{ij}) = 0$ . The translation tensor  $\alpha_{ij}$  prescribes the position of the center of the yield surface. The consistency rule (the current stress point is on the yield surface during plastic loading) requires that

$$d\phi(\sigma_{ij} - \alpha_{ij}) = 0. \quad (2.34)$$

However, the dependence of the translation tensor  $\alpha_{ij}$  on plastic strains  $\varepsilon_{ij}^p$  or stress  $\sigma_{ij}$  throughout the plastic loading process also needs to be determined so that the above rule could work effectively. Melan [18] suggested two definitions (original articles can be found at [19] and [20]) for the  $\alpha_{ij}$ , namely

$$d\alpha_{ij} = cd\varepsilon_{ij}^p, \quad (2.35)$$

or

$$d\alpha_{ij} = d\sigma_{ij}. \quad (2.36)$$

The first one is limited to the linear plastic hardening, while the latter may be used for an arbitrary nonlinear hardening material. Ishlinsky [18] (original article can be found at [21]) and Prager [22,23] later developed the first one. Therefore, it is generally called the Mellan-Ishlinsky-Prager (MIP) kinematic hardening rule, or simply, the Prager hardening rule. Ziegler [24] proposed a modified translation rule that better fits the experimental results. The modified translation rule assumes that the yield surface





translates in the direction of the lines connecting the current center of the yield surface to the current stress point (or, in other words, in the direction of  $\sigma_{ij} - \alpha_{ij}$ ),

$$d\alpha_{ij} = (\sigma_{ij} - \alpha_{ij})d\mu. \quad (2.37)$$

Here  $d\mu$  is a positive factor. Based on consistency condition

$$d\varphi = \frac{\partial \varphi}{\partial \sigma_{kl}} d\sigma_{kl} \big|_{\alpha_{kl}=\text{const}} + \frac{\partial \varphi}{\partial \alpha_{kl}} d\alpha_{kl} \big|_{\sigma_{kl}=\text{const}} = 0, \quad (2.38)$$

$d\mu$  can be determined as

$$d\mu = \frac{(\partial \varphi / \partial \sigma_{ij}) d\sigma_{ij}}{(\partial \varphi / \partial \sigma_{ij})(\sigma_{ij} - \alpha_{ij})}. \quad (2.39)$$

Once  $d\mu$  is known, the movement of the center of the yield surface can be obtained based on the current stress states.

Ellyin [25] and Ellyin and Wu [26] suggested an evolution rule suitable to reloading paths. After unloading, if the reloading path is still within the memory surface, the motion of the yield surface is defined as

$$d\alpha_{ij} = d\mu(\sigma_{ij}^m - \sigma_{ij}^y), \quad (2.40)$$

where  $\sigma_{ij}^y$  is the current stress point  $D$ ,  $\sigma_{ij}^m$  is a stress point on the stress memory surface,  $E$ , whose exterior normal is parallel to the outward normal at point  $\sigma_{ij}^y$  (Figure 2-6a ). This relationship guarantees that the yield surface and the stress memory surface will be tangent at the current stress point when the former approaches the latter.



The proportionality factor  $d\mu$  in equation (2.40) is determined by a consistency condition, i.e. the loading point is kept on the yield surface during plastic deformation, then

$$d\phi_y = \frac{\partial f_y}{\partial \sigma_{ij}} (d\sigma_{ij} - d\alpha_{ij}) - 2\sigma_y d\sigma_y = 0. \quad (2.41)$$

Substituting the above to (2.40) yields

$$d\mu = \frac{\frac{\partial f_y}{\partial \sigma_{ij}} d\sigma_{ij} - 2\sigma_y d\sigma_y}{(\sigma_{ij}^m - \sigma_{ij}^y) \frac{\partial f_y}{\partial \sigma_{kl}}}. \quad (2.42)$$

Therefore the motions of the yield surface are completely determined for each loading case.

For the monotonic loading (ML) case, an evolution equation that has the same form as equation (2.40) has been introduced, i.e.

$$d\alpha_{ij} = d\mu(\sigma_{ij}^{\text{lim}} - \sigma_{ij}^y) \quad (2.43a)$$

$$\sigma_{ij}^{\text{lim}} = \frac{R_{\text{lim}}}{\sigma_y} (\sigma_{ij}^y - \alpha_{ij}) \quad (2.43b)$$

where  $R_{\text{lim}}$  is a material constant. The above equation is equivalent to introduce another von-Mises surface with the center at origin and radius as  $R_{\text{lim}}$ . When  $R_{\text{lim}}$  is much larger than  $\sigma_y$ , then Ziegler's rule is recovered.

In the current application, for the ML loading case, Ziegler's rule is adopted ( $R_{\text{lim}} \gg \sigma_y$ ), and for RL case, equation (2.40) is used.



### 2.3.4 Determination of tangent modulus, $E_t$

The calculation of tangent modulus  $E_t$  is different for the monotonic loading and the reloading cases. For the monotonic loading, the tangent modulus is simply a function of the equivalent stress, and this function can be determined from the stress-strain curve of metal under uniaxial loading. For the reloading case, the tangent modulus no longer depends only on equivalent stress. Hence a ratio is introduced for any given point in multiaxial stress space, which is written as

$$r = \delta_1 / \delta_2, \quad (2.44)$$

here  $\delta_1$  is the distance between the loading point  $D$  (Figure 2-6a) and a corresponding point  $E$  on the stress memory surface. The exterior normal of point  $E$  is parallel to that of point  $D$ .  $\delta_2$  is defined as the distance between the point of the onset of plastic flow  $C$  and point  $D$ . The distance between any two points in the stress space is defined as

$$d = [(s_{ij}^{(2)} - s_{ij}^{(1)})(s_{ij}^{(2)} - s_{ij}^{(1)})]^{1/2}, \quad (2.45)$$

where  $s_{ij}^{(1)}$  and  $s_{ij}^{(2)}$  are deviatoric stress values of the two stress points, respectively.

Once the ratio  $r$  is determined for any point  $D$  in the stress space, there will be a corresponding point  $D'$  in the reversed uniaxial curve  $B'C'E'$  (Figure 2-6b). The relationship of point  $D$  and point  $D'$  is defined as

$$\delta_1 / \delta_2 = d_1 / d_2. \quad (2.46)$$

The uniaxial unloading curve can be related to the loading curve as

$$\Delta \varepsilon / 2 = F(\Delta \sigma / 2). \quad (2.47)$$



From the above equation, the tangent modulus can be determined for the reloading case.

## **2.4 Integral analysis model for the hybrid composite/metal pipe**

### **2.4.1 Basic assumptions**

To analyze the stress-strain response of a hybrid composite pipe, two assumptions are made:

First, the thickness of the hybrid composite pipe is relatively small compared to the diameter; thus it is reasonable to treat it as a thin-walled cylinder. This means that an average radius is used to describe the size of the hybrid composite pipe. In all, three parameters are used to represent the geometry of the hybrid composite pipe, the average radius  $r$ , the thickness of the metallic liner  $t_s$  and the thickness of the composite wrap  $t_c$ .

Second, it is assumed that there is perfect bonding between the metallic liner and the composite wrap. This gives the compatibility conditions of the hybrid composite pipe. This means that both the hoop and axial strains are the same for both the metallic liner and the composite wrap, i.e.,  $\varepsilon_{h,s} = \varepsilon_{h,c}$  and  $\varepsilon_{a,s} = \varepsilon_{a,c}$ .

### **2.4.2 Load analysis**

While transporting high-pressure hydrocarbons, the internal pressure is the major load to which the hybrid composite pipe is subjected. Axial loads can be introduced during installation of pipelines. Pipelines connecting a pressure vessel also have a loading





condition similar to that of a sealed cylinder (2H:1A). Figure 2-7 gives an illustration to the generalized loading conditions of a hybrid composite pipe.

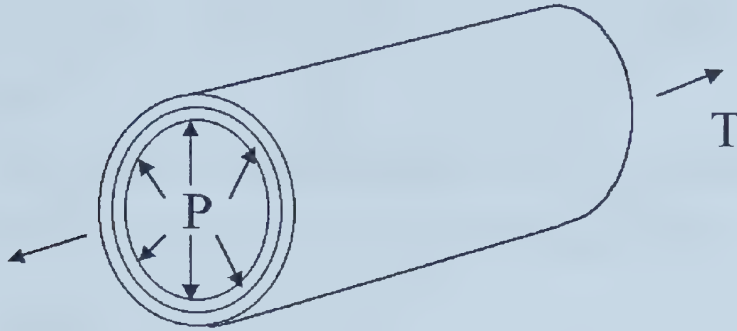


Figure 2-7 Loading status of the hybrid composite pipe

To account for different loading conditions, a factor  $\kappa$  is introduced to relate the total axial tension to the internal pressure. The axial tension is defined as

$$T = \kappa \pi r^2 P \quad . \quad (2.48)$$

Different values of the parameter  $\kappa$  stand for different loading conditions. For example,  $\kappa = 0$  produces pure hoop loading condition, which corresponds to the hybrid composite pipe subjected to internal pressure only. Another typical example is that  $\kappa = 1$ , which corresponds to the stress state of a sealed cylinder.

In the current study, the known parameters include:

- 1) Pipe geometry: average pipe radius  $r$ , thickness of metallic liner  $t_s$  and thickness of composite wrap  $t_c$ .
- 2) Material properties of the metallic liner:  
Poisson's ratio  $\nu$ .



Uniaxial stress-strain curve represented by certain amount of stress/strain points on the curve. The first point is at the origin, and the second point is the yield point.

The elastic modulus  $E_s$  is equal to the slope of the line between the two points.

- 3) Material properties of the composite wrap, i.e. the elastic constants and the ultimate strengths of the unidirectional lamina, and the ply angle of the laminate.

The loading history of the hybrid composite pipe can be divided into four stages, the elastic stage, the monotonic plastic stage, the elastic unloading and plastic reloading stage. Detailed analyses for each stage are given in the following sections.

### 2.4.3 Elastic stage

Referring to Figure 2-6a, this stage corresponds to path  $OA$ . This path stands for the elastic stage of the metal, and  $A$  is a point on the yield surface. Within this stage, the metallic liner is elastic and the stress-strain relationship of it can be described by the Hooke's law.

At the initial yield point, which corresponds to the point  $A$  in Figure 2-6a, the hybrid composite pipe is subjected to initial yield pressure  $P_y$  and axial tension  $T = \kappa \pi r^2 P_y$ .

To obtain the stress-strain relationship for the whole hybrid composite pipe, the hybrid composite pipe is decomposed into two separate parts, the metallic liner and the composite wrap. Figure 2-8 gives the free-body diagrams of them.



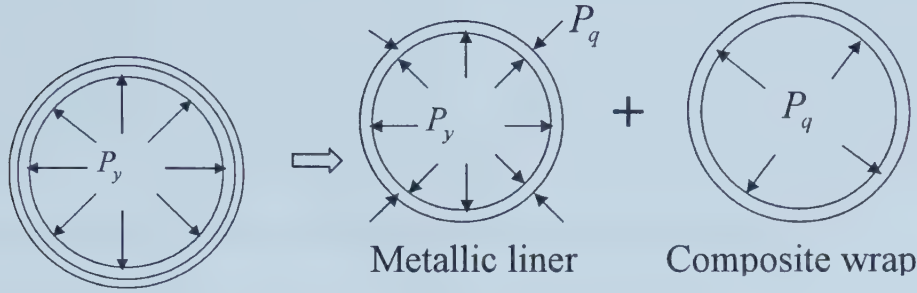


Figure 2-8 Free-body diagrams for the metallic liner and composite wrap

Assuming that the pressure between the metallic liner and the composite wrap is  $P_q$ , the total axial tension is  $T = \kappa\pi r^2 P_y$ , and the axial tension applied on the metallic liner is  $T_s$ , thus the axial tension applied on the composite wrap is  $T_c = T - T_s$ .

The hoop stress in the metallic liner is

$$\sigma_{hs} = (P_y - P_q)r / t_s, \quad (2.49a)$$

and the axial stress in the metallic liner is

$$\sigma_{as} = T_s / (2\pi r t_s). \quad (2.49b)$$

The hoop stress in the composite wrap can be written as

$$\sigma_{hc} = P_q r / t_c, \quad (2.50a)$$

and the axial stress in the composite wrap is

$$\sigma_{ac} = (T - T_s) / (2\pi r t_c). \quad (2.50b)$$

Based on the assumption that there is perfect bonding between the metallic liner and composite wrap, the strains are the same for the metallic liner and the composite wrap. The stress-strain relationship in the metallic liner can be determined as follows.



$$\begin{bmatrix} \varepsilon_a \\ \varepsilon_h \end{bmatrix} = \begin{bmatrix} \frac{1}{E_{s1}} & -\frac{\nu}{E_{s1}} \\ -\frac{\nu}{E_{s1}} & \frac{1}{E_{s1}} \end{bmatrix} \begin{bmatrix} \sigma_{as} \\ \sigma_{hs} \end{bmatrix}, \quad (2.51a)$$

The stress-strain increment relationship in the composite wrap is

$$\begin{bmatrix} \Delta\sigma_{ac} \\ \Delta\sigma_{hc} \end{bmatrix} = \begin{bmatrix} \bar{Q}_{11} & \bar{Q}_{12} \\ \bar{Q}_{12} & \bar{Q}_{22} \end{bmatrix} \begin{bmatrix} \Delta\varepsilon_a \\ \Delta\varepsilon_h \end{bmatrix}. \quad (2.51b)$$

The von-Mises yield criterion of the metallic liner is

$$\sqrt{\sigma_{hs}^2 + \sigma_{as}^2 - \sigma_{hs}\sigma_{as}} = \sigma_y. \quad (2.52)$$

Substituting equation (2.50) and (2.51a) into equation (2.51b) one obtains:

$$P_q r / t_c = a_1 \sigma_{hs} + a_2 \sigma_{as}, \quad (2.53a)$$

$$(T - T_s) / (2\pi r t_c) = b_1 \sigma_{hs} + b_2 \sigma_{as}. \quad (2.53b)$$

where

$$\begin{aligned} a_1 &= \bar{Q}_{22} / E_{s1} - \nu \bar{Q}_{12} / E_{s1}, & a_2 &= \bar{Q}_{12} / E_{s1} - \nu \bar{Q}_{22} / E_{s1}, \\ b_1 &= \bar{Q}_{12} / E_{s1} - \nu \bar{Q}_{11} / E_{s1}, & b_2 &= \bar{Q}_{11} / E_{s1} - \nu \bar{Q}_{12} / E_{s1}. \end{aligned} \quad (2.54)$$

Substituting (2.49) and  $T = \kappa \pi r^2 P_y$  into (2.53) and it yields

$$\begin{aligned} P_q c_1 + T_s c_2 &= P_y c_3 \\ P_q d_1 + T_s d_2 &= P_y d_3 \end{aligned} \quad (2.55)$$

where

$$\begin{aligned} c_1 &= r / t_c + a_1 r / t_s, & c_2 &= -a_2 / (2\pi r t_s), & c_3 &= a_1 r / t_s, \\ d_1 &= b_1 r / t_s, & d_2 &= -[1 / (2\pi r t_c) + b_2 / (2\pi r t_s)], & d_3 &= b_1 r / t_s - \kappa r / (2t_c). \end{aligned} \quad (2.56)$$





Solving (2.56) one can obtain

$$P_q = \frac{c_3 d_2 - d_3 c_2}{c_1 d_2 - d_1 c_2} P_y, \quad T_s = \frac{c_3 d_1 - d_3 c_1}{c_2 d_1 - d_2 c_1} P_y. \quad (2.57)$$

Substituting (2.57) into (2.49), one can obtain the stresses in the metallic liner as

$$\sigma_{hs} = e_1 P_y, \quad \sigma_{as} = e_2 P_y, \quad (2.58)$$

where

$$e_1 = \frac{r}{t_s} \left( 1 - \frac{c_3 d_2 - d_3 c_2}{c_1 d_2 - d_1 c_2} \right), \quad e_2 = \frac{1}{2\pi r t_s} \frac{c_3 d_1 - d_3 c_1}{c_2 d_1 - d_2 c_1}. \quad (2.59)$$

Substituting (2.59) into (2.51) one obtains

$$\sqrt{(e_1^2 + e_2^2 - e_1 e_2) P_y^2} = \sigma_y, \quad (2.60)$$

and thus the yield pressure is

$$P_y = \sigma_y / \sqrt{e_1^2 + e_2^2 - e_1 e_2}. \quad (2.61)$$

Now that  $P_y$  is known, by substituting it back into equations (2.57) and (2.51), respectively,  $\sigma_{hs}, \sigma_{as}, \sigma_{hc}, \sigma_{ac}, \varepsilon_h, \varepsilon_a$  can be obtained, and these parameters correspond to the values of stresses and strains at point  $A$  in Figure 2-6a.

At point  $A$ , the center of the yield surface center is at the origin, i.e.,  $\alpha_a = 0$  and  $\alpha_h = 0$ . The stresses at point  $A$  satisfy the von-Mises yield criteria

$$\sqrt{\sigma_{hs}^2 + \sigma_{as}^2 - \sigma_{hs} \sigma_{as}} = \sigma_y, \quad (2.62)$$

where  $(\sigma_{as}, \sigma_{hs})$  correspond to the stress state of the point  $A$  on the initial yield surface.



#### 2.4.4 Monotonic plastic loading stage

After the initial yielding, an increase in pressure will subject the metallic liner to the monotonic plastic loading stage. This stage corresponds to path  $AB$  in Figure 2-6a.

The metal is regarded as a multi-linear kinematic hardening material in this study. Its stress-strain relationship can be obtained from uniaxial test, i.e., Figure 2-9 gives a multi-linear stress-strain curve for the metal and  $oa$  is the elastic range, and  $a-b-c-d$  is the plastic range.

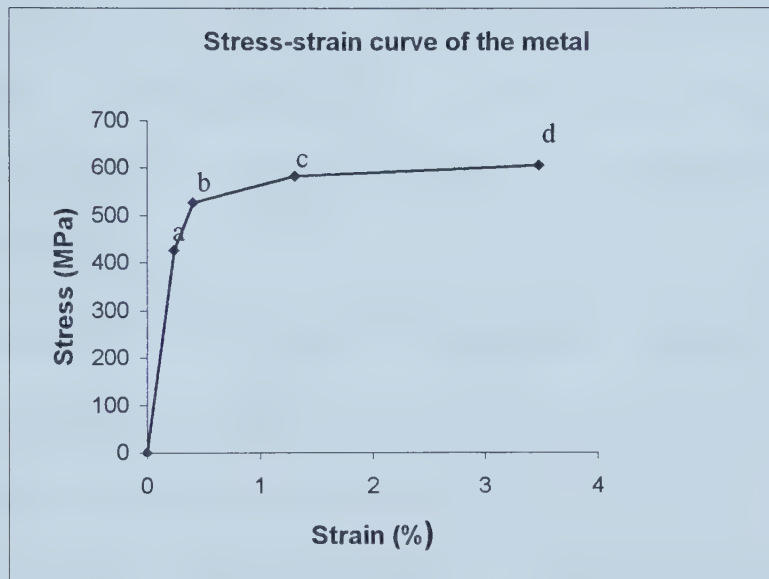


Figure 2-9 Multi-linear stress-strain curve of the metal

As discussed in the previous section, in the monotonic loading case, the tangent modulus is a function of the equivalent stress. For a multilinear hardening material, within each linear hardening part, the tangent modulus  $E_t$  is the same. It is only different



for each linear part. For example, in Figure 2-9, the tangent modulus for stage b-c

$$\text{is } E_t = \frac{\sigma_c - \sigma_b}{\varepsilon_c - \varepsilon_b}.$$

The criterion to enter another linear hardening stage, say, range  $bc$  in Figure 2-9 is

$$\sigma_b \leq \sqrt{\sigma_{hs}^2 + \sigma_{as}^2 - \sigma_{hs}\sigma_{as}} \leq \sigma_c, \quad (2.63)$$

where  $(\sigma_{hs}, \sigma_{as})$  stands for stress state of points on path  $AB$  in Figure 2-6, and  $\sigma_b$ ,  $\sigma_c$  stands for stress at points  $b$  and  $c$  in Figure 2-9.

Here we only discuss the calculation within the first linear plastic hardening part (range  $ab$  in Figure 2-9) after yielding, and the criterion to reach another linear range. This should suffice since the only difference for another linear plastic hardening part is in the value of tangent modulus  $E_t$ .

Increasing pressure to  $\Delta P + P_y$ , where  $\Delta P$  is the pressure increment, the stress and strain increment under  $\Delta P$  can be calculated and added to the previous stress and strain to obtain the current stress/strain state under  $\Delta P + P_y$ .

Assuming that the pressure increment between the metallic liner and the composite wrap is  $\Delta P_q$ , the total axial tension increment is  $\Delta T = \kappa \pi r^2 \Delta P$ , and the axial tension increment applied on the metallic liner is  $\Delta T_s$ , then the axial tension increment applied on the composite wrap is  $\Delta T_c = \Delta T - \Delta T_s$ .

The increment of hoop stress in the metallic liner is give by

$$\Delta \sigma_{hs} = (\Delta P - \Delta P_q) r / t_s. \quad (2.64a)$$



The increment of axial stress in the metallic liner is

$$\Delta\sigma_{as} = \Delta T_s / (2\pi r t_s). \quad (2.64b)$$

The increment of hoop stress in the composite wrap is

$$\Delta\sigma_{hc} = \Delta P_q r / t_c. \quad (2.65a)$$

The increment of axial stress in the composite wrap is

$$\Delta\sigma_{ac} = (\Delta T - \Delta T_s) / (2\pi r t_c). \quad (2.65b)$$

The stress-strain increment relationship of the metallic liner is

$$\begin{bmatrix} \Delta\varepsilon_a \\ \Delta\varepsilon_h \end{bmatrix} = \begin{bmatrix} g(2\sigma_a - \sigma_h)^2 + 1/E_{s1} & g(2\sigma_a - \sigma_h)(2\sigma_h - \sigma_a) - \nu/E_{s1} \\ g(2\sigma_a - \sigma_h)(2\sigma_h - \sigma_a) - \nu/E_{s1} & g(2\sigma_h - \sigma_a)^2 + 1/E_{s1} \end{bmatrix} \begin{bmatrix} \Delta\sigma_{as} \\ \Delta\sigma_{hs} \end{bmatrix} \quad (2.66)$$

where  $g = \frac{1}{4\sigma_y^2} \left( \frac{1}{E_t} - \frac{1}{E_0} \right)$  and  $(\sigma_a, \sigma_h)$  is the current stress state.

The stress-strain increment relationship of the composite wrap is

$$\begin{bmatrix} \Delta\sigma_{ac} \\ \Delta\sigma_{hc} \end{bmatrix} = \begin{bmatrix} \bar{Q}_{11} & \bar{Q}_{12} \\ \bar{Q}_{12} & \bar{Q}_{22} \end{bmatrix} \begin{bmatrix} \Delta\varepsilon_a \\ \Delta\varepsilon_h \end{bmatrix}. \quad (2.67)$$

The solution here is similar to that in the elastic stage with the only difference in stress-strain relationship for the metallic liner.

The final results are obtained as

$$\begin{aligned} \Delta\sigma_{hs} &= e_1' \Delta P, & \Delta\sigma_{as} &= e_2' \Delta P, \\ \Delta P_q &= \frac{c_3' d_2' - d_3' c_2'}{c_1' d_2' - d_1' c_2'} \Delta P, & \Delta T_s &= \frac{c_3' d_1' - d_3' c_1'}{c_2' d_1' - d_2' c_1'} \Delta P, \end{aligned} \quad (2.68)$$

$$\Delta\sigma_{hc} = \Delta P_q r / t_g, \quad \Delta\sigma_{ac} = (\Delta T - \Delta T_s) / (2\pi r t_c),$$





$$\Delta \varepsilon_h = ab1 * \Delta \sigma_{hs} - ab2 * \nu \Delta \sigma_{as},$$

$$\Delta \varepsilon_a = ab3 * \Delta \sigma_{as} - ab4 * \nu \Delta \sigma_{hs},$$

where

$$ab1 = g(2\sigma_a - \sigma_h)^2 + 1/E_{s1}, \quad ab2 = g(2\sigma_a - \sigma_h)(2\sigma_h - \sigma_a) - \nu/E_{s1},$$

$$ab3 = ab2, \quad ab4 = g(2\sigma_h - \sigma_a)^2 + 1/E_{s1},$$

$$a_1' = ab2 * \bar{Q}_{12} + ab4 * \bar{Q}_{22}, \quad a_2' = ab1 * \bar{Q}_{12} + ab3 * \bar{Q}_{22},$$

$$b_1' = ab2 * \bar{Q}_{11} + ab4 * \bar{Q}_{12}, \quad b_2' = ab1 * \bar{Q}_{11} + ab3 * \bar{Q}_{12}, \quad (2.69)$$

$$c_1' = r/t_c + a_1' r/t_s, \quad c_2' = -a_2'/(2\pi r t_s), \quad c_3' = a_1' r/t_s,$$

$$d_1' = b_1' r/t_s, \quad d_2' = -[1/(2\pi r t_c) + b_2'/(2\pi r t_s)], \quad d_3' = b_1' r/t_s - \kappa/(2t_c).$$

$$e_1' = \frac{r}{t_s} \left( 1 - \frac{c_3' d_2' - d_3' c_2'}{c_1' d_2' - d_1' c_2'} \right), \quad e_2' = \frac{1}{2\pi r t_s} \frac{c_3' d_1' - d_3' c_1'}{c_2' d_1' - d_2' c_1'}.$$

Based on the discussion in section 2.3.3, the movement of the center of the yield surface can be obtained from equation (2.37) and can be written as

$$\Delta \alpha_{hs} = (\sigma_{hs} - \alpha_{hs}) d\mu, \quad \Delta \alpha_{as} = (\sigma_{as} - \alpha_{as}) d\mu, \quad (2.70)$$

where

$$d\mu = \frac{(2\bar{\sigma}_{hs} - \bar{\sigma}_{as})\Delta \sigma_{hs} + (2\bar{\sigma}_{as} - \bar{\sigma}_{hs})\Delta \sigma_{as}}{(2\bar{\sigma}_{hs} - \bar{\sigma}_{as})\bar{\sigma}_{hs} + (2\bar{\sigma}_{as} - \bar{\sigma}_{hs})\bar{\sigma}_{as}}, \quad (2.71)$$

and

$$\bar{\sigma}_{hs} = \sigma_{hs} - \alpha_{hs}, \quad \bar{\sigma}_{as} = \sigma_{as} - \alpha_{as}. \quad (2.72)$$



Using  $\Delta P$  as step length, the stress states of all the points on path  $AB$  in Figure 2-6 can be obtained. Under load  $P_{\max} = P_y + \sum \Delta P$ , and by the superposition of the results of this section and the previous section, the stress and strain conditions can be obtained as

$$\begin{aligned}
 \sigma_{hs}^m &= \sigma_{hs} + \sum \Delta \sigma_{hs}, & \sigma_{as}^m &= \sigma_{as} + \sum \Delta \sigma_{as}, \\
 P_q^m &= P_q + \sum \Delta P_q, & T_s^m &= T_s + \sum \Delta T_s, \\
 \sigma_{hc}^m &= \sigma_{hc} + \sum \Delta \sigma_{hc}, & \sigma_{ac}^m &= \sigma_{ac} + \sum \Delta \sigma_{ac}, \\
 \varepsilon_h^m &= \varepsilon_h + \sum \Delta \varepsilon_h, & \varepsilon_a^m &= \varepsilon_a + \sum \Delta \varepsilon_a, \\
 \alpha_a^m &= \sum \Delta \alpha_{as}, & \alpha_h^m &= \sum \Delta \alpha_{hs}.
 \end{aligned} \tag{2.73}$$

The criterion to enter another linear hardening stage, say, range  $bc$  in Figure2-9, is

$$\sqrt{\sigma_{hs}^2 + \sigma_{as}^2 - \sigma_{hs}\sigma_{as}} \geq \sigma_b, \tag{2.74}$$

where  $(\sigma_{as}, \sigma_{hs})$  stands for stress state of points on path  $AB$  in Figure 2-6a, and  $\sigma_b$  stands for stress at point  $b$  in Figure2-9.

#### 2.4.5 Elastic unloading and plastic reloading

The first stage of unloading is elastic unloading, which corresponds to path  $BC$  in Figure 2-6a. Within this stage, the stresses satisfy the equation

$$\sqrt{(\sigma_{as} - \alpha_a^m)^2 + (\sigma_{hs} - \alpha_h^m)^2 - (\sigma_{as} - \alpha_a^m)(\sigma_{hs} - \alpha_h^m)} < \sigma_y. \tag{2.75}$$

The stresses and strains during the elastic unloading stage can be deduced in a similar way as before, and the stress-strain relationship for the metallic liner and the composite wrap are (2.32) and equation (2.19), respectively.



The center of the yield surface remains unchanged during this stage, i.e.  $\Delta\alpha_a = 0$  and  $\Delta\alpha_h = 0$ .

The criteria to enter the plastic unloading stage (Von Mises criteria) is

$$\sqrt{(\sigma_{as} - \alpha_a^m)^2 + (\sigma_{hs} - \alpha_h^m)^2 - (\sigma_{as} - \alpha_a^m)(\sigma_{hs} - \alpha_h^m)} = \sigma_y. \quad (2.76)$$

When the above criterion is satisfied, the stresses stand for those of point  $C$  in Figure 2-6a, i.e.,  $(\sigma_{aC}, \sigma_{hC})$ .

Based on the discussion in section 2.3.3, the movement of the center of the yield surface can be obtained based on the current stress state through equation (2.40), which can be written as

$$\Delta\alpha_{hs} = (\sigma_{hs}^E - \sigma_{hs}^D)d\mu, \quad \Delta\alpha_{as} = (\sigma_{as}^E - \sigma_{as}^D)d\mu, \quad (2.77)$$

where

$$d\mu = \frac{(2\bar{\sigma}_{hs} - \bar{\sigma}_{as})\Delta\sigma_{hs} + (2\bar{\sigma}_{as} - \bar{\sigma}_{hs})\Delta\sigma_{as}}{(2\bar{\sigma}_{hs} - \bar{\sigma}_{as})(\sigma_{hs}^E - \sigma_{hs}^D) + (2\bar{\sigma}_{as} - \bar{\sigma}_{hs})(\sigma_{as}^E - \sigma_{as}^D)}, \quad (2.78)$$

$$\bar{\sigma}_{hs} = \sigma_{hs} - \alpha_{hs}, \quad \bar{\sigma}_{as} = \sigma_{as} - \alpha_{as}, \quad (2.79)$$

and

$(\sigma_{as}^E, \sigma_{hs}^E)$  and  $(\sigma_{as}^D, \sigma_{hs}^D)$  stand for the stress states at point  $D$  and  $E$  in Figure 2-6a.

For the plastic unloading stage, the only difference is the method used to calculate tangent modulus  $E_t$ , and the criteria for it to reach the next linear stage. The stress-strain relationship for the metallic liner and the composite wrap are equation (2.33) and equation (2.19), respectively.



The tangent modulus  $E_t$  is determined by introducing the ratio  $r = \delta_1 / \delta_2$ , where  $\delta_1 = DE$ ,  $\delta_2 = DC$  (Figure 2-6a). The detailed procedure is given bellow.

Now the known parameters include  $\sigma_{aC}$ ,  $\sigma_{hC}$ ,  $\alpha_a$ ,  $\alpha_h$ , the radius of the stress memory surface ( $OB$  in Figure 2-6a)

$$R = \sqrt{\sigma_{aB}^2 + \sigma_{hB}^2 - \sigma_{aB}\sigma_{hB}}, \quad (2.80)$$

and the radius of the yield surface,  $\sigma_y$ . In this study, the expression of the yield surface is

$$\phi_y = f_y(\sigma_{ij} - \alpha_{ij}) - \sigma_y^2 = (\sigma_a - \alpha_a)^2 + (\sigma_h - \alpha_h)^2 - (\sigma_a - \alpha_a)(\sigma_h - \alpha_h) - \sigma_y^2 = 0. \quad (2.81)$$

The expression of the memory surface is

$$\phi_m = f_m(\sigma_{ij}) - R^2 = \sigma_a^2 + \sigma_h^2 - \sigma_a\sigma_h - R^2 = 0. \quad (2.82)$$

Here point  $D$  is located on the yield surface and point  $E$  is located on the memory surface. The normal direction at point  $D$  is  $\frac{\partial f_y}{\partial \sigma_{ij}}|_{\sigma_{ij}=\sigma_D}$ , and the normal direction at point

$E$  is  $\frac{\partial f_m}{\partial \sigma_{ij}}|_{\sigma_{ij}=\sigma_E}$ . Since these two points have the same normal directions, the following

equations can be deduced,

$$\frac{2\sigma_{aE} - \sigma_{hE}}{2\sigma_{aD} - \sigma_{hD}} = \frac{2\sigma_{hE} - \sigma_{aE}}{2\sigma_{hD} - \sigma_{aD}}. \quad (2.83)$$

As point  $E$  is on the memory surface, the following equation must also be satisfied

$$\sigma_{aE}^2 + \sigma_{hE}^2 - \sigma_{aE}\sigma_{hE} = R^2. \quad (2.84)$$

Solving the above two equations, one can obtain the stresses at point  $E$  as





$$\sigma_{aE} = \frac{R}{\sigma_y}(\sigma_{aD} - \alpha_a), \quad \sigma_{hE} = \frac{R}{\sigma_y}(\sigma_{hD} - \alpha_a). \quad (2.85)$$

Thus,

$$\delta_1 = \sqrt{(\sigma_{aE} - \sigma_{aD})^2 + (\sigma_{hE} - \sigma_{hD})^2 - (\sigma_{aE} - \sigma_{aD})(\sigma_{hE} - \sigma_{hD})}, \quad (2.86a)$$

$$\delta_2 = \sqrt{(\sigma_{aC} - \sigma_{aD})^2 + (\sigma_{hC} - \sigma_{hD})^2 - (\sigma_{aC} - \sigma_{aD})(\sigma_{hC} - \sigma_{hD})}. \quad (2.86b)$$

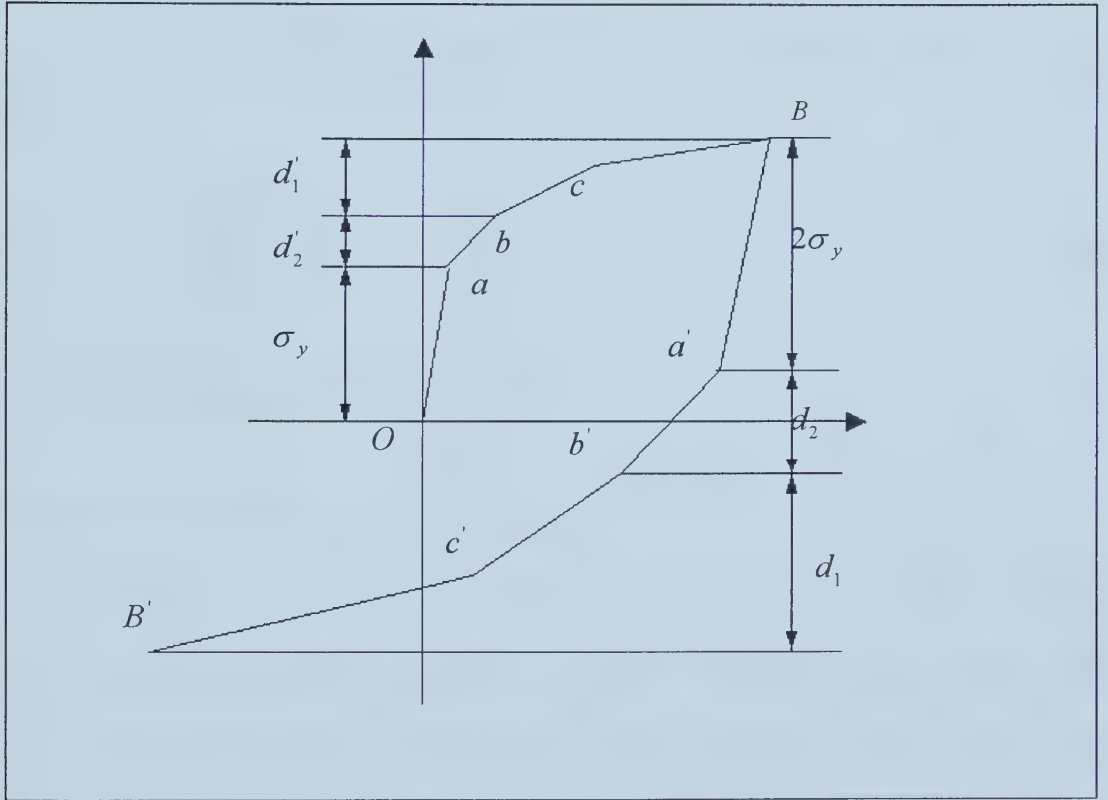


Figure 2-10 Schematic about determine tangent modulus

Based on Figure 2-10, the following equation is satisfied,

$$\frac{d_1}{d_2} = \frac{d'_1}{d'_2}, \quad (2.87)$$



where  $d'_1 = \sigma_{eq}^B - \sigma_{eq}^b$ , and  $d'_2 = \sigma_{eq}^b - \sigma_{eq}^a$ .

In the above,  $\sigma_{eq}^B = \sqrt{\sigma_{aB}^2 + \sigma_{hB}^2 - \sigma_{aB}\sigma_{hB}}$  is the equivalent stress at point  $B$  in Figure

2-6a,  $\sigma_{eq}^a$  and  $\sigma_{eq}^b$  is the stress input of point  $a$  and  $b$  in Figure 2-10.

$$\text{If } \frac{\sigma_{eq}^B - \sigma_{eq}^b}{\sigma_{eq}^b - \sigma_{eq}^a} = \frac{d'_1}{d'_2} < \frac{\delta_1}{\delta_2} \leq \infty, \text{ then tangent modulus } E_t = E_s^{ab},$$

where  $E_s^{ab}$  is the tangent modulus within range  $ab$ .

For the use of next tangent modulus  $E_t = E_s^{bc}$ , the following criterion must be satisfied

$$\frac{\sigma_{eq}^B - \sigma_{eq}^c}{\sigma_{eq}^c - \sigma_{eq}^a} < \frac{\delta_1}{\delta_2} \leq \frac{\sigma_{eq}^B - \sigma_{eq}^b}{\sigma_{eq}^b - \sigma_{eq}^a}. \quad (2.88)$$

## 2.5 Numerical program development

### 2.5.1 Input parameters

Two numerical programs are developed using the engineering software MatLab. These two programs are named as HPD1 and HPD2, respectively. The program HPD1 calculates the pressure (Proof test) required to obtain desired residual stress. Failure analysis is also carried out to provide more information for the proof pressure design. Several failure criteria are included in the program. For the metallic liner, the ultimate strength criterion is used. For the composite wrap, the transverse strength, the longitudinal strength and the shear strength of the composite wrap as well as Tsai-Wu criteria [17] are applied. The program HPD2 simulates any loading, unloading and



reloading history of the hybrid composite pipe and also records and plots the stress-strain response during the loading history.

The material properties of the composite laminate include those of the unidirectional lamina and the ply angle  $\theta$ . The material parameters for the unidirectional lamina include the following nine parameters:

Longitudinal elastic modulus  $E_1$

Transverse elastic modulus  $E_2$

Major Poisson's ratio  $\nu_{12}$

Shear modulus  $G_{12}$

Ultimate longitudinal tensile strength  $(\sigma_1^T)_{ult}$

Ultimate longitudinal compressive strength  $(\sigma_1^c)_{ult}$

Ultimate transverse tensile strength  $(\sigma_2^T)_{ult}$

Ultimate transverse compressive strength  $(\sigma_2^c)_{ult}$

Ultimate in-plane shear strength  $(\tau_{12})_{ult}$

The material properties of the metal include the Poisson's ratio  $\nu$ , the ultimate strength and the stress-strain curve. This curve is input as a multi-linear one and it can be obtained through experiment. The first point inputted is the origin (both stress and strain are zeros), and the second point is the elastic limit and the corresponding strain (Young's modulus  $E = \sigma_2 / \varepsilon_2$ ).



The input geometry parameters include the thickness of the metallic liner  $t_s$ , the thickness of the composite wrap  $t_c$ , and the average radius of the pipe  $r$ .

For HPD1, the inputted loading conditions include the loading ratio of axial/hoop loading  $k$ , and the ratio of the desired residual stress to the yield stress,  $\alpha$ . Here  $k$  is defined as  $T = k\pi r^2 P$ , where  $T$  is the axial loading; and  $\alpha$  is defined as  $\alpha = \sigma_{eq}^{res} / \sigma_y$ .

For HPD2, the inputted loading conditions include: the loading ratio of axial/hoop loading  $k$ , the number of cycles of loading and unloading, and the maximum and minimum pressure for each loading cycle.

### 2.5.2 Failure analysis of HPD1

The program HPD1 also carries out failure analysis based on several different failure criteria. This is to provide more information to the designer about what kind of failure may occur during the proof test procedure.

The failure criterion for the metallic liner uses the maximum equivalent stress as the parameter to determine whether the pipe may fail or not. Once the maximum equivalent stress in the liner is greater than the ultimate strength of the metallic liner, then failure will occur and the program will terminate.

Several failure criteria are used for the composite wrap. In the maximum stress failure theory [17], the stresses acting on the laminate are resolved into the normal and shear stress components in the local axes of each lamina. If any of the stresses is equal or exceed the corresponding ultimate strength of the unidirectional lamina, i.e. if any of the following criteria





$$-(\sigma_1^c)_{ult} < \sigma_1 < (\sigma_1^T)_{ult}, \quad (2.89a)$$

$$-(\sigma_2^c)_{ult} < \sigma_2 < (\sigma_2^T)_{ult}, \quad (2.89b)$$

$$-(\tau_{12})_{ult} < \tau_{12} < (\tau_{12})_{ult} \quad (2.89c)$$

is violated, then the laminate is considered to have failed.

The Tsai-Wu theory is based on the total strain energy failure theory of Beltrami. If the following formula

$$H_1\sigma_1 + H_2\sigma_2 + H_6\tau_{12} + H_{11}\sigma_1^2 + H_{22}\sigma_2^2 + H_{66}\tau_{12}^2 + 2H_{12}\sigma_1\sigma_2 < 1 \quad (2.90)$$

is violated, then the laminate is considered to have failed, too. In the above,

$$H_1 = \frac{1}{(\sigma_1^T)_{ult}} - \frac{1}{(\sigma_1^c)_{ult}}, \quad H_2 = \frac{1}{(\sigma_2^T)_{ult}} - \frac{1}{(\sigma_2^c)_{ult}}, \quad H_6 = 0,$$

$$H_{11} = \frac{1}{(\sigma_1^T)_{ult}(\sigma_1^c)_{ult}}, \quad H_{22} = \frac{1}{(\sigma_2^T)_{ult}(\sigma_2^c)_{ult}}, \quad H_{66} = \frac{1}{(\tau_{12})_{ult}^2}, \quad (2.91)$$

$$\text{and } H_{12} = -\frac{1}{(\sigma_{12}^T)_{ult}^2}.$$

### 2.5.3 Output parameters

Both programs can predict the stress-strain response for the metallic liner and the composite wrap during the entire loading history. The parameters recorded include the internal pressure and axial tension, the hoop strain and axial strain, the equivalent strain, the hoop and axial stresses and the equivalent stresses for the metallic liner and the composite wrap. All these parameters are stored in matrixes, and they can be easily listed.



By the built-in functions of MatLab, these parameters can also be arranged to plot different curves, e.g., the stress-hoop strain curve or the pressure-strain curve, etc.

### 2.5.3 Examples

In order to confirm the validity of the numerical programs, several specific examples are provided in the following sections.

#### 2.5.3.1 Example 1: Metallic liner alone

The objective of this example is to verify that the material model for the metallic liner is correct. Based on the theoretical model, the stress-strain curve for the kinematic hardening metal is shown in Figure 2-11.

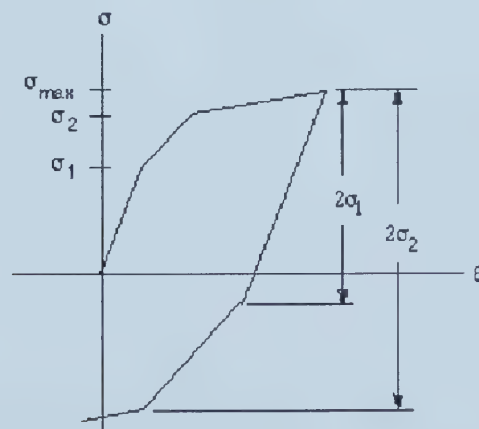


Figure 2-11 Stress-strain relationship for multi-linear kinematic hardening material

For this example, the input parameters include:

Geometry:  $t_s = 2mm$ ,  $t_c = .0001mm$ ,  $r = 25mm$ .

Stress-strain points of the metallic liner:  $[0,0]$ ,  $[100, 0.001]$ ,  $[200, 0.003]$ ,  $[400, 0.02]$ .

Loading conditions: Internal pressure only ( $\kappa = 0$ ), and the pressure loading path is



$0 \rightarrow 20\text{MPa} \rightarrow -20\text{MPa} \rightarrow 20\text{MPa}$ .

Note that the thickness of composite wrap takes a near-zero value to avoid singularity during calculation.

The stress-strain curve of the metallic liner obtained using HPD2 is shown in Figure 2-12.

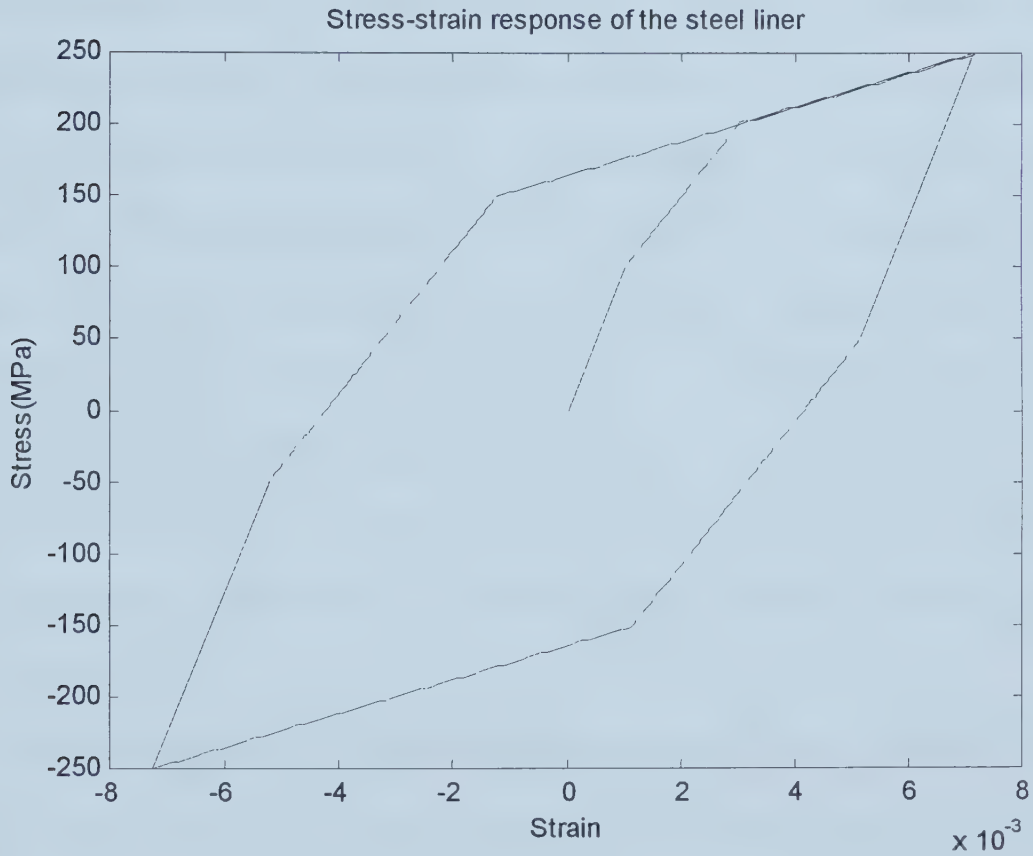


Figure 2-12 Response of the metallic liner

From the above result, it can be clearly seen that the stress-strain curve during monotonic loading is exactly the same as the input stress-strain curve. For the unloading curve, it fits exactly the relation as

$$\Delta\varepsilon/2 = F(\Delta\sigma/2),$$



which is the relationship predicted in theoretical analysis.

After reloading to the previous maximum pressure, the stress status comes back to the initial unloading point, which also fits the kinematic hardening rule.

### **2.5.3.2 Example 2: Proof pressure prediction with the use of program HPD1**

During manufacturing of composite pipe, it is beneficial to introduce some compressive residual stress within the internal metallic liner. This increases the elastic range of the pipe, and the pipe can thus work under higher working pressure. The compressive residual stress also suppresses the micro-crack from initiating and growing, thus improves the pipe's fatigue resistance. With compressive residual stress in the metallic liner, and tensile residual stress in the composite wrap, the bonding between the metallic liner and the composite wrap is also improved. The procedure to produce this compressive residual stress in the metallic liner is very much akin to the "autofrettage" in metal manufacturing, and the pressure required to produce the desired residual stress is called "proof pressure".

It is important to accurately predict the proof pressure in order to obtain desired residual stresses in the hybrid pipe and the program HPD1 serves to this objective. An example is provided bellow.

In this example, it is assumed that the desired compressive residual stress in the metallic liner is half of the yield stress of the metal material, and a biaxial loading condition (2H:1A) is applied. Other inputted geometrical and material parameters are





taken from the hybrid pipe specimen used in the experiments (see Chapter 3). The values for each parameters inputted are:

Geometry:  $t_s = 1mm$ ,  $t_c = 2mm$ ,  $r = 26.25mm$ .

Stress-strain points of the metallic liner: [0,0], [426, 0.00239], [476, 0.00284], [527, 0.00408], [551.7, 0.00547], [572.3, 0.00874], [583, 0.01322], [605.5, 0.03476].

Ultimate strength of the metal material:  $\sigma_{ult} = 605MPa$ .

Poisson's ratio:  $\nu = 0.3$ .

Material properties of the unidirectional lamina:

$E_1 = 43.2GPa$ ,  $E_2 = 10GPa$ ,  $\nu_{12} = 0.31$ ,  $G_{12} = 4.49GPa$ ,  $(\sigma_1^T)_{ult} = 1062MPa$ ,

$(\sigma_1^c)_{ult} = 610MPa$ ,  $(\sigma_2^T)_{ult} = 31MPa$ ,  $(\sigma_2^c)_{ult} = 118MPa$ ,  $(\tau_{12})_{ult} = 72MPa$ .

The ply angle is  $\theta = \pm 70^\circ$ .

Loading conditions: 2H:1A ( $\kappa = 1$ ), and the required residual stress in the metallic liner is  $\sigma_y / 2$ .

HPD1 performs the proof pressure prediction, and plots the stress-strain curve of the metallic liner (Figure 2-13). It also gives the following information:

The proof pressure is 45.723 MPa.

No failure of metal.

Failure pressure based on Tsai-wu criteria is 37.523 MPa.

Failure pressure based on transverse strength is 36.723 MPa.

Failure pressure based on longitudinal strength is 98.023 MPa.



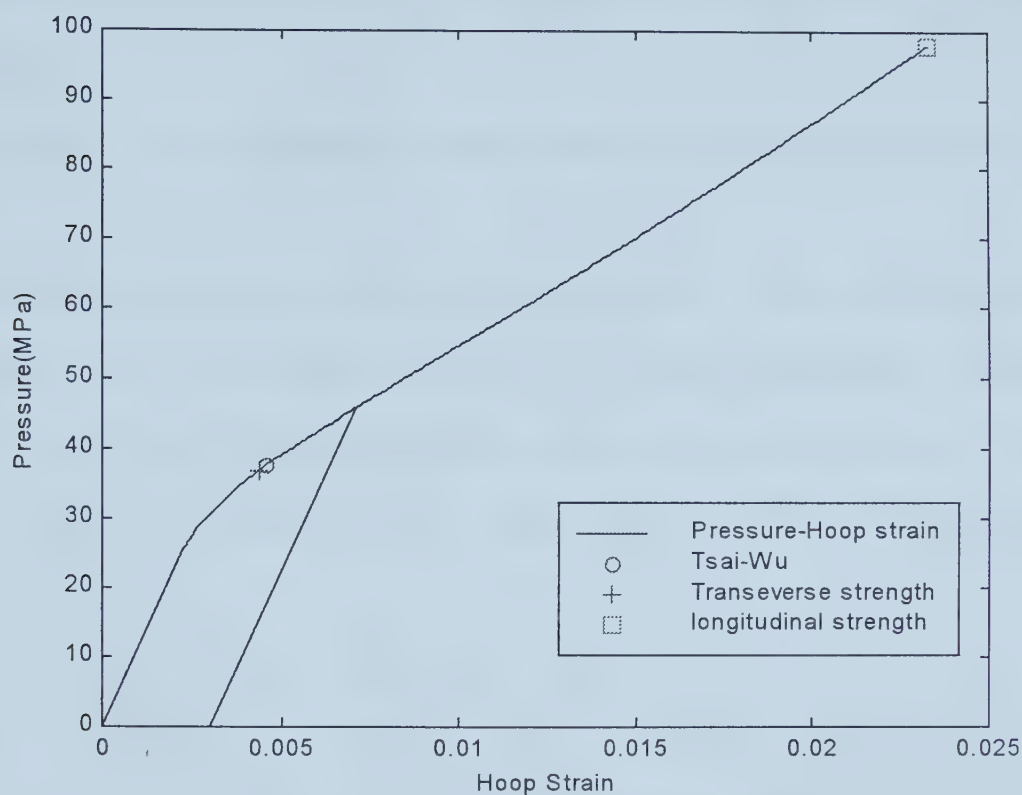


Figure 2-13 Proof pressure prediction and failure analysis by HPD1

Based on the analysis of the program HPD1, transverse failures occur before obtaining the desired residual stress. This is because of the very weak strength in the transverse direction of the lamina (The transverse ultimate strength is 31MPa only). However, here the transverse failure is not considered as final failure. The reason lies on the existence of the metallic liner. In the current application, the major load the pipe is suppose to take under working conditions is the internal pressure, the major load-carrying constituent of the composite laminate is the fiber. The matrix mainly acts to hold the fiber together. Transverse cracking of the matrix may cause leakage in purely composite pipes, but will not have significant effect on the loading carrying capacity of the hybrid pipe. For the hybrid composite pipe, the metallic liner prevents leakage even when transverse



cracking occurs in the composite wrap, thus the longitudinal strength is used as the final failure criterion.

### **2.5.3.3 Example 3: Uniaxial loading-reloading simulation with the use of program HPD2**

This example shows the loading-reloading characteristics of the hybrid composite pipe under uniaxial cyclic loading condition. The geometry sizes and the material properties for the metallic liner and composite wrap are the same as those in the last example. However, it is under pure hoop stress condition ( $\kappa = 0$ ), and the pressure loading cycle is

$0 \rightarrow 40\text{MPa} \rightarrow 0\text{MPa} \rightarrow 52\text{MPa} \rightarrow 0\text{MPa} \rightarrow 62\text{MPa} \rightarrow 0\text{MPa}$ .

Figure 2-14 shows the Pressure-hoop strain curve under uniaxial-loading condition. From this curve, it can be seen that the mechanical behavior of the pipe during the reloading procedure is different from the monotonic one. Due to introduction of the compressive stress in the metallic liner, the elastic limit is increased during the next reloading procedure.



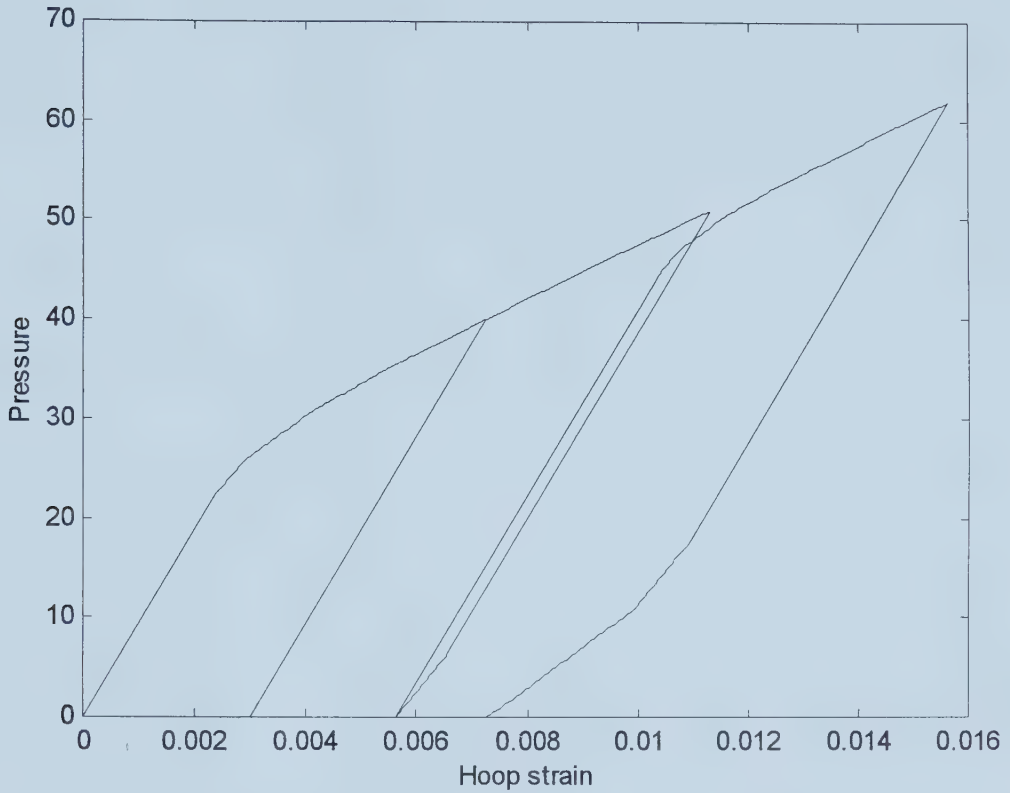


Figure 2-14 Pressure-hoop strain curve under uniaxial-loading condition

#### 2.5.3.4 Example 4: Biaxial loading-reloading simulation with the use of program HPD2

This example shows the loading-reloading characteristics of the hybrid composite pipe under biaxial loading condition. The only difference between this example and the previous one is in the loading condition. For this example, the pipe is under biaxial loading condition (2H:1A), and the pressure loading path is

$0 \rightarrow 45\text{MPa} \rightarrow 0\text{MPa} \rightarrow 55\text{MPa} \rightarrow 0\text{MPa}$ .

The Pressure-hoop strain curve for the metallic liner is shown in Figure 2-15.





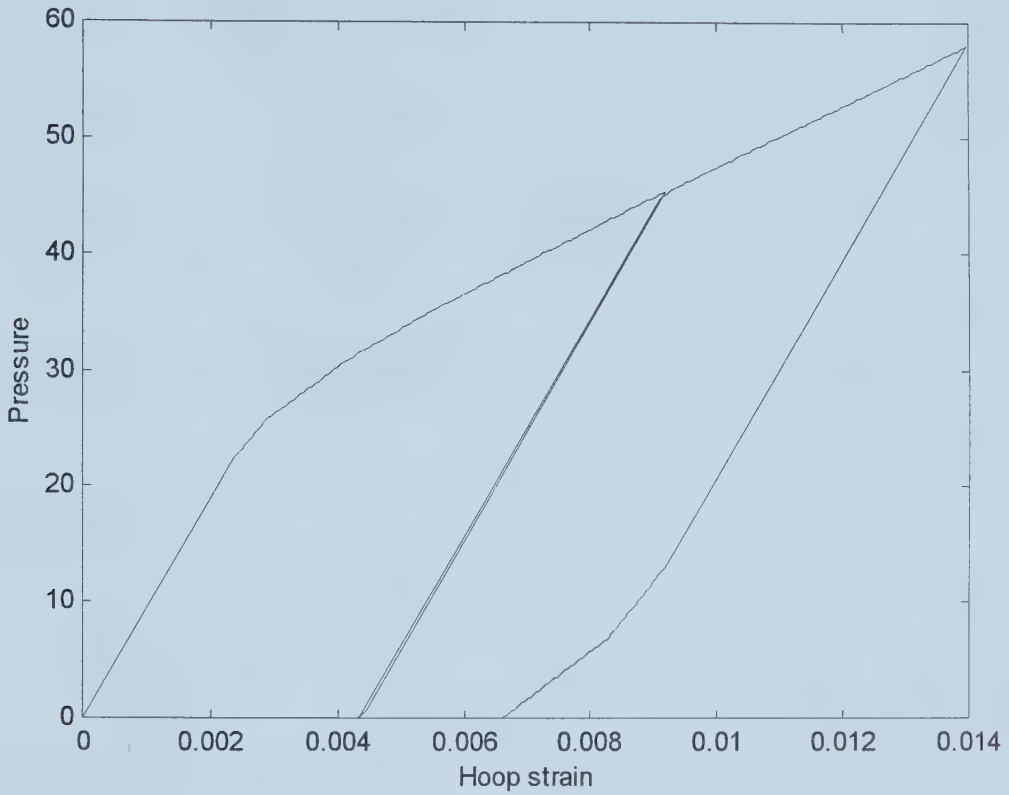


Figure 2-15 Pressure-hoop strain curve under biaxial-loading condition

### 2.5.3.5 Example 5: Weight saving calculation

This example aims to show how much weight the hybrid composite/metal pipe can save compared with purely metal pipe. A purely steel pipe is introduced here, and it has the same capacity and safety factors as the hybrid composite/steel pipe designed in the above example.

The thickness of this purely steel pipe must meet the following criteria

$$\frac{\sigma_y}{n_s} = \frac{P_{op} D_{in}}{2t_s}, \quad (2.92)$$

thus it is determined as



$$t_s = \frac{P_{op} D_{in} n_s}{2\sigma_y} = \frac{20 \times 52.5 \times 2}{2 \times 426} = 2.465 \text{ mm} . \quad (2.93)$$

The specific gravity of metal is 7.8, and that of the glass/epoxy is 1.8, thus the specific weight per unit length for the pure metal pipe here is

$$W_s = \pi D_{in} t_{s2} \rho_s , \quad (2.94)$$

and the specific weight per unit length for the hybrid composite/metal pipe is

$$W_h = \pi D_{in} (t_{s1} \rho_s + t_{c1} \rho_c) . \quad (2.95)$$

Thus the weight ration is

$$W_h / W_s = (t_{s1} \rho_s + t_{c1} \rho_c) / t_{s2} \rho_s = 0.54 . \quad (2.96)$$

Here it can be seen that the hybrid composite/metal pipe can save close to 50% weight compared with purely metal pipe.



## Chapter 3 Experimental verification

### 3.1 Introduction

To verify the theoretical predictions, both uniaxial and biaxial tests are carried out on the specimens of hybrid composite/metal pipes. Tubular specimens with an internal steel liner and an outside glass fiber/epoxy matrix composite wrap are designed based on the experimental objective and available instruments. To maintain repeatability of the experiments, the manufacturing procedure for the tubular specimens is specified. This chapter also describes the testing apparatus and gripping system as well as the data acquisition system. Several different kinds of experiments are carried out: steel liner test to obtain the stress-strain curve of the steel, uniaxial test and biaxial test on hybrid pipe specimens.

### 3.2 Tubular specimen design

Most of the earlier works about tubular specimen test were carried out to obtain composite materials properties in uniaxial tests, and most recent works are concerned with multiaxial loading. Halpin et al [27], Guess and Gerstle [28], Soded et al [29], and Daniel et al [30] were among those who first applied multiaxial loading to tubular composite specimens.

However, significant end effects exist among these researches [31]. In order to decrease the stress concentration between the reinforced region and the gage section, Pagano [31], Whitney et al [32] studied the geometric design of thin-wall tubular specimen, so that the elastic stress gradients can be reduced to a predetermined limit.



With the introduction of modern analysis techniques, such as finite element analysis, the design of tubular specimens becomes easier. Guess and Haizlip [33] examined two gripping methods on stress (strain) distribution within tubular composite specimens loaded in uniaxial and biaxial tension, using finite element analysis and strain-gage measurements. Guess [34] gave an experimental-theoretical comparison to the biaxial testing of composite cylinders and get good agreement. However, stress concentration is still significant in these tests.

Toombes et al [35] developed a tubular specimen to minimize the undesirable end effects, and used finite element method to analyze the stress concentration, which was shown to be greatly reduced. This specimen design was adopted in their subsequent work and was applied to a number of different test conditions and laminates, as reported in the literature of Toombes et al [35], Swanson and Christoforou [36, 37], and Swanson and Nelson [38], Swanson, Christoforou and Colvin [39]. In 1997, Smith and Swanson [40] further developed this design, to permit higher axial loads than previously achieved. FEM analysis showed that the load is introduced smoothly in both the axial and hoop directions. Experiment showed that the grip and apparatus design was successful in achieving gage section failures over wide range of biaxial test conditions.

In our study, in order to simplify the manufacture and assemble procedure, an integrated steel mandrel is designed. The gauge section will serves as the steel liner for the pipe, and the two convex ends will be used for gripping. While designing the steel mandrel, the following factors should be considered:





- 
- The gauge section should be long enough to keep the test results not affected by the stress caused by the two end grips.
  - The ratio of the diameter to the thickness must be large enough to ensure the finished tubular specimen can be regarded as a thin-walled cylinder.
  - The specimen should be easily fitted to the current gripping systems and available instruments.

Based on all these considerations, the final design is shown in Figure 3-1. The gauge section of the specimen is 100mm. The internal diameter is 50mm. The thickness of the steel liner and the thickness of the composite wrap are 1mm and 2mm, respectively. Therefore, the finished specimen meets the thin-walled cylinder assumption.



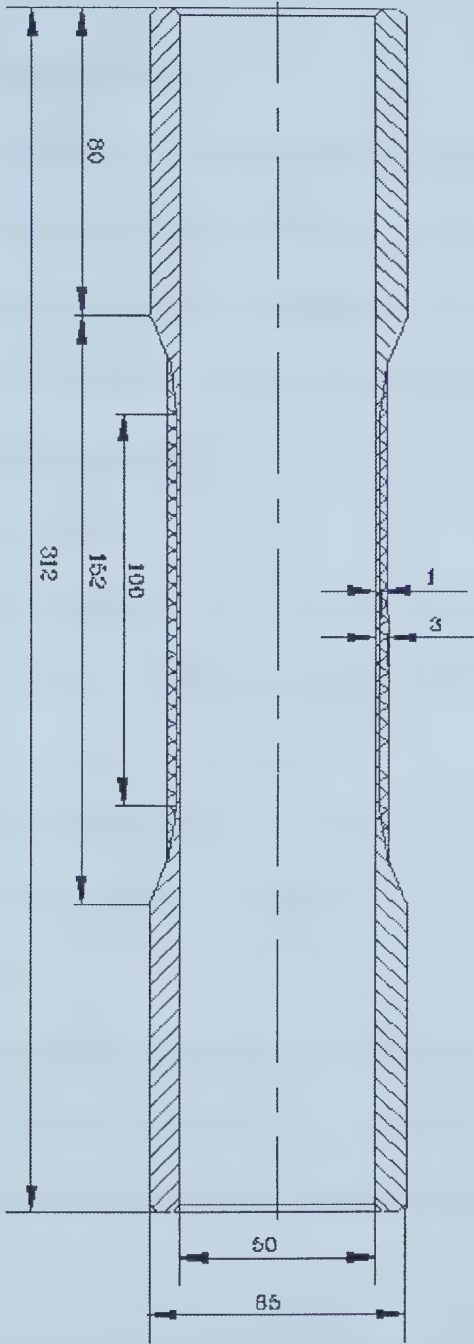


Figure 3-1 Drawing of the hybrid composite/steel specimen (Unit: mm)



### **3.3 Tubular specimen manufacturing**

When conducting experiments, one requirement is that the experimental results must be reproducible. Therefore, the quality control of the specimen manufacturing procedure is very important. The materials used, lay-up procedure and curing temperature and time should be kept the same for each specimen. The manufacturing procedure for the hybrid tubular specimens is outlined in the following:

#### ***Step 1: Steel mandrel preparation***

First, a steel mandrel must be manufactured. After it is machined, the outer surface of the gauge section should be sandblasted. This increases the bond between the steel liner and the composite wrap.

Once the steel mandrel is sandblasted, the outer surface of the gauge section should be thoroughly cleaned with acetone applied to a clean cloth.

#### ***Step 2: Rolling table setup***

A rolling table is used to apply successive layers of prepreg on the steel liner. A picture of the rolling table and the layout of it is shown in Figure 3-2. The main components of this table include a flat plate, a longitudinal guide and a mandrel support arm.

The cut layer of prepreg is put on the flat plate. This plate is made of plastic with a thickness of about 7mm and with a metal sheet glued to its surface. The total thickness is determined by the difference between the diameter of the gauge section and the two ends of the steel mandrel. The plate must be thick enough to allow the gauge section to bear on



the flat plate while the two ends remain suspended. With the metal surface, the flat plate is easy to be cleaned with acetone, and the resin stuck to it during the layer lay-up can be easily removed.

A ground steel strip is bolted to the table to serve as a longitudinal guide. It is precisely adjusted to make it perpendicular to the mandrel axis (and parallel to the rolling direction).

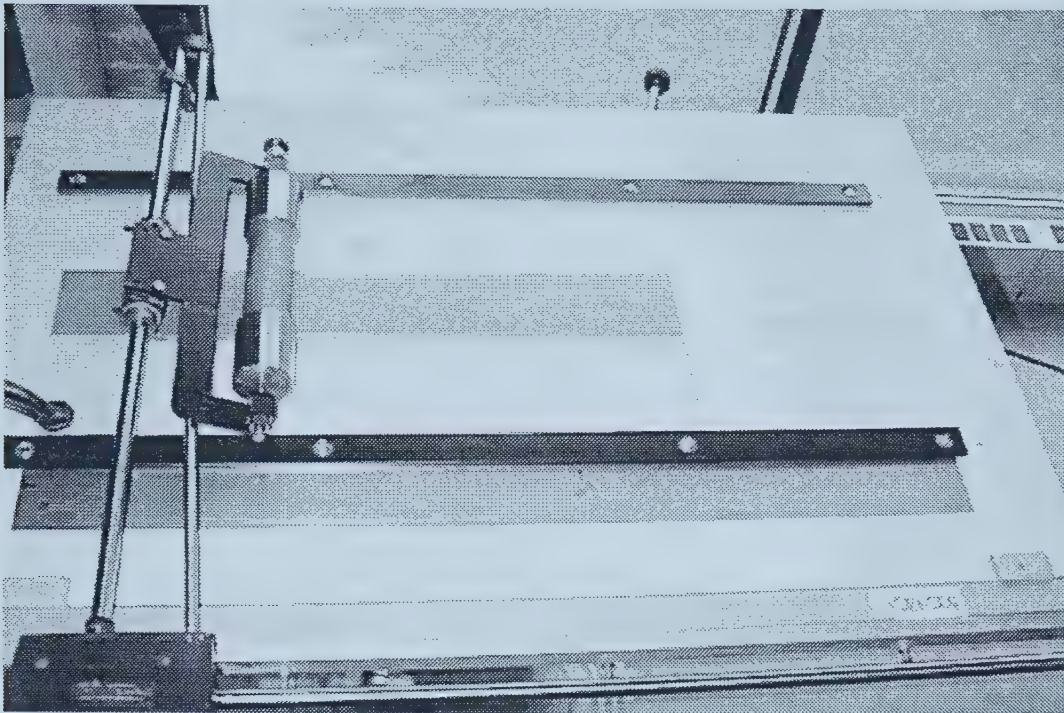
With two end plugs fitted into the convex ends of the steel mandrel, the steel mandrel can be mounted on the mandrel support center with fastening the centering nuts to prevent the release of the steel mandrel. In this position, the steel mandrel can be easily rotated.

Equally mark the steel mandrel ends with a pen along the circumference, which is to ensure stagger of successive layer start points.

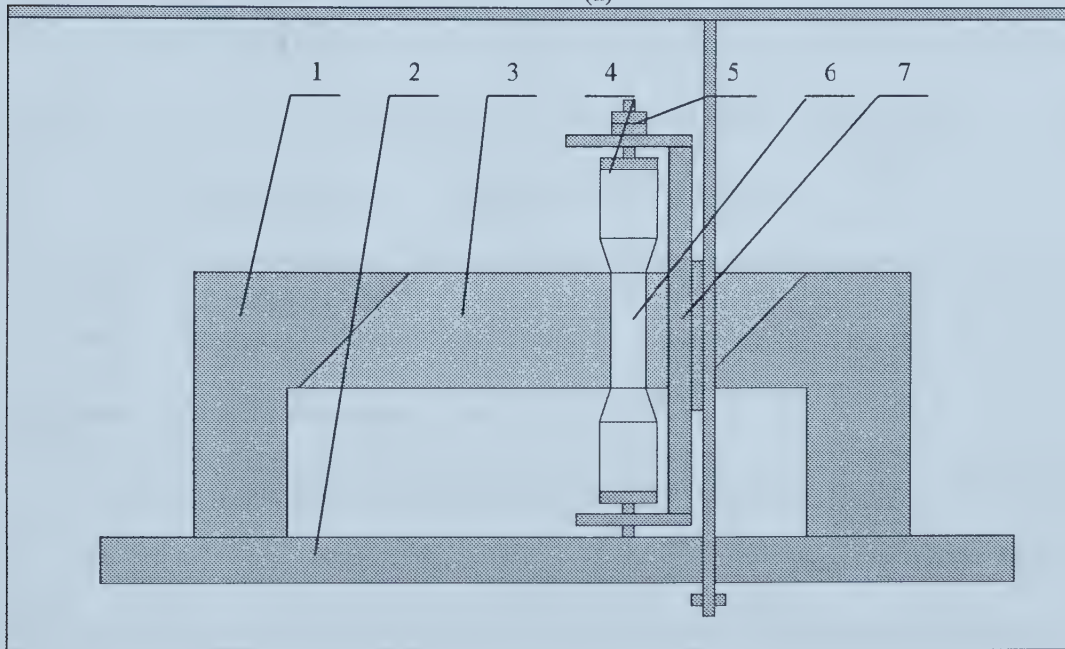
After the steel mandrel is mounted and marked, the surface of the flat plate is cleaned with acetone.







(a)



(b)

Figure 3-2 (a) Picture of the rolling table, (b) Layout of the rolling table. (1. Flat plate 2. Longitudinal guide

3. Cut prepreg 4. End plug 5. Centering nuts 6. Steel mandrel 7. Mandrel support arm)

### ***Step 3: Template preparation***



To save time and maintain the precision while cutting prepreg layers, several templates are made with high-quality metal sheet according to the pipe dimension and wrapping angle. Figure 3-3 gives an example for the template for the wrapping angle  $\theta$ . For the current study,  $\theta = 70^\circ$ .

The parameters for the laminate is determined from the expressions

$$W = w \quad \text{and} \quad D = \pi d.$$

The relationship between the template and the wrapping angle is also given in Figure 3-3.

#### ***Step 4: Prepreg cutting***

The 3M type 1003 (scotchply) E-glass-fiber/epoxy resin is used as the material of the composite wrap. This is in a form of the tape roll of Scotchply prepreg, the unidirectional glass fiber is in the roll direction, and backing paper is used to separate the layers of the prepreg on its roll. The tape roll is stored bellow  $0^\circ\text{C}$  to avoid premature of the epoxy. Before being used, it needs to be kept at room temperature for at least 3 hours to warm up; however, to avoid condensation on the prepreg, the tape roll should be kept in a plastic bag during storage or warm up.

Hoover [41] has examined the material properties of this material shown in Table 3-1. The materials he used come from the same stock as those used in the current study, and the same curing cycle is adopted. Thus, these material properties obtained by Hoover will be used in the current study to calculate the material properties of the composite wrap according to the classical laminate theory.



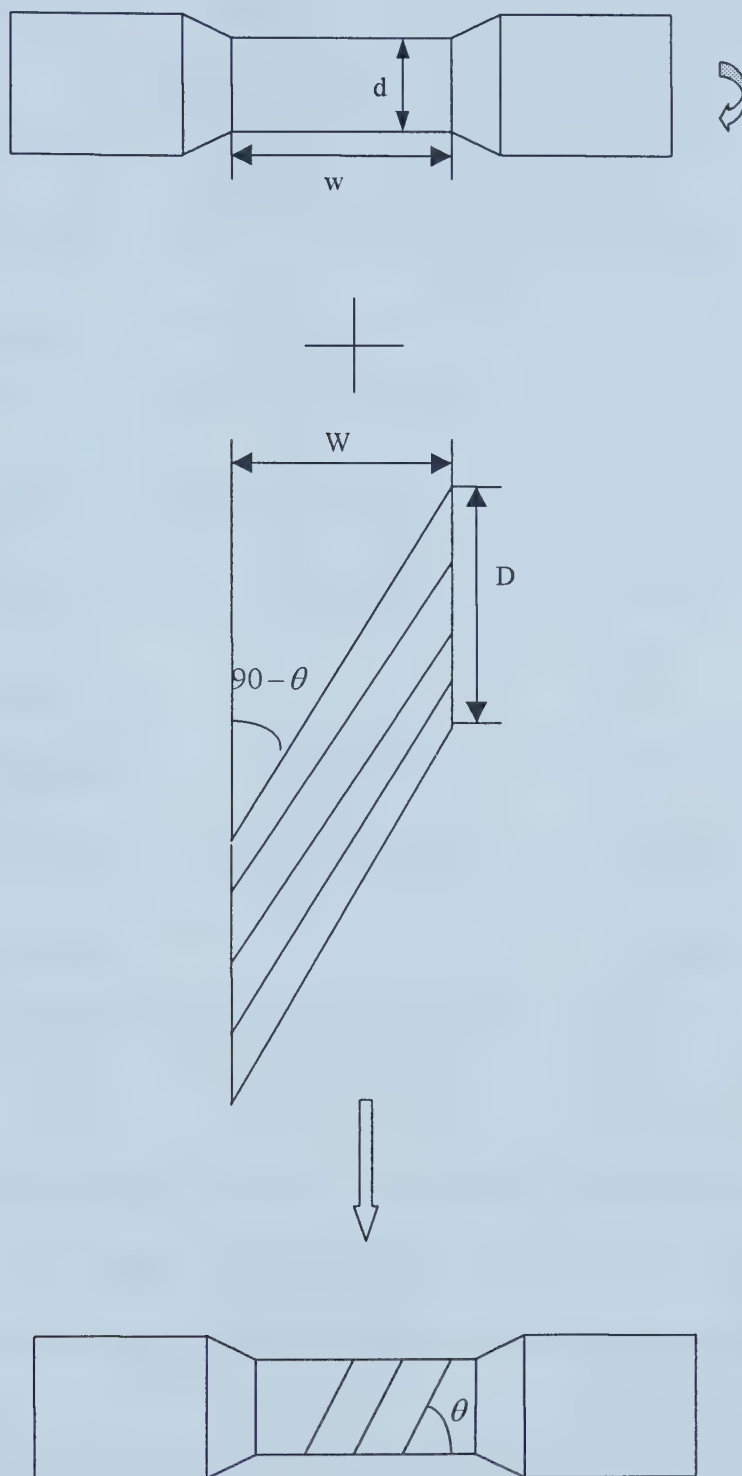


Figure 3-3 Relationship between the template and the steel mendral



Table 3-1 Material properties of 3M type 1003 E-glass fiber/epoxy resin composite as manufactured at the University of Alberta [41]

| Engineering Constant                                       | Value  |
|--|--|
| Longitudinal Modulus, $E_1$                                | 43.2 GPa   |
| Transverse Modulus, $E_2$                                  | 10.0 GPa   |
| In-plane Shear Modulus, $G_{12}$                           | 4.49 GPa   |
| Out-of-plane Shear Modulus, $G_{23}$                       | 4.17 GPa   |
| In-plane Poisson ratio, $\nu_{12}$                         | 0.31   |
| Out-of-plane Poisson ratio, $\nu_{23}$                     | 0.44   |
| Longitudinal co-efficient of thermal expansion, $\alpha_1$ | $8.6 \times 10^{-6} \text{ m/m/}^\circ\text{C}$  |
| Transverse co-efficient of thermal expansion, $\alpha_2$   | $22.1 \times 10^{-6} \text{ m/m/}^\circ\text{C}$ |
| Average Ply Thickness                                      | 0.210mm  |
| Fiber Volume Fraction (After cure),                        | 52%  |

Several laminate layers are cut with a scalpel knife according to the templates. A layer of release film should be put between the prepreg and the template to prevent contamination during cutting. Figure 3-4 gives an illustration to the laminate cutting.





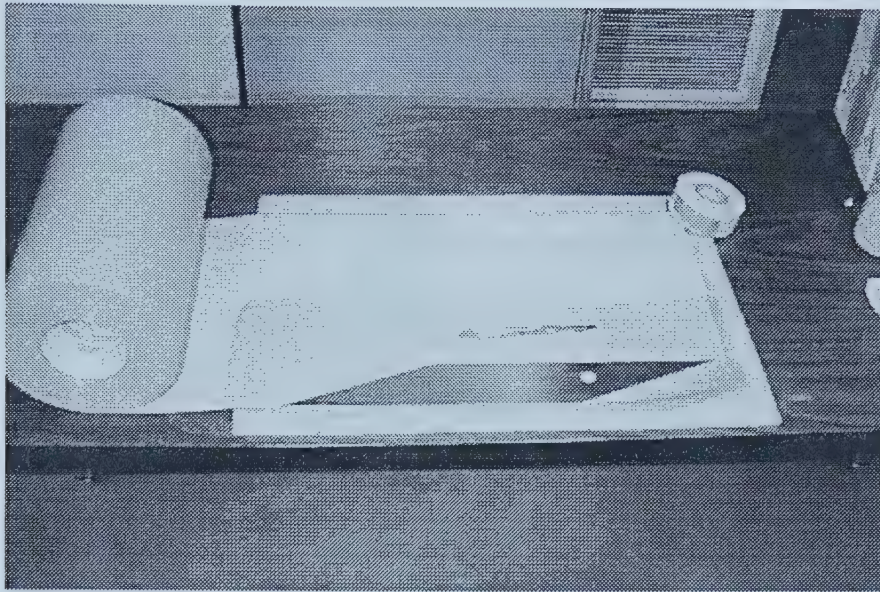


Figure 3-4 Laminate cutting

***Step 5: Put cut prepreg on the rolling table***

After cutting the prepreg layer, it is placed on the flat plate with back paper on the top (Figure 3-5). Pressure is slightly applied on the back of the prepreg to squeeze out the air trapped between the prepreg layer and the flat plate and to make the prepreg layer to stick to the flat plate. This pressure should be sufficient only to hold the prepreg in place. If it is too high, the prepreg will not be able to be properly peeled off the flat plate when it is applied to the steel mandrel.



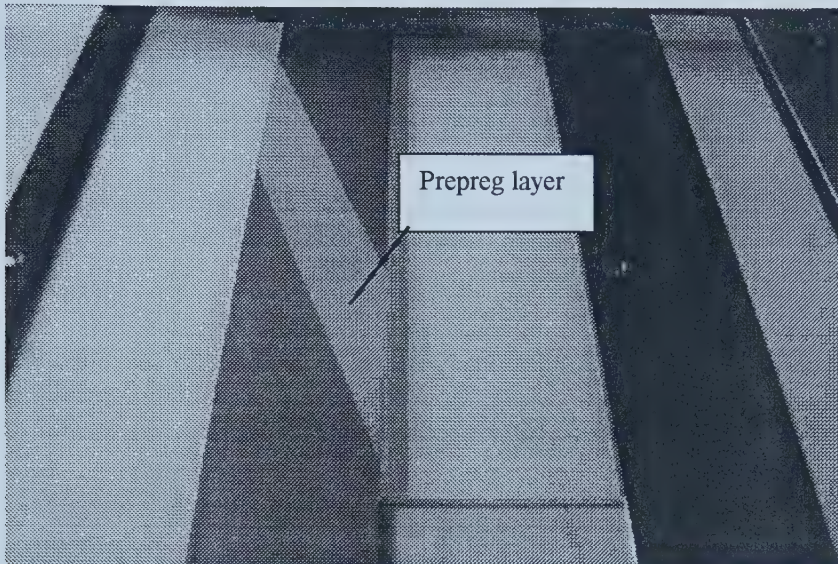


Figure 3-5 Place the prepeg layer on the flat plate

***Step 6: Locate the mandrel***

The scalpel knife is used to peel off the back paper at the start end of the prepeg. This paper provides support for the prepeg during handling and positioning, and should not be removed until the prepeg is correctly positioned and ready to be applied to the steel mandrel. Otherwise the lamina may easily fall apart due to the very weak nature of the matrix interface.

The steel mandrel is placed at the start end of the prepeg layer. The mandrel should also start from one marked position so that the next layer could start from the next marking.

***Step 7: Roll the steel mandrel***

The steel mandrel is pressed onto the start of the prepeg layer and rolled by hand using the two ends. Since the back paper is just peeled off, the upper side of the prepeg





layer is stickier than the other side in contact with the flat plate. Thus it has a tendency to adhere to the steel mandrel rather than to the flat plate. In cases when the prepreg adheres to the flat plate, the scalpel knife can be used to lift the start end of the lamina. After the lamina start to adhere to the mandrel, roll the mandrel slowly until all of the lamina is applied to the mandrel to avoid wrinkle during the wrapping.

When the prepreg layer is applied to the steel mandrel, the steel mandrel is rolled on the flat plate for several times. This would squeeze out the trapped air between the steel mandrel and the first prepreg layer.

***Step 8: Repeat step 5-7 until the last layer of wrapping***

After the first layer is done, the flat plate is cleaned with acetone again to get rid of the resins stuck on the flat plate during the rolling procedure. Step 5 to 7 are repeated until all the prepreg layers are applied on the steel mandrel. Since the prepreg layer is much tackier than the metal surface of the flat plate, it is easier to apply successive layers than the first one. For the current study, totally 8 layers of prepreg are wrapped outside the steel mandrel.

***Step 9: Wrap nylon release peel ply fabric***

After all the prepreg layers are applied to the steel mandrel, a nylon release peel ply fabric is wrapped on the surface. With slightly hand pressure, the fabric will stick to the outside prepreg layer. The two ends of the fabric should be slightly overlapped. The surface is smoothed with hand and no wrinkle or air bubble should exist. This fabric will facilitate the removal of the wraps applied to it later, and will help to produce a quality finished surface.



---

***Step 10: Wrap a thin layer of steel or metal sheet***

A steel sheet (0.076 mm in thickness) is also adopted to help to make a quality finished smooth surface. This layer evenly distributed the stress applied by the shrink tape during curing, thus produce a smooth and nice finished surface.

***Step 11: Wrap shrink tape***

Shrink tape is used to provide consolidation pressure during curing. To maintain a smooth surface, it must be equally distributed over the surface. High temperature tape is used to fix it in place.

After the shrink tapes are wrapped, all the seams between the shrink tapes are sealed with the high temperature tape, too. This is to avoid excessive resin flow.

***Step 12: Curing***

Dismount the wrapped up specimen from the mandrel support center. Put it inside the curing oven (Figure 3-6). Set the temperature to  $300^{\circ}F$ , and the time to 12 hours. Start the oven and the curing cycle begins. The curing cycle is to provide heat and pressure to the specimen to finalize cross-linking of the polymer matrix.





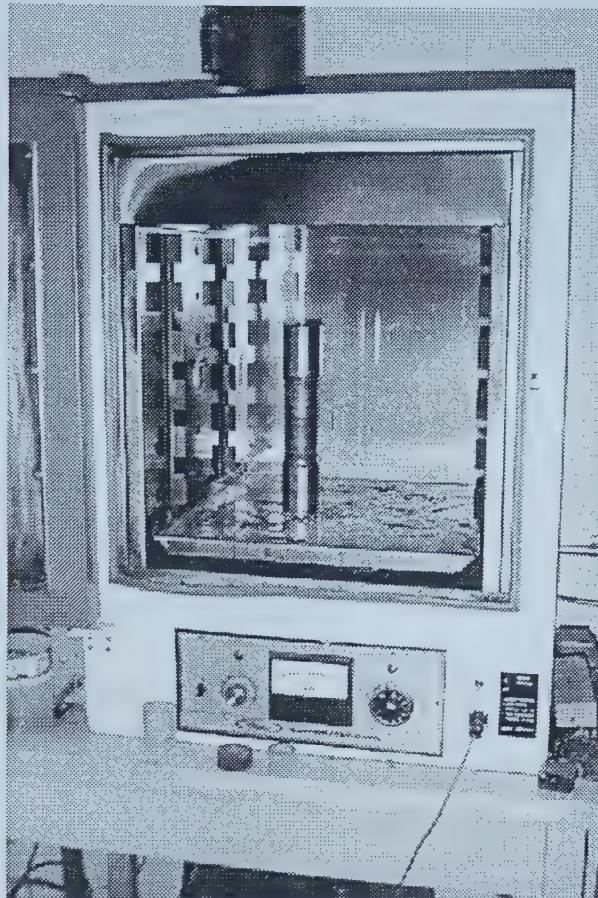


Figure 3-6 Specimen in the curing oven

***Step 13: Remove the shrink tape, steel sheet, nylon release peel ply fabric***

After the curing cycle, the specimen is allowed to cool down within the oven. Once at room temperature, it is taken out and the shrink tape, steel sheet and the nylon release peel ply are removed carefully. There maybe some excessive resin flow to the downside steel end, thus it is necessary to clean it by hand using Si-C grit papers (600 grit or higher). After all these steps, the hybrid tubular specimen is ready (Figure 3-7).



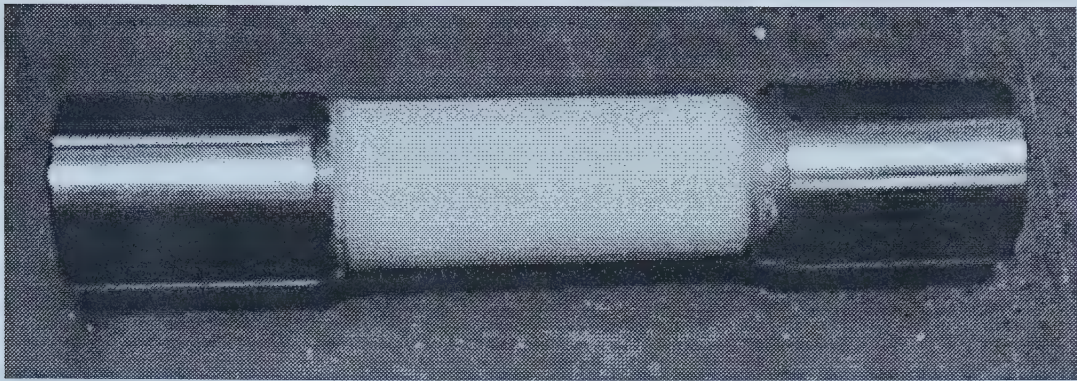


Figure 3-7 Finished tubular specimen

### **3.3 Testing apparatus**

#### **3.3.1 MTS testing machine**

Considering the requirements of the experiment, the testing machine to be used must be able to perform the following:

- Provide uniaxial loading condition
- Provide biaxial loading condition
- Provide different loading histories (Loading, unloading and reloading)
- The maximum load must be able to keep the steel liner in a prescribed plastic range

From the analysis in Chapter 2, the following predictions are made concerning the capacities of the present tubular specimen:

- Under uniaxial loading condition, the yield pressure is 22.33Mpa. The proof pressure required to produce residual stress of approximately half the yield stress is 41.33MPa.



- Under biaxial loading condition, the yield pressure is 25.42MPa, The proof pressure required to produce residual stress of approximately half the yield stress is 46.42MPa, and the axial loading at this pressure is 100KN.

Based on the above considerations, a 650KN MTS machine with a maximum 70MPa internal pressure source is chosen (Figure 3-8).





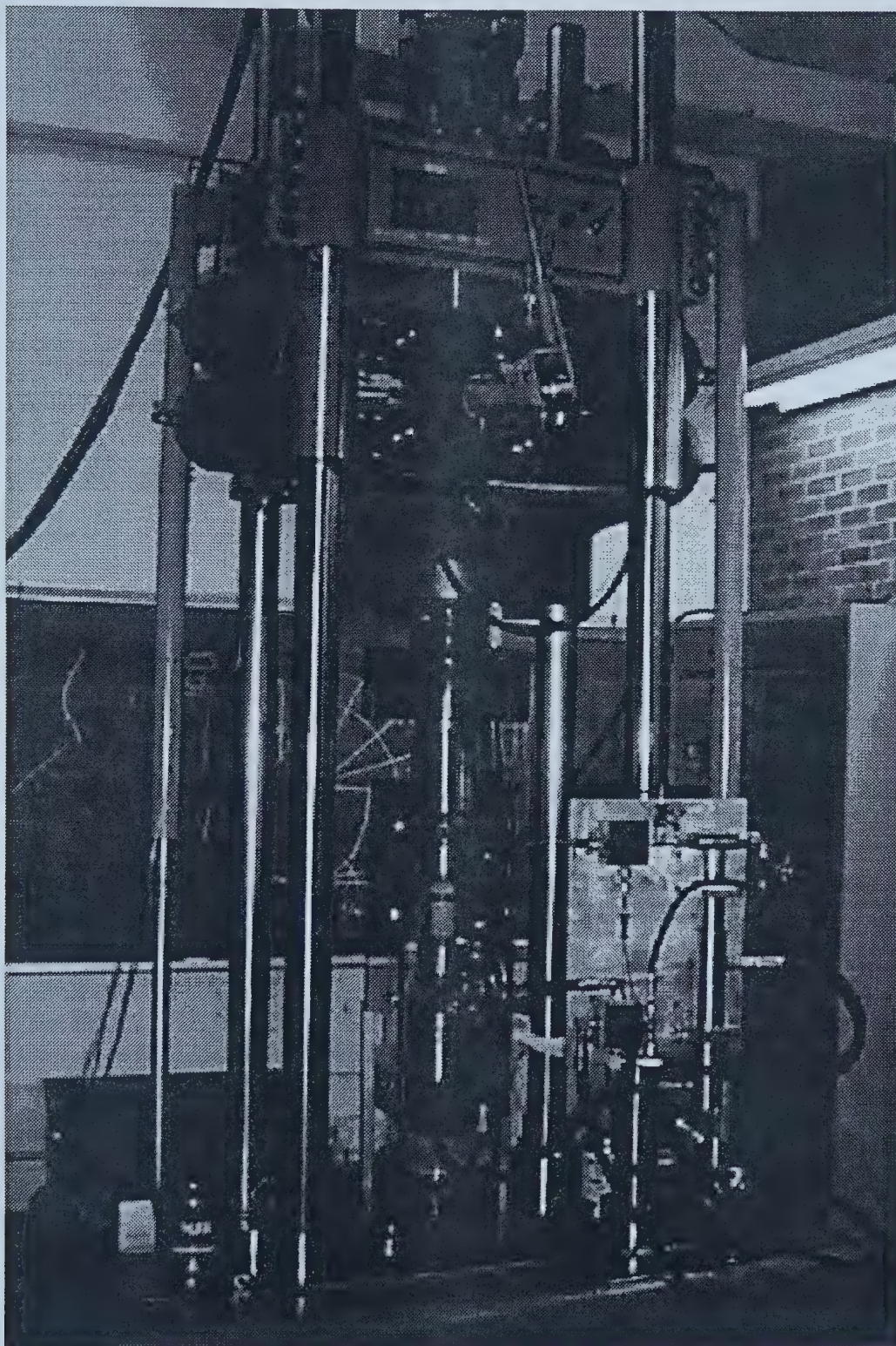


Figure 3-8 MTS machine





### 3.3.2 Gripping system

To mount the specimen on the MTS machine, a gripping system is required. This gripping system must be able to hold the specimen in such a way that there is no axial slippage even under the highest axial loading experienced. It must also have good seal so that there is no leakage during the experiment.

A specially designed double collet gripping system is used in this investigation. Martens [42] developed this system to perform biaxial monotonic tests on composite pipe specimens. The original design comes from Carroll [43], who developed a double collet system for biaxial monotonic testing of filament wind tubular specimens without any end reinforcement. A schematic illustration of the grip assembly is shown in Figure 3-9, and major components of this system include: inside collet, outside collet, collar, mandrel and base plate.

An O-ring is placed on the outside surface of the mandrel, and another O-ring is placed on the outside surface of plug. These two O-rings act as the seal to prevent leakage. The plug is made of high strength steel (ASTM 4340), which will kept the plug at elastic status during the test, and thus minimize the internal deflection. The plug was placed below the internal collets to ensure a proper seal. Anti-extrusion rings were also added to ensure that the O-ring did not extrude through the gap between the plug and the internal wall of pipe during assembling.

To provide sufficient radial loading to hold the specimen during the test without causing any detrimental effects to the gauge section, both the gripping system and the specimen need to be carefully designed.



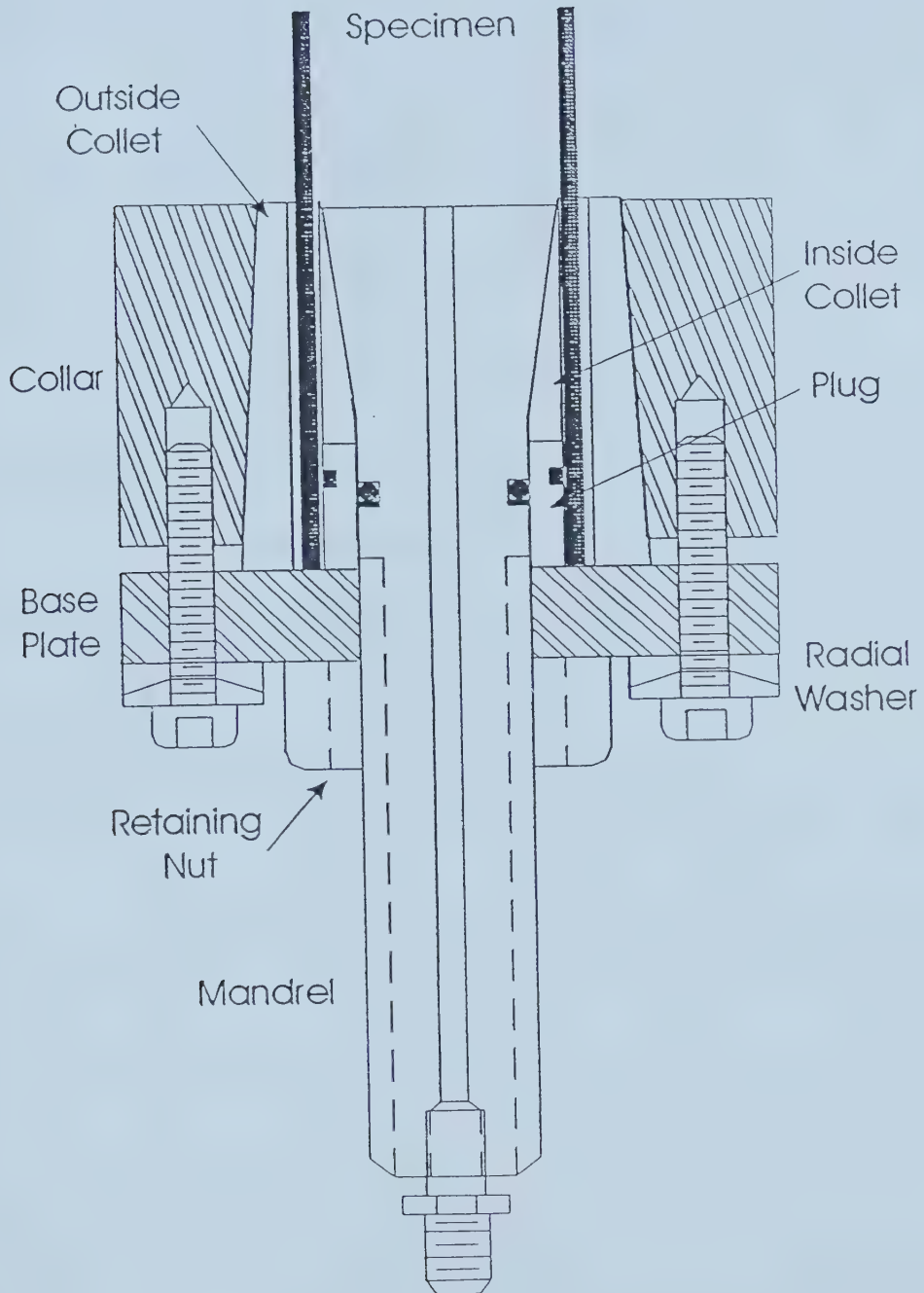


Figure 3-9 Schematic drawing of the gripping system [42]



Based on the fact that this is a specimen of hybrid composite pipe with an internal steel liner, the two ends of the specimen are made of steel and they are integrated to the internal steel liner. The steel ends could stand the highest preload applied during the assembly. The surface of steel ends could also be easily machined to the required dimension. In contrast, it is usually more difficult to accurately control the dimension of a composite end.

A set of collets made of high strength steel (ASTM 4340) is adopted to provide the high axial preload to prevent slippage during the experiment. The taper of the outside collet and the assembly sequence ensure the collets are self-tightening when axial load exceeds the total preload. An INSTRON hydraulic screw driven testing machine (Figure 3-10) is used to perform the assembly of the gripping system. The sequence of assembly is important for a good quality of assembly. The inside collets were first loaded to 88,964N (20,000lbs) to ensure internal support for the specimen. Outside collets were then loaded to 177,928N (40,000lbs). Radial washers were added to the base plate to lower the amount of stress concentration. Figure 3-11 gives the picture of the unfinished and finished specimen mounted in the gripping system.



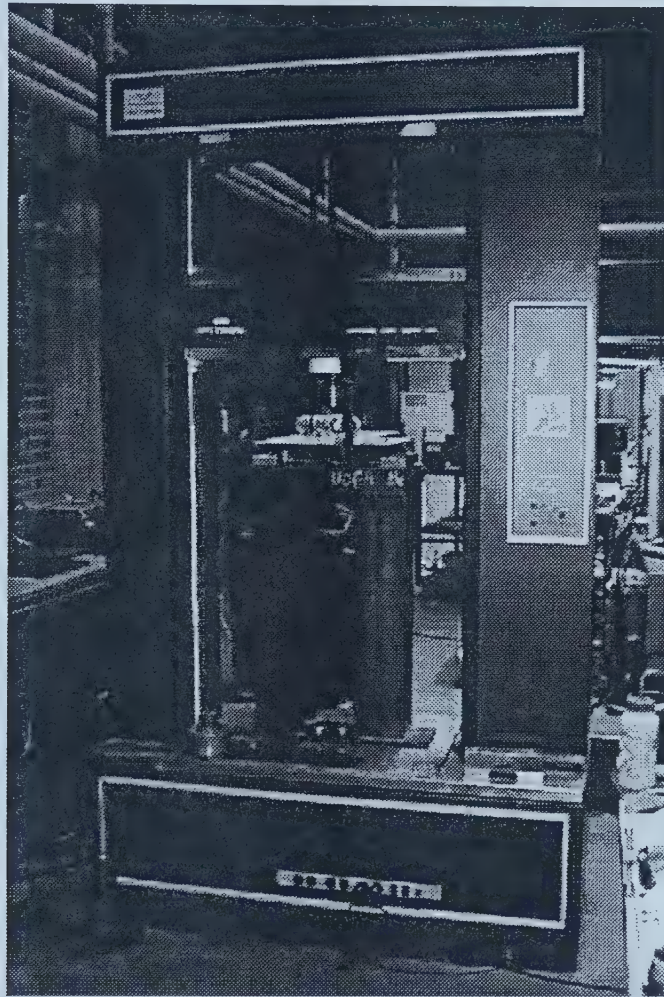


Figure 3-10 INSTRON hydraulic screw driven testing machine





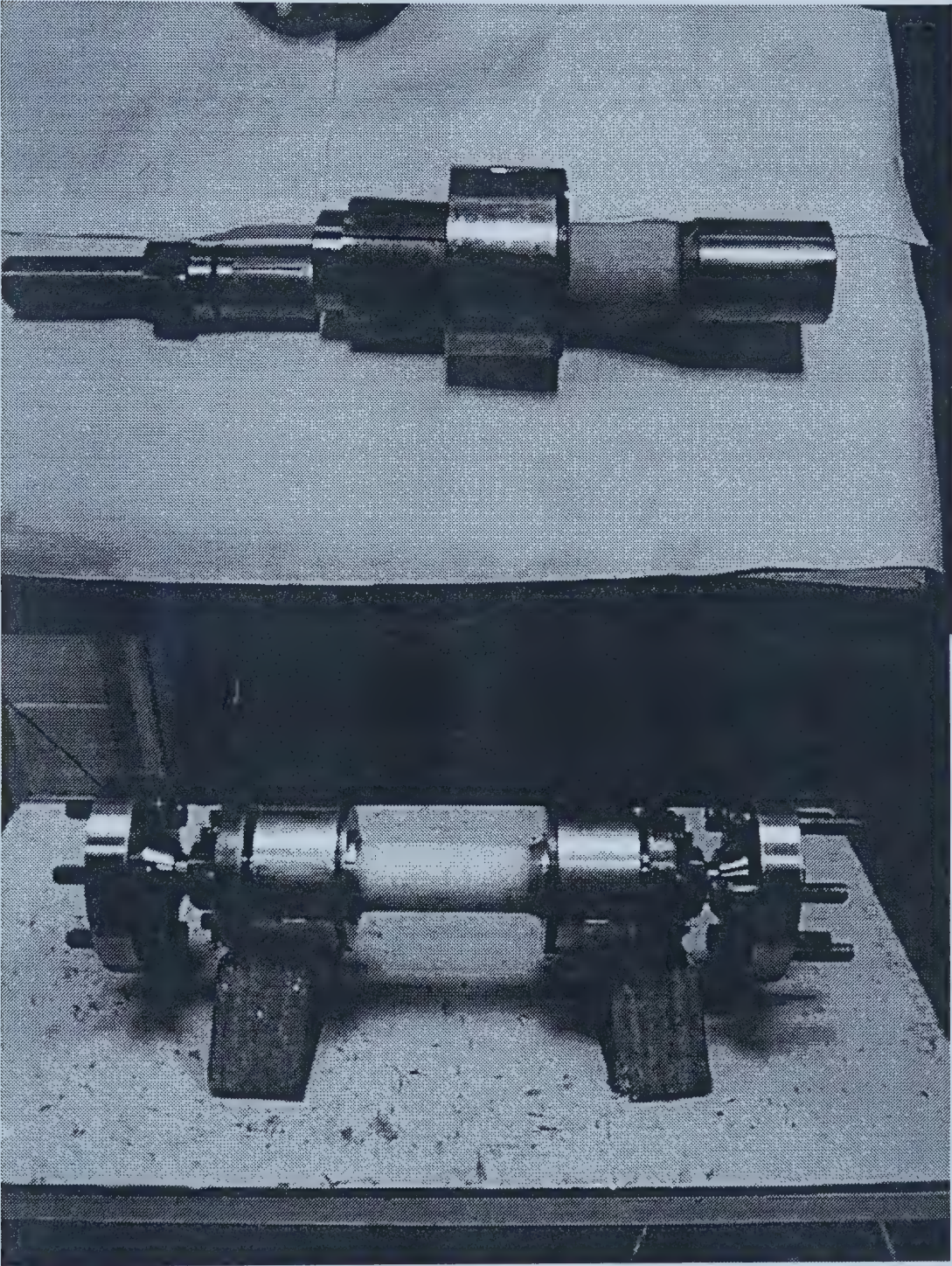


Figure 3-11 Finished specimen mounted in the gripping system





### 3.3.3 Data acquisition

Hoop and axial extensometers (Figure 3-12) are used to measure the hoop and axial strains for both uniaxial and biaxial tests. The axial and hoop extensometers have gauge length of 50.80mm (2 inches) and 62.23mm (2.45 inches), respectively. Both of them are calibrated before each test in a range that covers the maximum strains that will be encountered during test.

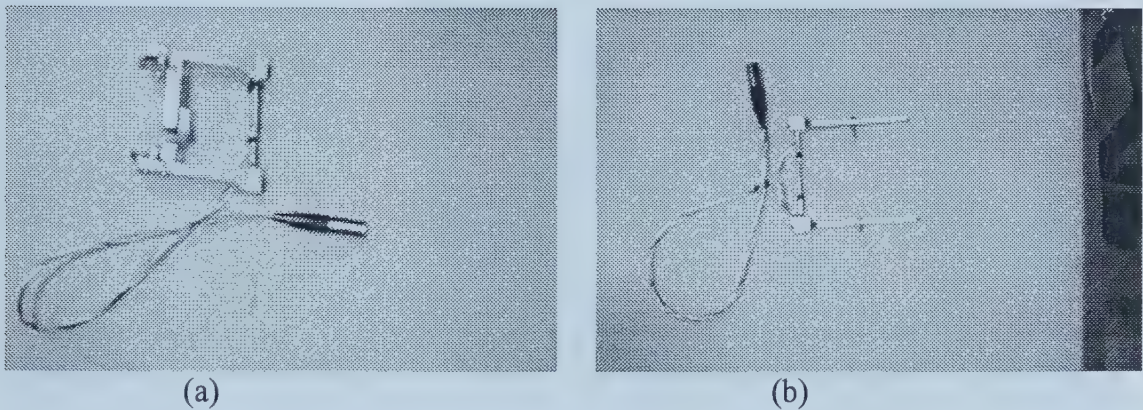


Figure 3-12 (a) axial extensometer (b) hoop extensometer

The axial extensometer is held to the surface of the specimen by the contact force applied by the knife-edges through the use of springs. In the case of the hoop extensometer, instead of the knife-edges, pins are used to apply the contact force. The contact force is approximately several Newtons in value, which is sufficient to keep the extensometers in position without causing detrimental effects to the test results. To further prevent slippage of the extensometers, fast cold-cure epoxy is also added to the knife-edges of the axial extensometers as well as the pins of the hoop extensometers.

The position of the extensometers is also critical to minimizing errors during measuring, especially for the hoop extensometer. A height gauge used together with a



horizontal lay-up table (Figure 3-13) to mark the positions on the specimen that would be in contact with the extensometers. This set could ensure that the points of the hoop extensometer pass through the diameter of the specimen.

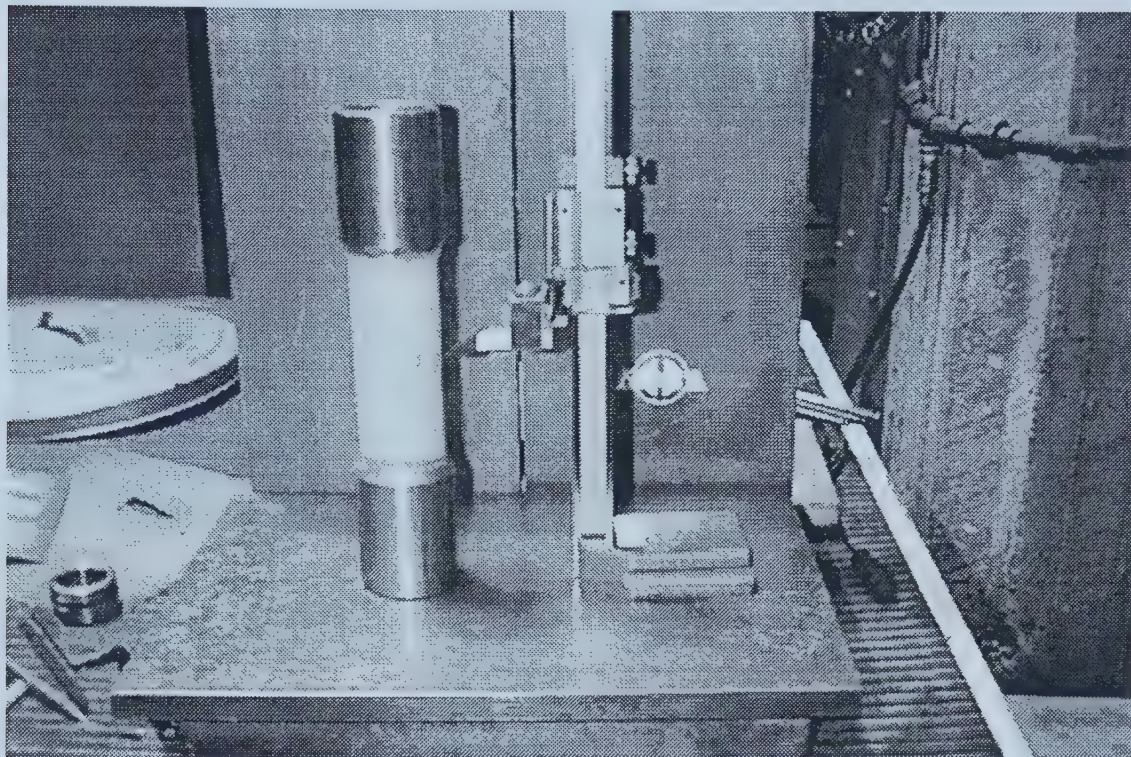


Figure 3-13 Marking the position of extensometers on the specimen

A Tektronix TDS 410A two channel digitizing oscilloscope is used to collect and record data throughout the whole test. At the same time, two X-Y recorders are also used to plot pressure-hoop strain and pressure-axial strain curves in order to give an illustration of the loading procedure. Figure 3-14 gives an illustration of these instruments.





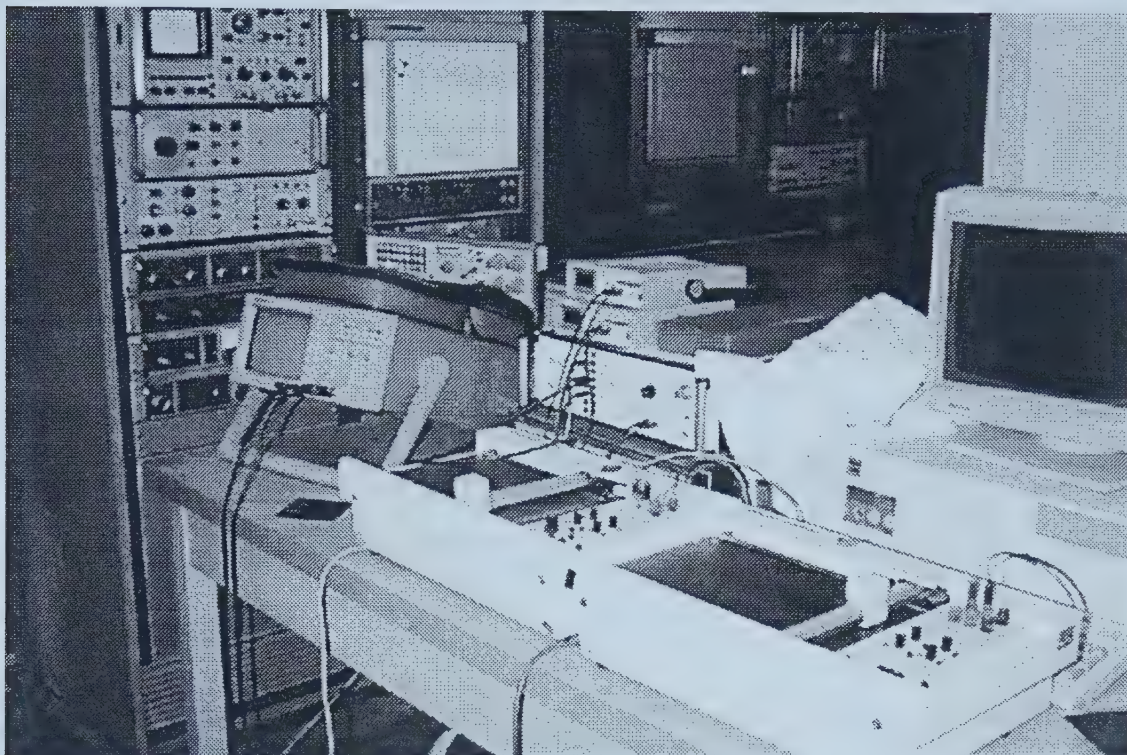


Figure 3-14 Data acquisition system

### ***3.4 Testing procedure & results***

#### ***3.4.1 Introduction***

Four tests are carried out during this study. The specimens tested include one steel liner only specimen and three hybrid composite/metal tubular specimens. A detailed description about the specimens and loading conditions is given in Table 3-2.





Table 3-2 Specimens tested

| Specimen                   | A     | B     | C     | D     |
|----------------------------|-------|-------|-------|-------|
| Liner thickness $t_s$ (mm) | 1     | 1     | 1     | 1     |
| Wrap thickness $t_c$ (mm)  | 0     | 1.8   | 2     | 1.8   |
| Average radius $r$ (mm)    | 25    | 26.2  | 26.3  | 26.2  |
| Loading condition          | 1H:0A | 1H:0A | 2H:1A | 2H:1A |

### 3.4.2 Steel liner test

The first experiment carried out was on specimen A to obtain the uniaxial stress-strain curve of the steel.

Without any composite wrap outside, the internal steel liner was mounted onto the gripping system and put on the MTS test machine. The positions of the extensometers are carefully marked with the use of height gauge and lay-up table. The surface of the steel liner is cleaned thoroughly with acetone to minimizing any containment that may cause error during test. After mounting the extensometers on the steel liner, they are connected to the oscilloscope and the X-Y recorders to record the hoop and axial strains.

This test is referred to as a 1H:0A test, which means that only hoop pressure will be applied, and there is no axial loading during the whole testing procedure. As internal pressure is applied by pumping oil into the specimen, a 2H:1A loading condition is generated automatically. Thus axial loading must be compensated to obtain a 1H:0A



loading condition. The axial compensation is applied in the compressive form with the value as

$$T = P\pi r^2,$$

where  $P$  is the internal pressure applied, and  $r$  is the internal radius of the specimen. This would fully compensate the tension produced by the internal pressure, and the required 1H:0A loading condition is generated.

The stress-strain curve obtained from this test is shown in Figure 3-14. To be used in the theoretical calculation, several interpolation points are chosen to produce a multi-linear curve, which is also marked in Figure 3-15. The values for these data points are shown in Table 3-3.

Table 3-3 Stress-strain curve points for the steel

|              |   |       |       |       |       |       |       |       |
|--------------|---|-------|-------|-------|-------|-------|-------|-------|
| Stress (MPa) | 0 | 426.2 | 476.5 | 527   | 551.7 | 572.3 | 583   | 605.5 |
| Strain (%)   | 0 | 0.239 | 0.284 | 0.408 | 0.547 | 0.874 | 1.311 | 3.476 |



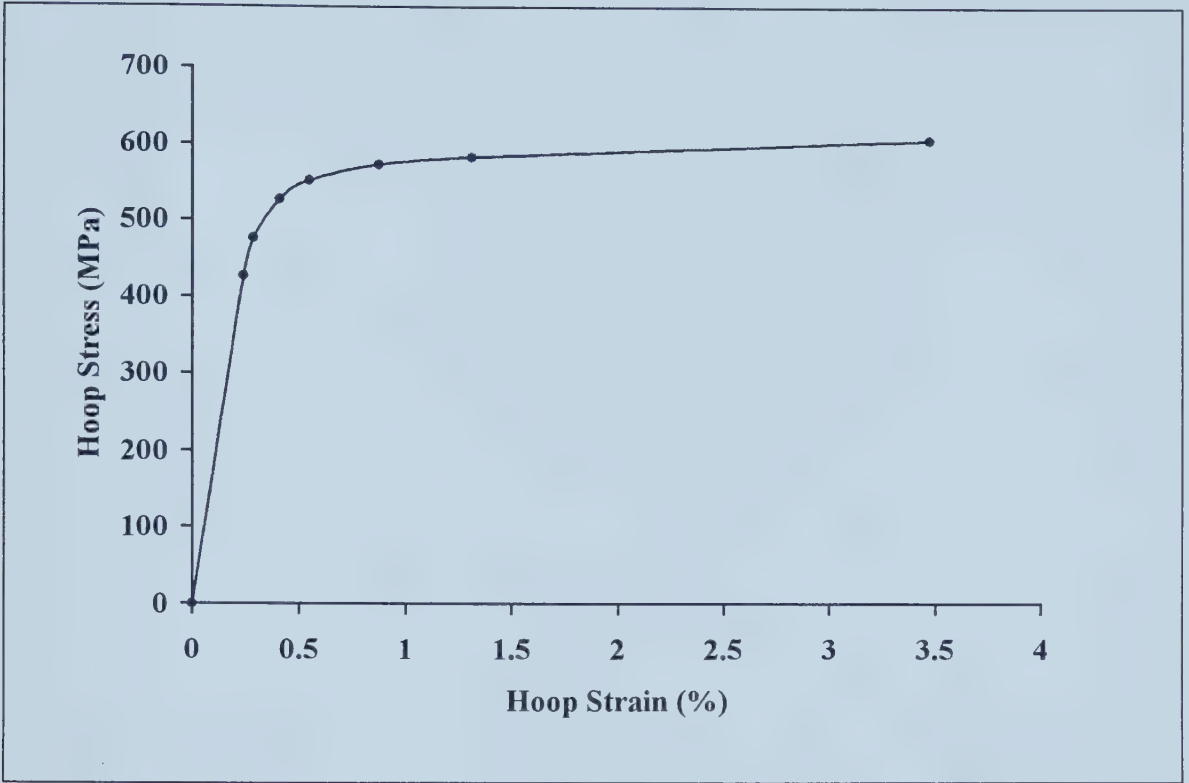


Figure 3-15 Experimental stress-strain curve of steel with points used in multilinear kinematic hardening model

### 3.4.3 Hybrid pipe specimen test

#### 3.4.3.1 Uniaxial test (1H:0A)

This test was carried out on a fully finished specimen B with composite layers wrapped outside the internal steel liner. A compressive axial force ( $T = P\pi r^2$ ) was applied to compensate the tension produced by the internal pressure. The test on specimen A is a monotonic loading one, while this test has some unloading and reloading procedure during the plastic range. The load history was  $0 \rightarrow 40\text{MPa} \rightarrow 0 \rightarrow 51.5\text{MPa} \rightarrow 0 \rightarrow 62\text{MPa} \rightarrow 0$ .



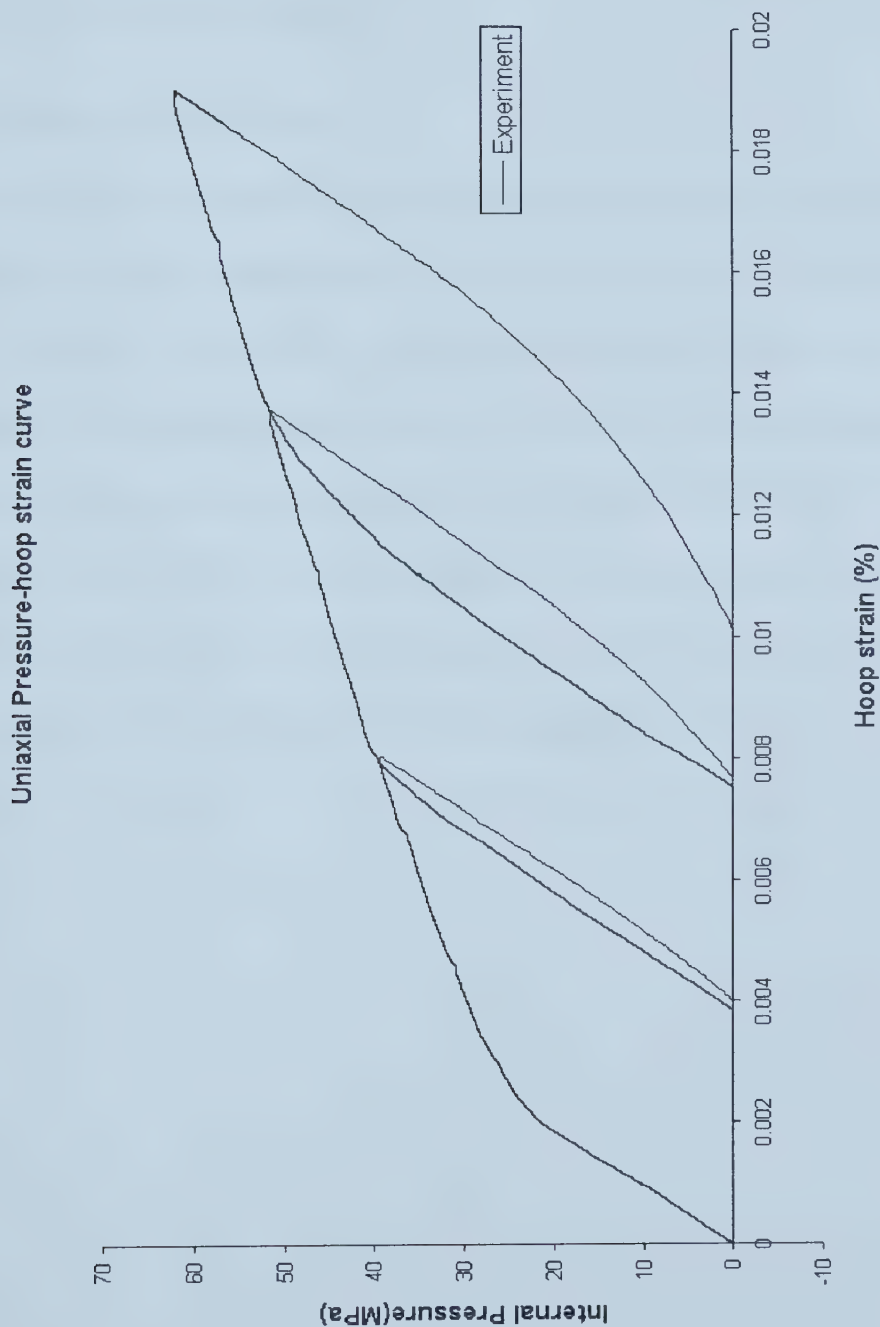


Figure 3-16 Uniaxial  $P - \varepsilon_h$  curves





Since pressure and strain are the two parameters directly being measured with instruments, the pressure-strain curve is used. Figure 3-16 gives the pressure-hoop strain curves obtained from experiment.

### 3.4.3.2 Biaxial test I (2H:1A)

This test is on specimen C, and it is under a 2H:1A loading case, which is generated by applying internal pressure without any axial compensation. This test also includes some unloading and reloading procedure in the plastic range (steel) to study the unloading and reloading characteristics of the hybrid composite/metal pipe with an internal steel liner. The load history was  $0 \rightarrow 45.5\text{MPa} \rightarrow 0 \rightarrow 55\text{MPa} \rightarrow 0$ .

Due to the limitation of the two-channel digitizing oscilloscope, only two parameters can be recorded digitally during the test and these are the pressure and the hoop strains. X-Y recorder will be used to record the axial pressure-strain curve.

Figure 3-17 (a) gives the  $P - \varepsilon_h$  curve and Figure 3-17 (b) gives the  $P - \varepsilon_a$  curve.



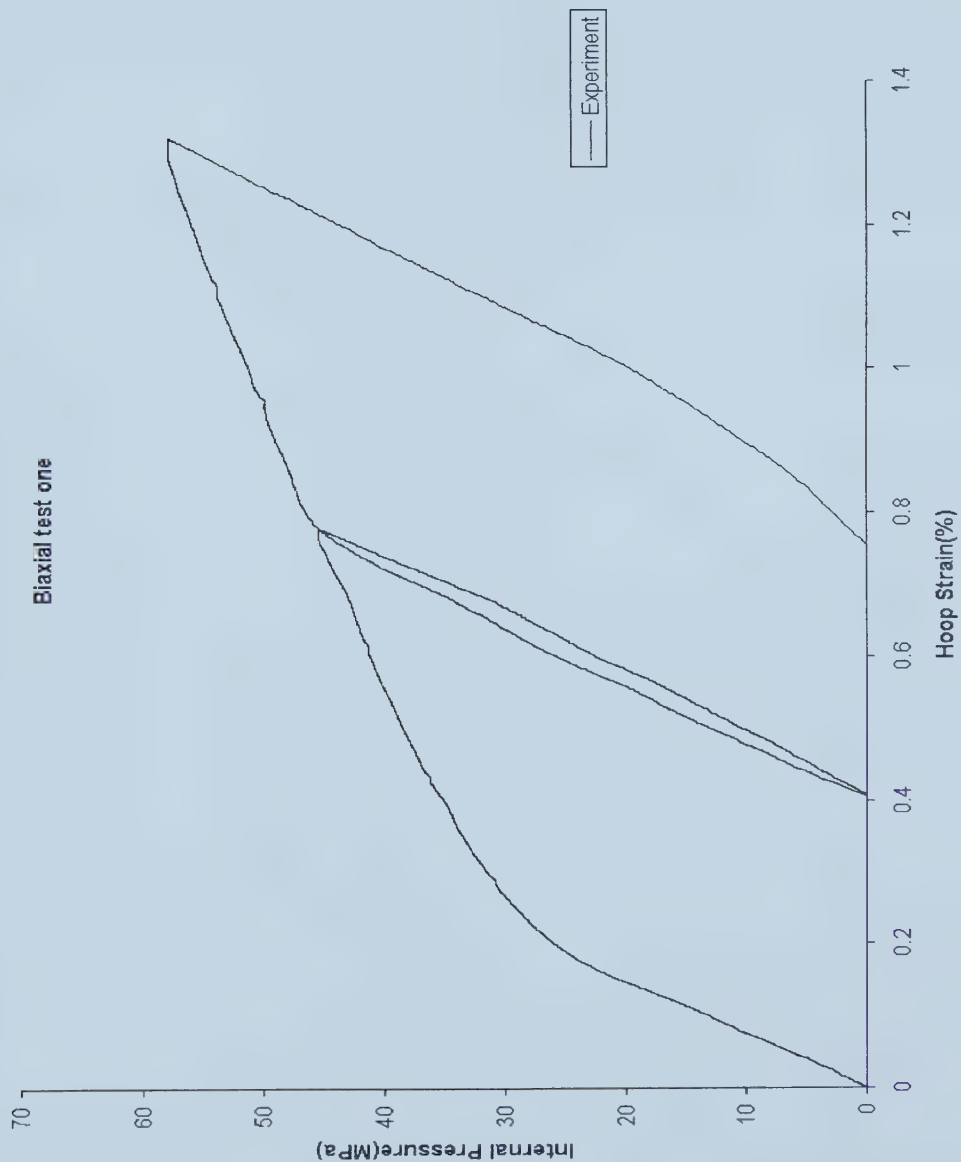


Figure 3-17 (a)  $P - \varepsilon_h$  curve of biaxial loading test one



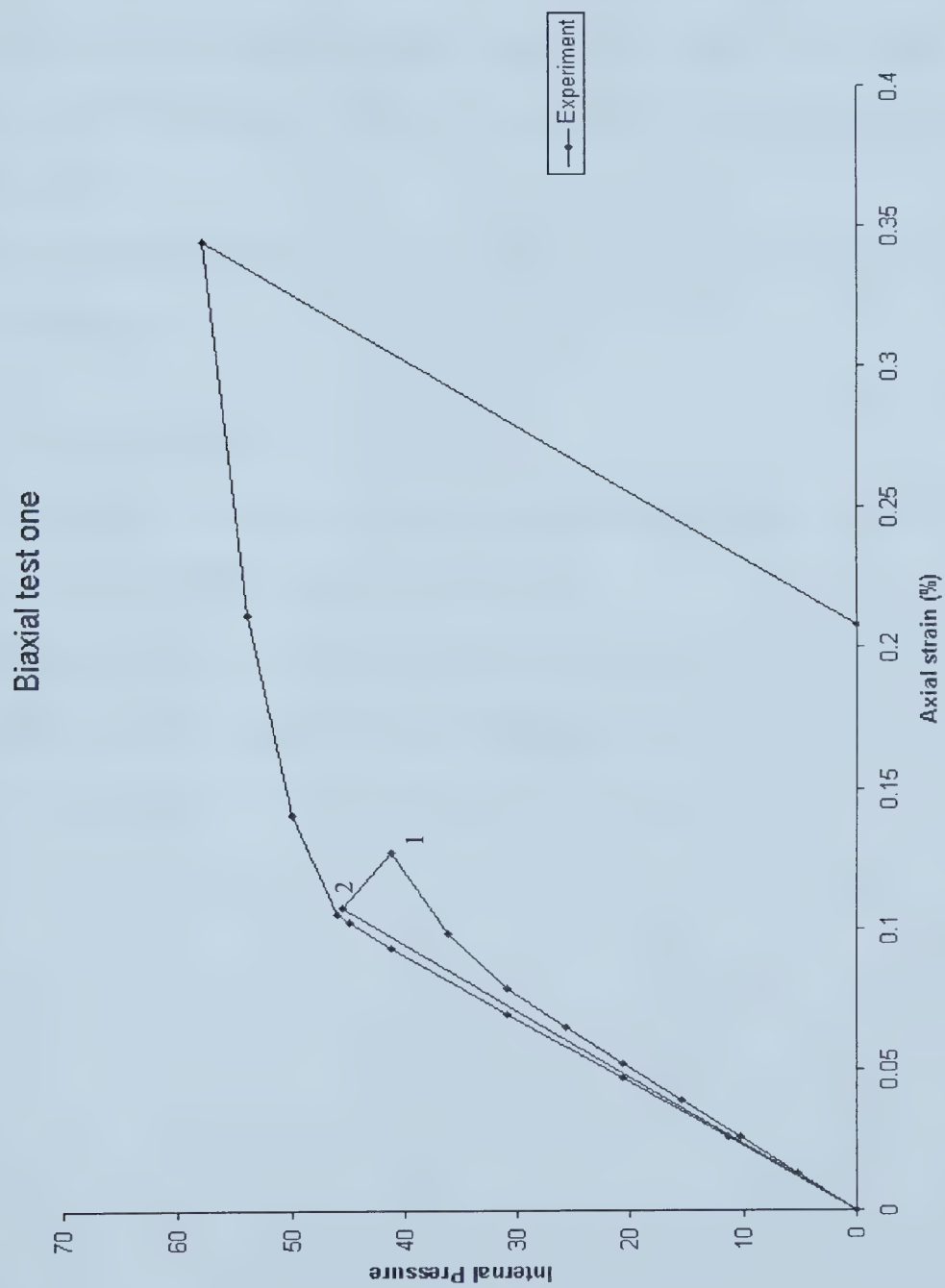


Figure 3-17 (b)  $P - \varepsilon_a$  curve of biaxial loading test one



From the axial pressure-strain curve, it could be seen from the curve that something unusual occurred between data point 1 and 2. At data point 1, the strain suddenly become smaller, which obvious violates theoretical predictions. Possible reason causing this anomaly might be the slippage of the axial extensometer when the load was increased from data point 1 to 2.

As a result of this anomaly during axial loading, another biaxial test was carried out for further verification.

#### 3.4.3.3 Biaxial test II (2H:1A)

This biaxial test is the same as the above, and the specimen tested is specimen D. The loading path was also  $0 \rightarrow 45.5\text{MPa} \rightarrow 0 \rightarrow 55\text{MPa} \rightarrow 0$ .

In this experiment, the pressure and the axial strain were recorded digitally, and the X-Y recorder was used to record the hoop pressure-strain curve.

Figure 3-18 (a) gives the  $P - \varepsilon_h$  curve and Figure 3-18 (b) gives the  $P - \varepsilon_a$  curve.





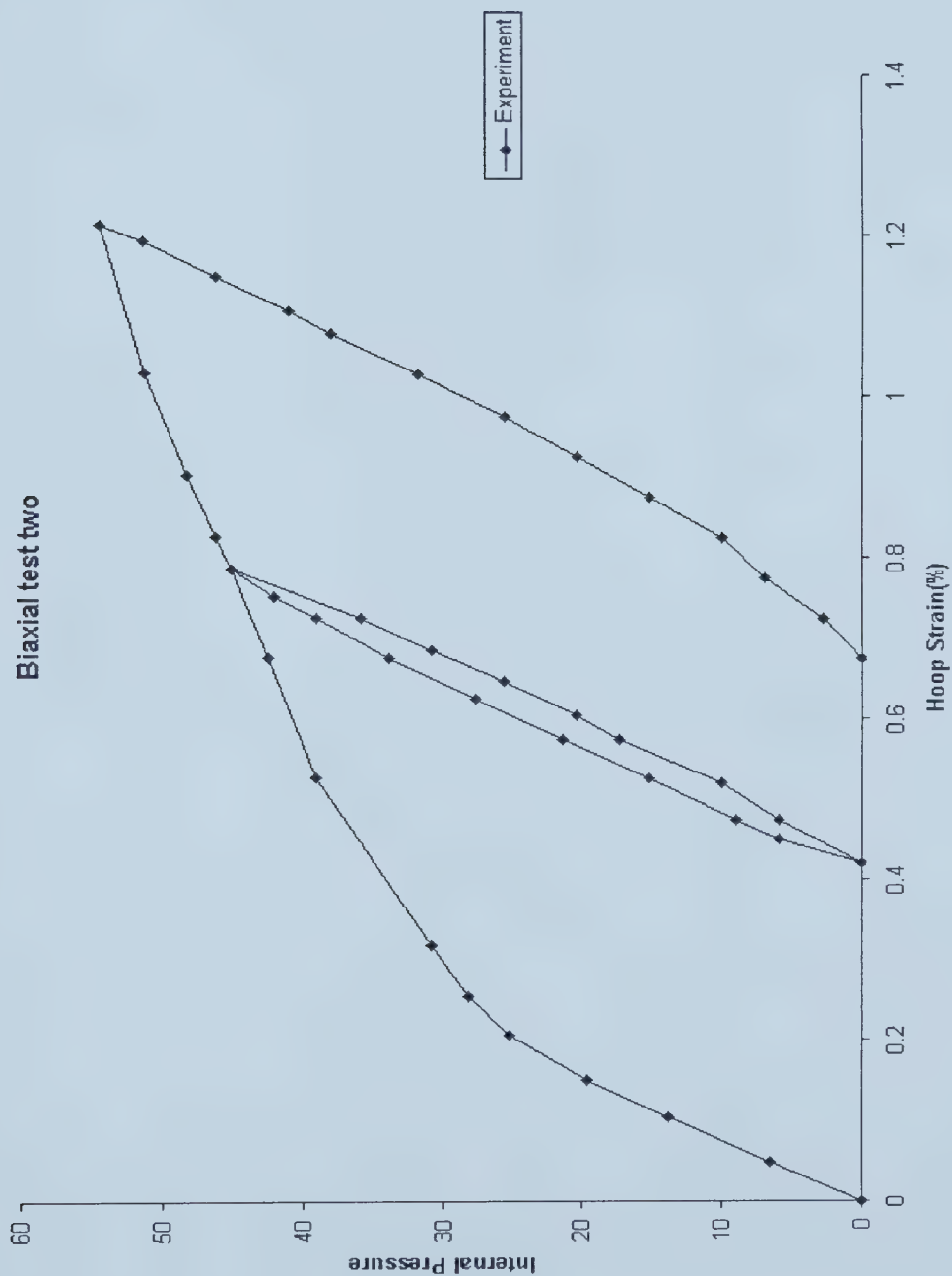


Figure 3-18 (a)  $P - \varepsilon_h$  curve of biaxial loading test two



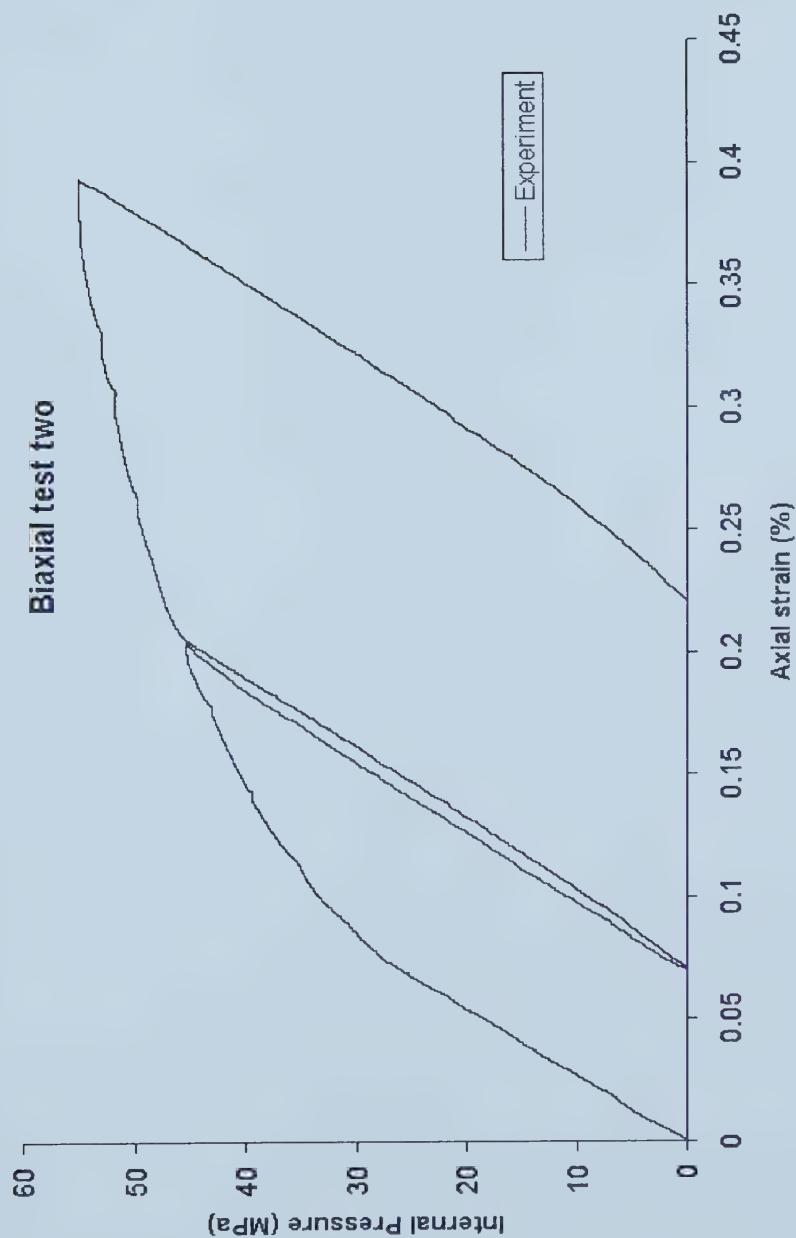


Figure 3-18 (b)  $P - \varepsilon_a$  curve of biaxial loading test two



---

Following this experimental investigation, the test results are compared with the theoretical predictions and finite element analysis in the following chapter.



---

## Chapter 4 Finite element analysis and comparisons

### **4.1 Introduction**

Finite element method is now widely used in engineering analysis. With the help of various FEM packages, such as ANSYS, ADINA, MARC, etc., one can obtain close predictions for the physical behavior of the actual structures, provided that appropriate model is adopted. In this study, a finite element analysis is also carried out with ANSYS 5.6 for the hybrid pipe. Both uniaxial and biaxial loading conditions are modeled, and the loading and unloading procedures are simulated. All the FEM numerical results are compared with the theoretical predictions described in Chapter 2 and the experimental results in Chapter 3, and they are found to be in a good agreement.

### **4.2 Finite element model**

In the current study, the hybrid composite pipe is subjected to axisymmetric loads, i.e., internal pressure and axial tension (Figure 4-1). The geometry, material properties and loading conditions of the pipe are also axisymmetric. Thus all field variables (displacements, strains, stresses, etc.) are independent of the coordinate  $\theta$ , and this problem can be reduced to a 2-D axisymmetric problem.





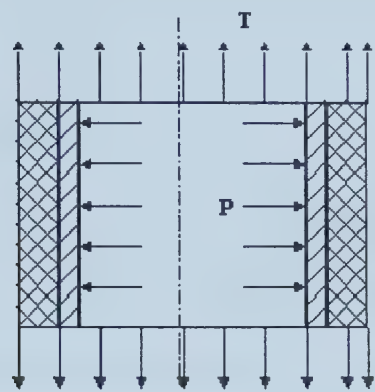


Figure 4-1 Axisymmetric loading conditions of the hybrid composite pipe

4.3 Element type

A 2-D structural solid element PLANE42 is used for this study. The element can be used as a plane element (plane stress or plane strain) or as an axisymmetric element. The element is defined by four nodes with two degrees of freedom at each node: translations in the x and y directions. The element has plasticity, creep, swelling, stress stiffening, large deflection, and large strain capacity [44]. Figure 4-2 shows the pictorial summary of element PLANE42.

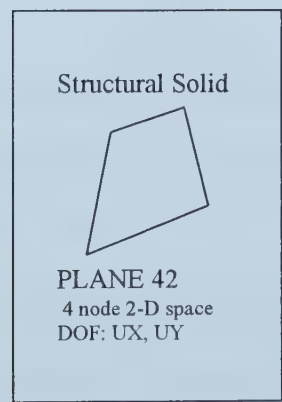


Figure 4-2 Pictorial summary of element PLANE42



## 4.4 Material properties

### 4.4.1 Material properties of the steel

The steel is an isotropic elastic-plastic material with Young's modulus  $E = 200GPa$ , and Poisson's ratio  $\nu = 0.3$ . In this study, the steel is regarded as a kinematic-hardening material. Multilinear kinematic hardening material was chosen and the input points was obtained from experiment. Figure 4-3 shows the stress-strain relationship for this multilinear kinematic hardening material.

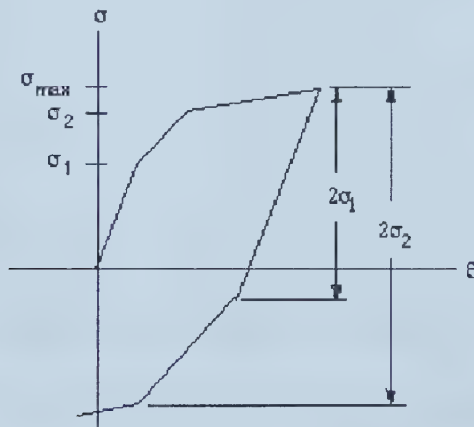


Figure 4-3 Stress-strain relationship for multilinear kinematic hardening material

In ANSYS, the multilinear kinematic hardening material adopts the von Mises yield criteria, and using associative flow rule, and kinematic hardening rule. The implementation of the analysis is using the Besseling model also called the sublayer or overlay model. This allows a multilinear stress-strain curve that exhibits the Bauschinger (kinematic hardening) effect as shown in Figure 4-3.



#### 4.4.2 Material properties of composite wrap

The composite wrap is assumed to be homogenous and orthotropic. In this study, it is assumed to be a linear elastic material. Based on classical laminate theory and material properties of the individual lamina, the material properties of the composite wrap in this study was determined to be:

$$E_z(E_\theta) = 33544 \text{ MPa},$$

$$E_x(E_r) = E_y(E_z) = 10026 \text{ MPa},$$

$$G = 7600 \text{ MPa},$$

$$\nu_{\theta r} = \nu_{\theta z} = 0.5664,$$

$$\nu_{rz} = 0.4.$$

#### 4.5 Loading conditions

The hybrid composite pipe is subjected to internal pressure and axial loading. Due to the axisymmetric properties, only half of the cross-section is studied. Based on the assumption of long pipe, and the stresses and strains do not vary along the length, only a unit length of pipe, i.e., one element along the axial direction, is required. In the thickness direction, 28 elements are used.

Since this is a long pipe, all the nodes on the top surface have the same displacement in the Y direction, which corresponding to the axial direction. For all the nodes on the bottom surface, symmetric boundary conditions are imposed.



---

## 4.6 Loading history

There are two different types of loading conditions and histories: one is the uniaxial (1H:0A) loading, unloading and reloading, and the other is the biaxial (2H:1A) loading, unloading and reloading path. The results of these two different loading conditions are compared with the experimental results and the analytical results obtained from the programs HPD1 and HPD2.

## 4.7 Comparisons

### 4.7.1 Uniaxial tests ( $\kappa = 0$ )

This is a 1H:0A test, and it is carried out on specimen B (Chapter 3). The first unloading pressure is chosen as the proof pressure to obtain residual stress at the value of half of the yield stress, and the subsequent two unloading pressures were chosen to be evenly distributed between the first unloading pressure and the estimated failure pressure. Therefore, the loading path is  $40\text{MPa} \rightarrow 0 \rightarrow 51.5\text{MPa} \rightarrow 0 \rightarrow 62\text{MPa} \rightarrow 0$ . The Pressure-Hoop strain curve is shown in Figure 4-4, which contains the curves obtained from HPD2, and from ANSYS, and from the experiment.





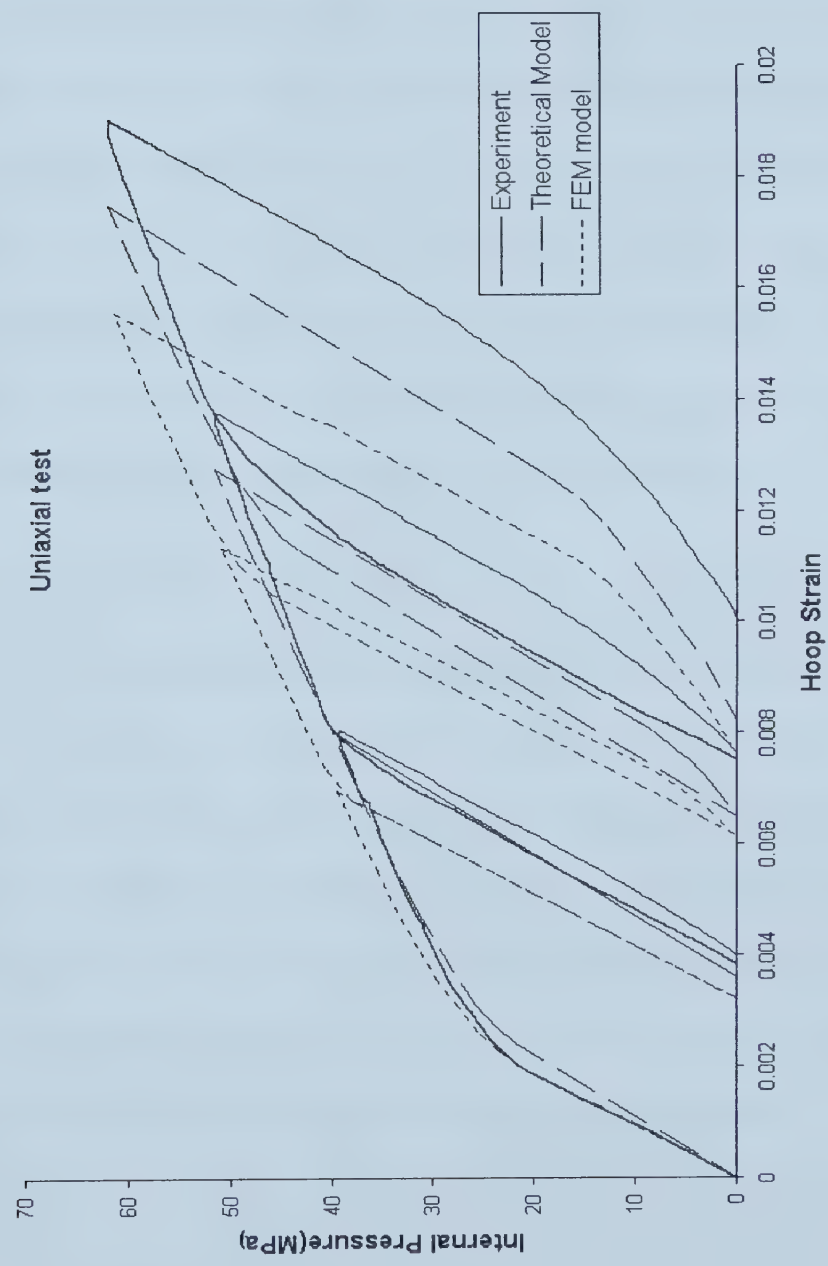


Figure 4-4 Uniaxial Pressure-Hoop strain curves



From Figure 4-4, it can be seen that all the three curves have similar shape and trend during both loading, unloading and reloading procedures. It is also noted that the prediction of the current theoretical model and the test curve are closer to each other. The difference is that the numerical and analytical results tend to be stiffer than the experimental results in plastic range. The reason for this may lie on the assumption that the composite wrap is totally elastic. In fact, the  $[\pm 70]_n$  cross-ply composite laminate are visco-elastic, which may show some softening behavior at the higher load, and this could cause the softness of the experimental results during the plastic range. However, the well agreements of these three curves could still prove that the current theoretical model can effectively simulate the response of the hybrid composite/steel pipe.

#### 4.7.2 Biaxial loading case I ( $\kappa = 1$ , 2H:1A)

Under biaxial loading condition, the specimen is under 2H:1A stress state, which is generated by applying internal pressure to the sealed specimen without applying any axial compensation. This test is carried out on specimen C (Chapter 3). The loading history for this case has two unloading and reloading procedures and the pressures are determined in a similar manner as the previous one. The load history for this case was  $0 \rightarrow 45.5\text{MPa} \rightarrow 0 \rightarrow 58\text{MPa} \rightarrow 0$ . Figure 4-5 shows the pressure-hoop strain curves obtained from the current theoretical model, the FEM model and the experiment.



Bi-axial test one

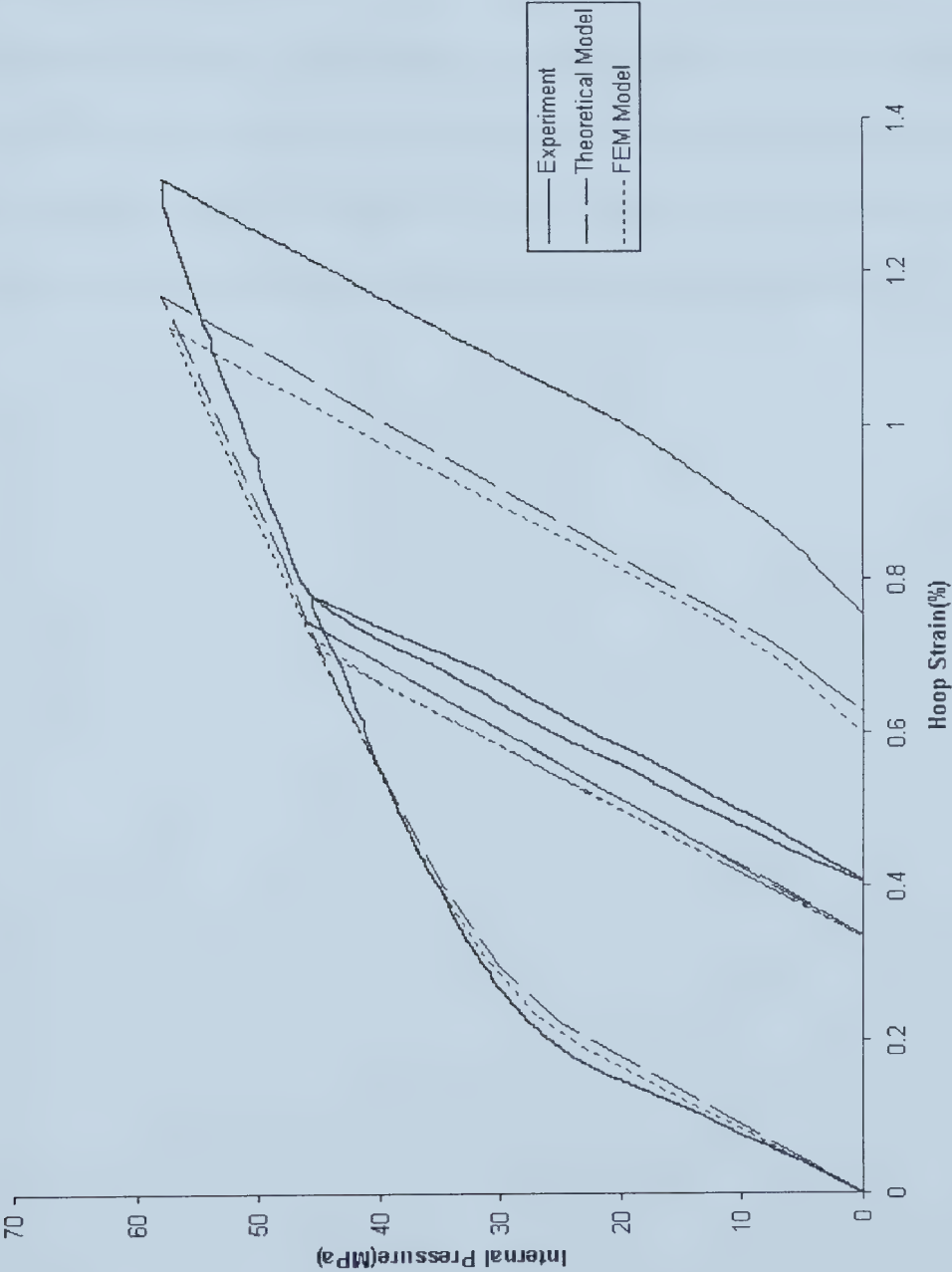


Figure 4-5 Pressure-Hoop strain curves of bi-axial test one



---

From Figure 4-5, similar conclusions can be drawn as the uniaxial loading case: All the three curves are very close to each other, and the current theoretical model can simulate the experiment very well.

As described in Chapter 3, abnormality occurred in the experimental pressure-axial strain curve. Thus the comparisons of the pressure-axial strain curves are given only for the FEM and theoretical ones. The following biaxial loading case will give the pressure-axial strain curve, and further confirmation about the pressure-hoop strain curve.





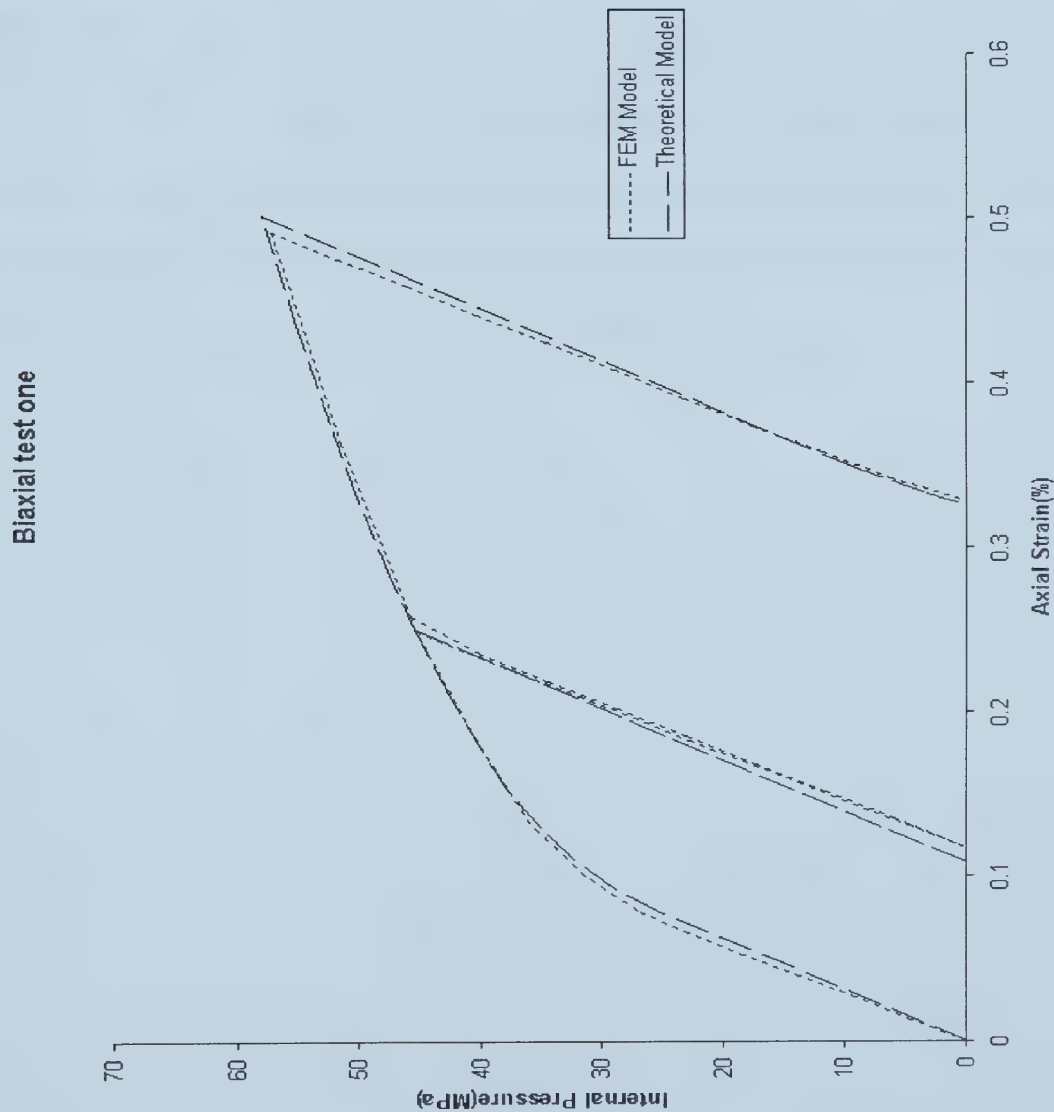


Figure 4-6 Pressure-Hoop strain curves of biaxial test one



### 4.7.3 Biaxial loading case II ( $\kappa = 1$ , 2H:1A)

This biaxial test is carried out on specimen D (Chapter 3). The load history for this case was  $0 \rightarrow 45.5\text{MPa} \rightarrow 0 \rightarrow 55\text{MPa} \rightarrow 0$ . Figure 4-7 shows the pressure-hoop strain curves and Figure 4-8 gives the pressure-axial strain curves. The  $P - \varepsilon_h$  curve was recorded by the X-Y plotter and the  $P - \varepsilon_a$  curve was recorded using the oscilloscope.

It is seen that both hoop and axial pressure-strain curves under biaxial loading condition are in good agreement for the results obtained from the three different methods: numerical (ANSYS), theoretical (HPD2) and experimental methods. This shows that the theoretical model is appropriate and the program is effective and useful.



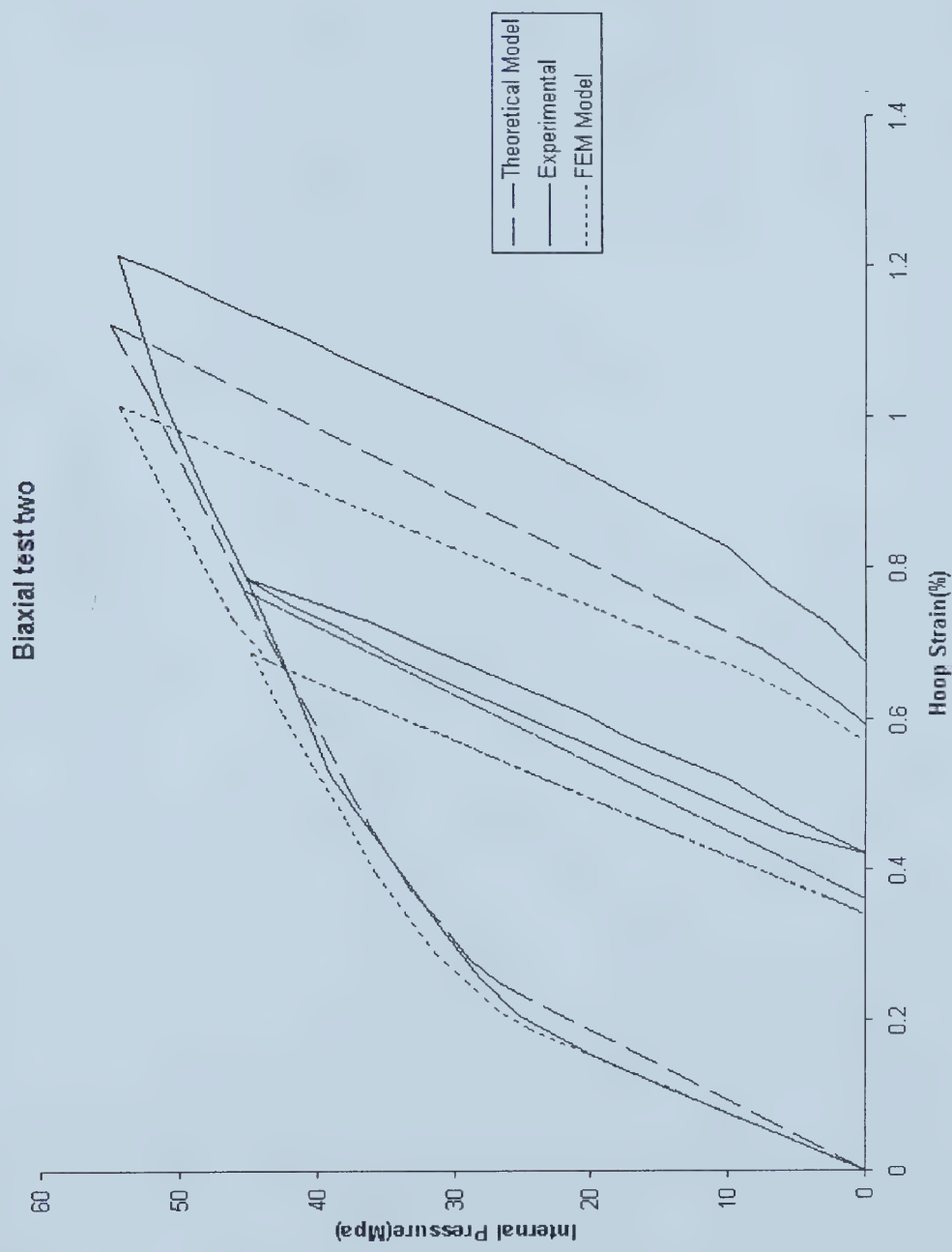


Figure 4-7 Pressure-Hoop strain curves of biaxial test two



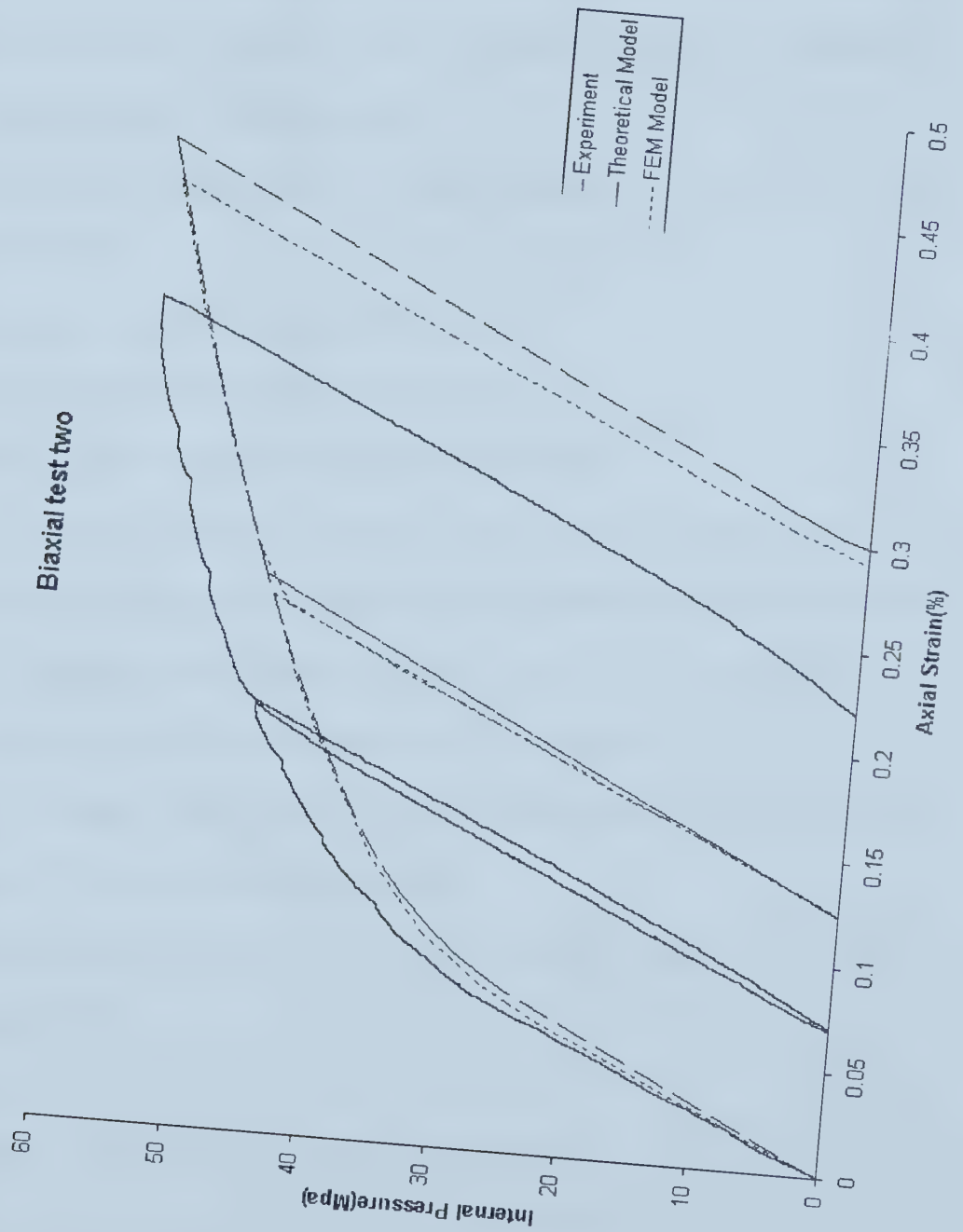


Figure 4-8 Pressure-Axial strain curves of biaxial test two





#### 4.7.4 Failure observation

Though not the major purpose of this study, failure predictions are also included in the developed program HPD1, and here gives some data obtained from the experiments to provide some insight into the failure analysis.

Under the uniaxial loading condition, the failure predictions given by the program HPD1 are listed below:

Failure pressure based on shear strength is 60.927 MPa.

Failure pressure based on Tsai-wu criteria is 62.427 MPa.

Failure pressure based on longitudinal strength is 92.227 MPa.

Under uniaxial loading condition, transverse failure occurs at a pressure much higher than the one that fiber breaks. For the  $\pm 70^\circ$  ply angle laminate in this study, fiber is the major load-carrying constituent, thus fiber failure is considered to be the final failure, and any failure that occurs after the fiber breaks will not be predicted.

From the uniaxial loading experiment, final failure happened at pressure around 68MPa. At proof pressure, no failure was observed.

Under the biaxial loading condition, the failure predictions given by the program HPD1 are listed below:

Failure pressure based on Tsai-wu criteria is 36.475 MPa.

Failure pressure based on transverse strength is 35.775 MPa.

Failure pressure based on longitudinal strength is 90.775 MPa.



In this example, shear failure occurs after the fiber breaks. Due to the same reason stated above, fiber failure is considered to be the final failure, and the shear failure is not included here.

During the biaxial loading case I, the loading path is  $0 \rightarrow 45.5\text{MPa} \rightarrow 0 \rightarrow 58\text{MPa} \rightarrow 0$ . After the first unloading ( $45.5\text{MPa} \rightarrow 0$ ), transverse failure was observed during the proof test stage, but no final failure happens. When try to reload to a higher pressure, final failure happened at pressure of  $56\text{MPa}$ .

Based on the above observations, it could be seen that:

1. Under uniaxial loading condition, no transverse failure happened during the proof test for the  $\pm 70^\circ$  angle ply composite wrap. For the biaxial case, transverse failure happens before reaching the proof pressure, but final failure happens at a much higher pressure.
2. During both tests, final failure happened well below the longitudinal fiber failure prediction. One reason for this fact is the cyclic loading path, which is not considered in the failure predictions. The loading-unloading-reloading procedures may decrease the strength of the composite wrap and the metallic liner. Another fact that may account for this difference is that the strength of the composite wrap is assumed to be the same after the transverse failure happens. In fact, the strength of the composite wrap is decreased after transverse failure happens.
3. For the proof test, 1H:0A loading condition is recommended to avoid the occurrence of transverse failure.



## Chapter 5 Summary & Conclusions

The newly developed hybrid composite/metal pipe has many advantages over the purely metallic or purely composite pipes and it is necessary to better understand its mechanical behavior. This thesis mainly aims to study the mechanical behavior of the pipe, to provide an analysis tool for the design of hybrid pipes and to predict the proof pressure. Through careful numerical and analytical modeling and analysis, in conjunction with experimental verification, a better understanding of the mechanical behavior of the hybrid composite/metal pipe is achieved, and an effective way to design and to predict the proof pressure is obtained.

The theoretical model is built based on the separate constitutive models for the metallic liner and the composite wrap. The constitutive model for the metallic liner is based on Ellyin and Xia's [14, 15 and 16] advanced elastic/plastic constitutive model, which characterizes the mechanical behavior for monotonic loading as well as unloading and reloading history. Under the assumptions that there is perfect bonding between the metallic liner and the composite wrap, and the pipe is a thin-walled cylinder, the integral model for the pipe is obtained. In order to calculate the proof pressure and obtain the mechanical behavior of the hybrid composite/metal pipe, two programs (HPD1 and HPD2) are developed using MatLab. The program HPD1 predicts the pressure required to obtain desired residual stress under any combination of biaxial loadings. It also carries out failure analysis based on Tsai-Wu theory, transverse strength, shear strength and longitudinal strength for the composite wrap, and the failure point based on strength of the metallic liner is also given to provide more information for the pipe design. The program HPD2 simulates the loading and



unloading history of the hybrid composite/metal pipe and record and plot the stress-strain response during loading, unloading and reloading.

Tubular specimens were designed and fabricated for experimental verification. The specimen consists of an integral steel mandrel with pre-impregnated composite tapes (prepregs) wrapped over the steel mandrel using a tube rolling method. The tubular specimen manufacturing methodology is inexpensive and easy to implement, and produces good quality laboratory specimens with repeatable material and geometrical characteristics.

The gripping system used to mount the specimen on the testing machine adopts the double collet gripping system that is developed by Martens [42]. The gripping system provides a high preload to prevent from slippage occurring during testing. The taper of the outside collet and the assembly sequence ensure the collets are self-tightening when axial load exceeds the total preload. An INSTRON hydraulic screw driven testing machine is used to perform the assembly of the gripping system, which ensures repeatable preloading applied to the specimen.

Hoop and axial extensometers are used to measure the hoop and axial strains for both uniaxial and biaxial tests. A Tektronix TDS 410A two channel digitizing oscilloscope is used to collect and record data throughout the whole test. At the same time, two X-Y recorders are also used to plot pressure-hoop strain and pressure-axial strain curves. As pressure and strain are the two parameters directly measured, the pressure-strain curve is plotted and compared with the theoretical and numerical analysis.





FEM numerical analysis is also carried out using ANSYS. Both uniaxial and biaxial loading conditions are modeled, and the loading, unloading and reloading procedures are simulated. All the numerical results were compared with the theoretical predictions and the experimental results, and they were found to be in good agreement.

The following conclusions are drawn from this study:

1. The hybrid composite/metal pipe has numerous advantages when compared with metal pipes or purely composite pipes, especially in the application of high-pressure natural gas transportation. It saves the total weight without affecting the total capacity. When compared with purely metal pipes, example calculations show that the weight saving can be up to approximately 50%. The metallic liner can work as a seal to prevent leakage, which is a main problem for purely composite pipes. The metallic liner can also work as a mandrel, which avoids the need to remove the internal mandrel which is required when fabricating purely composite pipes. The metallic liner can also introduce a beneficial compressive residual stress state through the proof test. This will increase the elastic range, increase fatigue resistance, and help improve the bonding between the metallic liner and the composite wrap.
2. Cross-ply composite wrap can be modeled as an elastic orthotropic homogeneous material using the macromechanical material properties obtained with classical laminate theory. The agreement of the pressure-strain curves for the experimental, numerical and analytical results confirms that this model is appropriate to model the cross-ply composite wrap. However, the



slight difference between the theoretical prediction and the experimental results in the plastic range indicates that while the elastic material assumption is generally sufficient, more accurate results can be obtained if the visco-elasticity of the composite materials is considered.

3. The metallic liner can be effectively modeled by the Ellyin and Xia's constitutive model. This model distinguishes two different types of plastic loading: monotonic plastic loading (ML) and plastic reloading (RL). For these two types of plastic loading, the evolution rule for the yield surface and the calculation of the tangent modulus are also different.
4. The numerical programs developed are effective in proof pressure prediction and in pipe design, and they can greatly ease the design of hybrid composite/metal pipe.
5. The failure analysis based on different failure criteria gives more insight into the pipe design. It indicates when the failure occurs and what kind of failure it is. For the current materials (3M type 1003 (scotchply) E-glass-fiber/epoxy resin) used, with  $\pm 70^\circ$  angle plies, it is very likely to have transverse tensile failure before reaching the proof pressure if the pipe is subjected to biaxial (tension in axial direction) loading condition. This is because of the very weak nature in the transverse direction of the lamina (The transverse ultimate strength is only 31MPa). As for uniaxial loading condition, the proof pressure can always be obtained without reaching the transverse failure limit. However, due to the existence of the metallic liner, the transverse failure is not considered as final failure. In the current application, the major load under



working conditions is internal pressure, and the major load-carrying constitute of the composite laminate is the fiber. The matrix mainly acts to hold the fibers in place. Transverse cracking of the matrix may cause leakage in purely composite pipes, but it will not have significant effect on the load carrying capacity. For the hybrid composite pipe, the metallic liner prevents leakage even when transverse cracking occurs in the composite wrap. Thus, the longitudinal strength is used as the final failure criteria. However, the experiments show that final failure happens well below the longitudinal failure prediction, and this may be due to the occurrence of the transverse and shear failure modes. Therefore, for the proof test, uniaxial loading condition is recommended, which will avoid the occurrence of any kinds of failure.

6. Experiments also confirmed that the theoretical predictions based on the current model could better simulate the real mechanical behavior of the hybrid composite/metal pipe than the FEM model. Thus the numerical programs developed based on the theoretical model can be safely used in pipe design and could better exploit the capacity of the materials, thus providing more accurate design solutions.



---

## Bibliography

1. A. Murrey, "Pipeline design and construction." International Pipeline Conference & Technology Exposition 2000, Calgary, Alberta, Canada, ASME, October 1-5, 2000.
2. M. Mohitpour, T. V. Egmond, and W. Wright. "High pressure gas pipelines—trends for the new millennium", Proc. World Petroleum Congress, Calgary, the Institute of Petroleum (Publisher), June 2000.
3. Pipeline information and education project, Discussion papers: first discussion leaders workshop, Canada, August 2-16, 1972.
4. Pipeline performance in Alberta 1980-1997, Alberta Energy and Utilities Board, Report 98-G, Dec. 1998.
5. L. Gaverick (Editor). Corrosion in the petrochemical industry. ASM International, 1994.
6. R.H. Lea and K. Schmit. "Twenty-year history of successful applications of composite pipe in seawater service", in: Composite Materials for Offshore Operations, Proceedings of the First International Workshop, Houston, TX, 26-28 Oct. 1993, National Institute of Standards Technology, Gaithersburg, MD, pp. 261-268, 1995.
7. S. V.Kulkarni and C. H. Zweben (eds), Composites in Pressure vessels and Piping, PVP-PB-021, ASME, 1977.
8. R. F. Lark, "Recent advances in lightweight, filament-wound composite pressure vessel technology", in: Composites in Pressure Vessels and Piping (eds Kulkarni, S.V. & Zweben, C. H.) PVP-PB-021, ASME, 1977, pp. 17-49.





- 
9. M. M. Shorkrieh and H. M. Rad, "The effect of internal liner on mechanical behavior of composite pressure vessels", Proceedings of the 12<sup>th</sup> International Conference of Composite Materials, T. Massard and A. Vautrin (eds), Paris, July 5-9, 1999.
  10. J. M. Lifshitz, "Filament-wound pressure vessel with thick metal liner", Composite Structure, **32**, pp. 313-323, 1995.
  11. M. Z. Kabir, "Finite element analysis of composite pressure vessels with a load sharing metallic liner", Composite Structures, **49**, pp. 247-255, 2000.
  12. J. Liu and T. Hirano, "Design and analysis of FRP pressure vessels with load-carrying metallic liners", in: Analysis and design of composite, process, and power piping and vessels, **368**, pp. 95-101, ASME, 1998
  13. S. R. Swanson and M. Offolter, "Analysis of a fiber composite cylinder laminated with an elastic-plastic aluminum liner under internal pressure loading", Journal of Thermoplastic Composite Materials, **11**, pp. 466-477, 1998.
  14. F. Ellyin, Z. Xia and J. Wu, "A new elasto-plastic constitutive model inserted into the user-supplied material model of ADINA," Computers & Structures, **56**, pp. 283-294, 1995.
  15. F. Ellyin, "An anisotropic hardening rule for elastoplastic solids based on experimental observations", Journal of Applied Mechanics, **56** or **111**, pp. 499-507, 1989.
  16. Z. Xia and F. Ellyin, "Nonproportional multiaxial cyclic loading: experiments and constitute modelling", Journal of Applied Mechanics, **58** or **113**, pp. 317-325, 1991.
  17. A. K. Kaw, Mechanics of Composite Materials, CRC Press LLC, 1997.



- 
18. J. J. Skrzypek, Plasticity and creep—theory, examples and problems. CRC Press, Inc. R. B. Hetnarski (English edition editor), 1993.
  19. E. Melan, “Zur Plastizität der räumlichen kontinuums”, Ing. Archiv, **9**, pp. 116-126, 1938.
  20. E. Melan, “Der Spannungszustand eines Mises-Hencky Schen Kontinuums Bei veränderlicher Belastung”, Sitz. Akad. Wiss., Ser IIa, **147**, pp. 73-87, 1938.
  21. Ishlinsky, A. Yu, “A general theory of plasticity with linear hardening”, (in Russian) Ukr. Mat. Zhurn., **6**(3), pp. 314-324, 1954.
  22. W. Prager, “The theory of plasticity: a survey of recent achievements”, Proc. Inst. Mech. Eng., pp. 41-57, 1955(169).
  23. W. Prager, “A new method of analyzing stresses and strains in work-hardening plastic solids”, J. Appl. Mech., **23**(4), pp. 493-496, 1956.
  24. H. Ziegler, “A modification of Prager’s hardening rule”, Quart. Appl. Math., **17**(1), pp. 55-65, 1959.
  25. F. Ellyin, “On the concept of initial and subsequent yield load”, in: Failure criteria of structural media, J. P. Boehler ed., A. A. Balkema Publishers, Rotterdam, the Netherlands, 1983.
  26. F. Ellyin and J. Wu, “A description of elastoplastic behavior based memory and yield surface in plane stress state”, in: Constitutive laws for engineering materials—theory and application, Elsevire, New York, pp. 531-538, 1987.



- 
27. J. C. Halpin, N. J. Pagano, J. M. Whitney and E. M. Wu, "Characterization of anisotropic composite materials," in: *Composite Materials: Testing and Design*, ASTM STP 460, pp. 37-47, 1969.
  28. T. R. Guess and F. P. Gerstle, "Deformation and fracture of resin matrix composites in combined stress states", *Journal of Composite Materials*, **11**, pp. 146-163, 1977.
  29. P. D. Soden, P. R. Leadbetter, P. R. Griggs and G. C. Eckold, "The strength of a filament wound composite under biaxial loading", *Composites*, **9**, pp. 247-250, 1978.
  30. I. M. Daniel, T. Liber, R. Vanderby and G. M. Keller, "Stress analysis of tubular specimen for biaxial testing of composite laminates", *Proc. 16<sup>th</sup> Mtg. Soc. Of Eng. Sci.*, Evanston, IL, September 1979.
  31. N. J. Pagano and J. M. Whitney, "Geometric design of composite cylindrical characterization specimens", *Journal of Composite Materials*, **4**, pp. 360-378, 1970.
  32. J. M. Whitney, N. J. Pagano and R. B. Pipes, "Design and fabrication of tubular specimens for composite characterization", in: *Composite Materials: Testing and Design*, ASTM STP 497, pp. 52-67, 1971.
  33. T. R. Guess and C. B. Jr. Haizlip, "End grip configurations for axial loading of composite tubes", *Experimental Mechanics*, **20**, pp. 31-36.
  34. T. R. Guess, "Biaxial testing of composite cylinders: experimental-theoretical comparison", *Composites*, **11**, pp. 139-148, 1989.
  35. G. R. Toombes, S. R. Swanson and D. S. Cairns. Biaxial testing of composite tubes. *Experimental Mechanics*, **25**, pp. 186-192, 1985.



- 
36. S. R. Swanson and A. P. Christoforou, "Response of quasi-isotropic carbon/epoxy laminates to biaxial stress", *Journal of composite materials*, **20**, pp. 457-471, 1986.
  37. S. R. Swanson and A. P. Christoforou, "Progressive failure in carbon/epoxy laminates under tension-compression biaxial tests", *Journal of Engineering Materials and Techniques*, **109**, pp. 12-16, 1987.
  38. S. R. Swanson and M. Nelson, "Failure properties of carbon/epoxy laminates under tension-compression biaxial stress", *Proc. Third Japan-US Conf. On Comp. Mat.*, Tokyo, pp. 279-286, 1986.
  39. S. R. Swanson, A. P. Christoforou and G. E. Jr. Colvin, "Biaxial testing of fiber composites using tubular specimens", *Experimental Mechanics*, **28**, pp. 238-243, 1988.
  40. L. V. Smith and S. R. Swanson, "Design of a cylindrical specimen for biaxial testing of composite materials", *Journal of Reinforced Plastics and Composites*, **16**, pp. 550-565, 1997.
  41. J.W. Hoover, J. D. Wolodko and F. Ellyin, "Transverse cracking of  $[\pm\theta/90_3]_s$  composite laminates, Part one—Experimental Results", 1999. (In preparation).
  42. Michael G. Martens, "Biaxial monotonic and fatigue behavior of a multidirectional glass fiber reinforced epoxy pipe", Master's thesis, Department of Mechanical Engineering, University of Alberta, Edmonton, Alberta, Canada, 1999.
  43. Carrol, "Lay-up and rate effect on fiber glass/epoxy laminates and tubulars", Master's thesis, Department of Mechanical Engineering, University of Alberta, Edmonton, Alberta, Canada, 1994.





---

44. ANSYS User's Manual for Revision 5.5, Volume 3.















University of Alberta Library



0 1620 1423 2472

**B45617**